# STUDIES OF ROTATING FLUIDS:

a) Plane Axisymmetric Flow,

b) Forced Oscillations in a Rotating Fluid,

c) The Ranque-Hilsch Vortex Tube

by

Alan James Reynolds

B.A.Sc., D.I.C.

September, 1960

A thesis submitted for the degree of Doctor of Philosophy

in the Faculty of Engineering

of the University of London

Volume II

The Ranque-Hilsch Vortex Tube


| | | |
|---|---|---|
| 1. | Introduction | 233 |
| 2. | Basic Apparatus | 241 |
| 3. | Experiments with Air | 247 |
| 4. | Experiments with Water | 278 |
| 5. | Theoretical Treatment | 303 |
| 6. | Conclusions | 356 |
| 7. | References | 357 |
| | Tabulated Test Data | 361 |
| | Figures | 365 |

# 1. Introduction

## 1.1. The Vortex Tube and the Ranque Effect

We begin by describing the usual form of the Ranque-Hilsch vortex tube and the physical effect which has aroused interest in it.

The chief component is a tube of constant circular cross-section, its length several times its diameter. Near one end the tube wall is pierced to allow the entry of fluid (usually air), the inlet ports or nozzles being so disposed that a swirling flow is set up within the tube. The fluid escapes at the ends of the vortex chamber, some through an orifice plate near the inlet, the rest through a second throttling device at the end of the tube distant from the inlet. It is usually found expedient to supply air at some pressure above atmospheric and to allow it to exhaust to atmospheric conditions at both exits.

Under certain operating conditions (notably, for reasonably high supply pressures and flow speeds) it is observed that the air emerging through the orifice near the inlet has a lower total temperature than on entering the tube, and that the air leaving at the other exit has a higher temperature than the air supplied; temperature differences equivalent to several times the maximum dynamic head can be obtained. This phenomenon of energy separation has been named the "Ranque effect" after its discoverer. These effects lead naturally to the terminology

"cold end" for that part of the tube containing the inlet ports and "hot end" for the far end.

This basic form can be modified in various ways while still retaining the interesting Ranque effect. For example, vortex tubes have been constructed with tapering barrels and have been water-cooled. A form which has been considered by several investigators is the so-called uniflow vortex tube, in which the cold air is withdrawn through a small tube concentric with the main tube.

## 1.2. Historical

The device just described is associated with the names of two men: Ranque, the French engineer who first fashioned it in 1931, and Hilsch, the German physicist who studied its performance in detail and applied it to the liquefaction of gases in 1944. Hence the device has been variously termed the Ranque tube, Ranque's tube, the Hilsch tube, and the Ranque-Hilsch tube, or any of these with the word "vortex" inserted appropriately.

Earlier investigators concentrated on performance, measuring the temperature changes and exit mass flows associated with particular geometrical configurations and pressure differentials. Most workers were interested in the application of the vortex tube as a refrigerator; their interest died when it became apparent that its efficiency is lamentably low. The only really successful application is to in-flight thermometry, for which the efficiency is not important. It has been found possible

to balance the recoverory temperature rise using the cooling effect of the vortex tube and thus to obtain the true air temperature by measuring that in the core of a vortex fed with ambient air.

Investigations within the tube began with flow visualization, techniques such as liquid injection being necessary for the high speed flows that are of interest. Later experimenters have made detailed measurements within the vortex chamber. Instead of finding the simple flow patterns that were expected, they encountered axial flows in both directions throughout the length of the vortex chamber. Similar complex reversal patterns had been noted previously in swirling flows of liquids.

Theoretical studies have been carried on in parallel with the experiments. Earlier investigators suggested semi-empirical methods of performance prediction, based upon not very clearly formulated theories of the separation mechanism. Attention then turned to the separation process. The most plausible theories are those suggesting that turbulent mixing is the efficient mechanism. But this conclusion is not encouraging for detailed extensions of the analysis since the theory of turbulent shear flows is not sufficiently well-developed to cope with a complex basic flow and the complications of important compressibility effects.

A few of the applications of the vortex tube have been mentioned already. The range of attempts to use the

device is conveyed by a list of the firms in whose laboratories it has been studied: de Havilland, du Pont, General Electric, Hoover, Kodak, Republic Aircraft, Shell.

1.3. Recent Literature on the Vortex Tube

Vortex tube literature published before 1953 has been listed and discussed by Westley. More recent work will now be discussed briefly. Some of the contributions will be discussed more critically in later sections devoted to particular aspects of the problem.

Since the publication of his review of previous work Westley has presented very extensive performance data, for supply pressure and inlet and outlet areas varying over wide ranges. Another recent performance study is that of Otten. He investigated a water-cooled tube with a tapered bore, basing his design on seemingly unpublished experimental data obtained at Royal Dutch Shell laboratories in the Netherlands. A patent has recently been taken on the idea of a water-cooled vortex tube. Some thought-provoking experimental results are reported by Sprenger. He has compared the performance of a vortex tube and a similar resonance tube at the same pressure ratio, finding their energy separating abilities to be very much alike. On this basis he suggests that the separation mechanism must be the same in each case.

Several detailed investigations of the flow within vortex tubes have been made recently. The most detailed are that of Hartnett and Eckert and that of Lay. They

present pressure, temperature and velocity profiles for a number of axial stations and for several supply pressures. Lay also presents the results of flow visualization by liquid injection. Scheller and Brown report less detailed internal flow data.

Several extensions have been made to the theory of the vortex tube. Savet attempts a semi-empirical approach to performance prediction; Lay gives an analysis of the spiraling flow of a compressible inviscid fluid; Pengelley has slightly extended the work of Dornbrand on plane axi-symmetric flow of a viscous fluid; Rott has carried their work into three dimensions by considering a swirling stagnation-point model.

Deissler and Perlmutter attack the three-dimensional viscous vortex and extend their treatment to the turbulent vortex by assuming a constant eddy viscosity and adiabatic radial lump movements during turbulent mixing. Hinze raises the concept of energy flow due to turbulent mixing across a pressure gradient to a new level of sophistication by showing the place of this energy transfer in Reynolds' energy equation.

A new university investigation of the vortex tube is that of Wenig referred to by Scheller and Brown. His work has not been examined.

The investigations discussed above were all made with the Ranque effect in mind and make direct reference to the Ranque-Hilsch vortex tube. A number of other recent

investigations are also of interest, although concerned in the first instance with other problems.

Vulis and Ustimenko present the results of investigations of the flows within several cyclone furnace models and attempt an analysis of such flows taking into account their turbulent nature using approximate equations; unfortunately, incorrectly approximated. These workers studied the mixing within the cyclone chamber by supplying air at a temperature higher than ambient and interpreting the resultant isothermals as lines of constant mixing. They were not aware of the Ranque effect, not realizing that processes other than straightforward mixing could affect the energy distribution.

Centrifugal separation processes involve flows with complex eddy patterns similar to those encountered in the Ranque tube. Hughes reviews work on centrifugal separators, giving sketches of typical swirl distributions and of a typical flow pattern in an axial plane.

Fundamental studies of rotating liquids also bear on the vortex tube problem. Many such investigations have been made by Binnie and his co-workers. Long also reports experimental and theoretical investigations of swirling flows, being primarily interested in meteorological applications. Gartshore has recently reviewed their work and has made detailed investigations of water flows in vortex tubes.

1.4. The Scope of the Present Investigation

At the time when this investigation was begun the results of detailed studies of the flow within vortex tubes were not available. Most of the available experimental data were concerned with performance and were not well adapted to study of the mechanism of the Ranque effect. As a result, attempts at analysis were based on quite arbitrary flow models.

It seemed that the time had come for a critical assessment of the various theoretical contributions in the light of a real knowledge of the situation within the vortex chamber. The same idea had occurred to other investigators several years before. Their results were published simultaneously with the completion of the apparatus for the present investigation. They supplied information of precisely the kind that the apparatus to be described in the next section had been designed to obtain. Nevertheless, numerous measurements have been made within the present vortex tube, a greater variety of flows being examined than in previous studies.

In order to gain further insight into the problem the original brass barrel was replaced by a Perspex tube and water was passed through the chamber. Although observation was confined to the liquid/air interface, it was possible to study a number of interesting phenomena.

The report of this experimental work begins with a

description of the apparatus utilized and moves on to describe the tests and the results obtained. Previous theoretical contributions are then discussed in the light of these data under two categories: qualitative theories of the Ranque effect, and mathematical models of vortex flows.

Finally, the analysis is advanced by deriving from Reynolds' equations approximate relations appropriate to flows with high swirl and by the study of a class of axi-symmetric solutions of the Navier-Stokes equations.

## 2. Basic Apparatus

In this section we describe the apparatus common to the several experimental investigations. Originally it was proposed to use the equipment solely to generate an air vortex. However, it proved capable of adaptation to the investigation of swirling water flows. The modifications are described in the section devoted to experiments with water.

The major components of the apparatus are shown in Figures 1, 2, and 3.

### 2.1. Mechanical Design

The chief loads to be resisted by the components and fittings are those due to internal pressurization during operation and the weight of the apparatus itself. To satisfy these strength requirements and to allow for the convenient introduction of instruments, it was decided to make the device primarily from metal. Brass was chosen for its corrosion-resistance.

The swirl chamber proper is a cylinder 3.05" in diameter (after polishing) and 48.0" long, formed from a tube with wall thickness of about $\frac{1}{4}$". The intake is a flat drum (some 12" by $1\frac{1}{4}$" externally) fitting around one end of the tube proper. It is composed of two side plates (thicknesses 3/16" and 1/8") containing between them a curved peripheral strip (thickness 1/8", depth 0.95"). This sturdy structure supports the end of the tube.

Eight tie-rods pass through the intake and provide the means of holding plates against the end of the tube proper passing through the intake. The tube is threaded and screws into a flange in the intake.

Support at the other end of the tube and means of fitting end plates there is provided by a second threaded flange.

2.2. Aerodynamic Design

The design of the flow passages was governed by two considerations: the desire to obtain as large a temperature drop as possible from a convenient pressure ratio (limited to 3:1 for convenient measurement using liquid columns while exhausting to atmosphere), and the desire to have set up within the tube a symmetrical flow, simplifying the experimental study and facilitating comparison with mathematical models. Fortunately, these two requirements were not contradictory. The design of the intake drum was also governed by the requirement of keeping it thin in order that it might not prevent access to the tube.

Early investigators utilized a single peripheral jet to set up a swirling flow, but later, more sophisticated investigations involved multiple-slot inlets with air flowing in form a plenum chamber. Another possibility is a large swirl chamber whose core forms one end of the tube proper. An attempt has been made to combine the advantages of the multiple-jet and swirl-chamber intakes to achieve high efficiency and symmetrical flow. Eight

slots have been cut tangentially through the tube wall. They are surrounded by a swirl chamber fed by a single duct.

McGee investigated the symmetry of flow resulting from the use of various numbers of symmetrically disposed inlet slots. He found that eight slots gave rise to a quite symmetrical flow, while lesser numbers might result in an easily discernable asymmetry. Westley's detailed tests involved a tube with eight inlet slots, perhaps as a result of McGee's work. An inlet very like that used by Westley was chosen so that his results might be used in other facets of the design. The experimental results of Westley and Dornbrand were used to choose the original sizes of the flow passages (inlet slots, outlet orifices) so that a maximum temperature drop might be attained for a pressure ratio of 2.5 to 1. The flow passage manufactured on this basis is as follows: the total area of the eight inlet slots is 1.36 square inches; the diameter of the intake end orifice is 1.25"; the diameter of the far end orifice plate is 1.35".

Several other end plates were utilized in the tests. They are described in Table I.

2.3. Fixed Instrumentation

Here we describe the sensing instruments that remained in position during all tests: those on the walls of the tube proper and those in the inlet line providing reference data.

Four symmetrically disposed taps allowed the pressure in an annular slot just outside the inlet slots to be measured. A thermometer was introduced into the inlet line just outside the intake. Thus the control data---inlet pressure and temperature---were determined. An orifice meter was also introduced in the inlet line: 48" downstream of a 135° bend, orifice diameter 1.100", line diameter 1.521".

Twenty-two stations down the length of the tube were chosen for fixed instrumentation and the introduction of probes. Their positions are shown in Table II. Entries plugged with screws were provided at the top and bottom at each section to allow traversing, as well as a pressure tap and another plugged entry intended for wall temperature measurement. The final polishing of the tube was done with all the plugs in place so that they might blend smoothly into the tube wall.

2.4. Traversing Arrangements

2.4.1. Entry to the Tube

Provision was made for probes with shank diameters up to 1/8". The entry holes along the top of the tube were designed to let hooked probes into the tube: the tapped portions have a diameter of 0.35" but do not pass right through the wall; the holes in the inner wall are 1/8" in diameter.

2.4.2. Lateral Traversing Gear

This mechanism is mounted on the tube itself. Its base is formed of two closely interlocking parts, each resting in one of two slots milled along the tube. When the halves are drawn together by a screw the base is clamped to the tube. The actual traversing mechanism is pivoted in the base thus provided. A vertical scale and drum scale indicate movements of the traversing head and a protractor measures probe rotations.

This gear is manufactured primarily from light alloy.

2.4.3. Longitudinal Traversing Gear

This rests on a platform supported by three screwed rods. It allows a probe to be traversed parallel to the axis of the vortex chamber anywhere within the bore of the tube. The platform and its supports are made of mild steel, cadmium-plated; the upper parts, of brass.

2.5. Installation and Control

The vortex tube was mounted on a table sufficiently long to allow the longitudinal traversing mechanism to be set up at either end. The air supply line rises vertically, then descends at $45^{\circ}$ to the intake. This configuration was adopted to give a reasonable length of straight pipe upstream of the orifice meter, and later proved useful in allowing the apparatus to be moved simply by rotating the whole about the upright portion of the supply line.

The vortex tube was connected to the high pressure air lines of the Department of Aeronautics. The reservoirs of this system are so large (2400 cubic feet at up to 1000 psi.) that very nearly constant supply conditions can be maintained without great difficulty. The chief problem is that of reducing the pressure from the high reservoir level to a few atmospheres at the intake of the vortex chamber.

The pressure control system consisted of a Hale-Hamilton RH-3DB controller in the line supplying the tube and a subsidiary Hale-Hamilton L-15 controller to set the dome pressure of the main valve. Various stop valves were located in the system, one being downstream of the main controller. During the tests the outlet pressure of the main controller was set at about 100 psig., the downstream stop valve being used to control the actual supply pressure to the vortex tube (generally about 30 psig.). This technique utilized a more satisfactory part of the controller's operating characteristic. By manipulating the stop valve occasionally during a run it was possible to keep the supply gauge pressure within about 1% of a mean.

## 3. Experiments with Air

After considering some preliminary tests chiefly concerned with probe design and calibration we shall turn to the main body of the tests, first the pressure measurements leading to a knowledge of dynamic effects within the tube, and then the temperature measurements giving insight into the energy flows.

It had been planned to make some measurements relating to the turbulent fluctuations within the vortex chamber. However, this project had to be dropped when it became apparent that the loud noise produced by the vortex tube was having an increasingly damaging physical effect.

### 3.1. Preliminary Tests

#### 3.1.1. Fixed Instrumentation

A number of early tests were made using only the fixed pressure taps. We consider them first.

Using a temporary flow meter the mass flow was found (with the two orifice plates fitted at the ends of the vortex tube) to be 32 pounds per minute for an inlet pressure of 40 inches of mercury. This information allowed the choice of a more suitable diameter for the orifice of the meter, that given in Section 2.3. The pressure drop across the tube fitted with the two orifice plates was found to be related to the mass flow, $q$ , by a law of form $\Delta p \propto q^k$ where $K = 1.7$ or $1.8$

Pressures were measured at tappings in various plates at the ends of the vortex chamber. By progressively

rotating the end plates the symmetry of the flow was checked. No deviation from symmetry could be detected. It was observed that the variation in end-plate pressures with inlet pressure was usually very nearly linear. This was later found to be true of pressures measured in the interior of the vortex chamber, both static and total.

The scatter of wall pressure measurements along the length of the tube indicated that some of the tappings gave erroneous readings, despite the care taken to ensure that they were flush with the tube wall. It had been hoped that detailed wall pressure measurements would indicate the location of reversal points within the tube. In fact, the wall pressures proved to be of little interest in the investigation. They did not tie in well with the static pressures measured using probes.

The pressures measured at the four intake pressure taps were found never to differ by more than 1/10" of mercury.

3.1.2. Pressure Probes

The two traversing mechanisms described previously were used to support probes during the following tests.

a) Longitudinal Traversing

It was discovered very early that longitudinal traversing was complicated by an unexpected aeroelastic phenomenon, seemingly a form of "whirling." Probes inserted longitudinally could adopt a stable whirling motion like that of a conical pendulum. If a probe were

inserted gradually into the tube filled with swirling gas the tip would suddenly move away from the axis and begin to spin with the rotating fluid. The probe could be returned to the stationary condition by slightly reducing the length exposed to the swirling gas. A loud singing was produced by probes while rotating. Several probes that had experienced the rotating mode repeatedly snapped off within the tube.

Tests were made on various probes, but it proved impossible to find one of practical size capable of extending more than a few inches into the tube, except at very low air speeds. For this reason, it was not possible to obtain reliable data by longitudinal traversing and attention was concentrated on lateral traversing.

b) Lateral Traversing

The early lateral traverses were made with hooked probes and consisted of determinations of swirl angle and of total and static pressure distributions across the tube. The tube configuration considered was that with both orifice plates fitted.

Traverses with a hooked Conrad type yawmeter (shank 1/8", sensing tubes 0.032") revealed an annular region of reversed flow within the tube. The use of this type of direction indicating device in the complex flow field was not at all straightforward as several null readings could be found on rotating the probe.

The degree to which conditions within the tube varied due to the insertion of a probe was investigated while total head surveys were being made using another hooked probe (shank 1/8", sensing tube 0.020" at the end). With inlet pressure held constant the wall pressure was measured as the probe was moved across the tube. Not only was the disturbance large (a total change during the traverse of about 8% of gauge pressure), but its variation across the chamber was far from linear. Correction is therefore difficult.

Measurements of static pressure were also made with a hooked probe (sensing tube 0.032"). The Mach number distribution was then computed using the two sets of pressure readings made with hooked probes. The lack of symmetry of the various profiles about the geometric centre-line attested to the disturbing effect of the probes.

A series of traverses were then made under the same conditions using a probe passing completely across the vortex chamber, a 1/16" diameter tube pierced by a single 0.010" hole. The way in which it was used will be explained in detail later. The total and static pressures and flow directions obtained agreed quite well with those determined using hooked probes, but the Mach number distribution was very different near the vortex core (a maximum of 0.44 for the straight-through probe data, 0.94 for the hooked probes). The most likely causes of this discrepancy are errors in locating the probes and differing position errors for the

for the two hooked probes. The significance of such errors is suggested by the high pressure gradients near the core. Under the conditions of the tests, pressure gradients as high as 240" of mercury per inch were measured, indicating a difference of 8 inches of mercury across a 0.032" sensing tube.

The straight-through probe was utilized for all further internal pressure measurements. By its use positioning errors are avoided. Also, conditions within the tube remain unaltered during any one traverse, although introducing the probe at different stations must still alter conditions during a series of traverses. However, a somewhat thinner probe can be used if supported at both ends. Finally, data is obtained more easily using a single probe for both total and static pressure measurements.

A probe passing through both walls does have the disadvantage that conditions near both walls are disturbed, not only by the presence of the tube, but also by the radial outflow around the probe. Hence, little attention was given to the flow very near the walls.

3.1.3. Thermocouple Probe

It had been hoped to obtain temperature profiles across the tube by butt welding two wires together to form a thermojunction and stretching the resulting transducer across the tube. The procedure has the advantages of introducing only small disturbances into the flow (since the wires can be made quite thin) and that the disturbance

which is introduced is like that of the cylindrical pressure probe. It did not prove possible to obtain dependable welds using the equipment available, so this plan was dropped.

a) Design of Probe

The probe consists of an 1/8" brass tube through which passes a stainless steel sheath containing the wires of the thermocouple imbedded in silica. The sheath and contents are available commercially. The thermocouple materials are chromel and alumel; the thermoelectric power for the range of interest (-20°C to 60°C) is about 0.0405 mV/C deg.

An Araldite probe tip extends some ¼" beyond the brass tube, the wires of the thermocouple being imbedded in it. The Araldite is formed into a shallow cone at the end (semi-apex angle about 60°), the actual junction forming the tip. This design utilizes the low conductivity of Araldite to reduce conduction errors.

b) Calibration of Probe

The probe was calibrated in the small supersonic wind tunnel of the Department of Aeronautics, the subsonic liner being fitted for the purpose. A fitting was manufactured to hold the probe in the working section; the probe projected some 1-3/4" into the test section. A long thermometer was introduced into the centre of the settling chamber to measure tunnel total temperature, the bulb being placed in a region of relative stagnation.

The relationship between total and recovery temperatures and Mach number is indicated in Figure 4a. The recovery temperature was got by assuming the thermoelectric power to be 0.0405 mV/C deg and the Mach number directly from settling chamber and working section pressures. The potentiometer used to measure thermoelectric emf's will be described later.

Air was bled slowly from the tube supporting the total temperature thermometer to reduce its lag. Nevertheless, total temperature lags seem to be the most likely causes of the systematic errors in the experimental results.

c) Interference of the Probe

The extent to which the introduction of the probe into the flow affects conditions within the tube can be judged from the results given in Figure 4b. Both curves were obtained by traversing at Station 6, but during the traverse represented by the upper curve a second probe (3/32" diameter) extended completely across the tube at Station 4. It will be noted that this additional disturbance raised the temperatures at Station 6 by about 7 C deg. But the shift was not constant across the bore; the central drop was flattened out to some extent by the disturbance. The lack of symmetry in the profiles is another indication of disturbance by the probe.

The profiles show that the required correction is far from linear; simple correction does not seem possible. We must content ourselves with noting that the introduction

of probes tends to raise the temperature level generally and that the apparent axis of the tube is shifted in the resultant profile. It should be noted that part of this shift will be due to the finite resolution of the sensing element and to conduction effects.

A check on conduction error was made by introducing a mercury thermometer along the tube centre-line to Station 21 (configuration as for Series V) and comparing its reading with simultaneous thermocouple measurements. The thermocouple recorded lower temperatures than did the thermometer (48°C vs. 52°C). Even allowing for the size of the thermometer (bulb diameter 1/10") and for possible misalignment, this suggests that the conduction errors are not more than a degree or so, even in the core.

### 3.2. Pressure and Mach Number Distributions

#### 3.2.1. Method of Obtaining Data

The 1/16" cylinder with an 0.010" sensing hole was used for all internal pressure measurements. The total pressure at a particular position was determined by rotating the cylindrical probe until a maximum pressure, $p_m$, was achieved for a protractor angle of $\theta_m$. The probe was then rotated to $\theta_m + 33^\circ$ and a pressure reading, $p_1$, made, then to $\theta_m - 33^\circ$ where the pressure, $p_2$, was again noted.

It will be appreciated that position errors introduced by this process will be relatively small. In order to allow approximately for the effects of viscosity and compressibility (both of which move the free-stream

recovery position further back) the angle of $33^\circ$ has here been assumed to correspond to the position at which the free-stream static pressure is regained, rather than the $30^\circ$ indicated by perfect fluid theory.

The total pressure was taken to be $p_m$ ; the static pressure was computed as $p = \frac{p_1 + p_2}{2}$. A correction of $\Delta\theta = -9.1 \frac{p_1 - p_2}{p_m - p}$ degrees was applied to $\theta_m$ to determine the flow angle more accurately. This correction was usually $3^\circ$ or less, although in the core larger corrections were often necessary. Its justification is as follows.

We assume that the pressure distribution on the surface of the cylindrical probe is given by

$$C_p = C_{pm}\left[2\cos\left(\frac{2}{1.1}\theta\right) - 1\right]$$

Then $C_p = 0$ for $\theta = 33^\circ$

$$\frac{dC_p}{d\theta} = -\frac{2\sqrt{3}}{1.1} C_{pm} \quad \text{for } 33^\circ.$$

The difference in angular setting for the two measurements near $33^\circ$ is given by $d\theta = -\frac{1.1}{2\sqrt{3}} \frac{dC_p}{C_{pm}}$ radians. The error in $\theta_m$ is then corrected by half of this quantity.

Static and total pressure distributions throughout the vortex chamber can be obtained by traversing at a number of sections, holding the overall pressure ratio nearly constant. For the earlier tests corrections were applied to measured pressures to refer all readings to a standard pressure ratio. But it was found that the inlet conditions could be controlled so precisely that, even allowing for day-to-day variations in atmospheric pressure, a series of tests could be made with essentially constant

pressure ratio. Also, great care in reducing data to standard conditions is not of especial value since the effects of introducing probes into the vortex chamber at different places are evidently very large compared to these small variations.

The Mach number distributions within the vortex tube were obtained from pressure readings using isentropic flow tables for ratio of specific heats of 7/5. The axial and swirl velocity distributions were then obtained (in the form of Mach number distributions) using the swirl angles.

The aerodynamic data were themselves used to determine the radial position of the sensing hole. Since the traversing cylinder passes right across the vortex chamber, the various distributions may be expected to be symmetrical about the centre-line of the chamber. The corrected flow angles were plotted and the axis of the vortex tube found as the point about which the results were symmetrical. As might be expected, variations of a few hundredths of an inch were found along the tube, corresponding to inaccuracies in machining the clamping slots.

3.2.2. Details of Tests

Lateral traverses were made for eight configurations of the vortex tube, as detailed in Table III. The first five series investigate the effect of simple orifice restrictions at the ends of the tube; the last three, the effects of altering the geometry of the throttling device.

In orifice plate (d) the outlet area is distributed near the periphery of the vortex chamber, while plates (c) and (e) were designed to approach uniform distribution of outlet area across the bore.

The possible extensions to these tests are, of course, very numerous. A good idea of the potential complexity of such tests can be gained by noting that the number of geometric variables to be specified in fixing a particular configuration for a vortex tube (inlet and outlet areas; length, bore and taper of vortex chamber; radial distribution parameters for outlet areas; etc.) is of the same order as the number of parameters to be specified in fixing the basic shape of an aeroplane (wing and tailplane aspect, thickness and taper ratios; fuselage fineness ratio; etc.).

It will be noticed that the tests were done for a pressure ratio of about 2.32, except for those configurations for which air consumption was especially high when the pressure ratio was near 2.00.

The justification for investigating each configuration at only one flow rate is that the flow patterns are thought to remain essentially unchanged as the pressure ratio is varied over a wide range, so long as it does not become too low. This view is supported by the detailed measurements in air made by Hartnett and Eckert and by Lay and by the previously mentioned linear correlation of pressures everywhere within the apparatus considered here.

At low speeds other, generally simpler, flow patterns

may be expected. Considerable attention has been given to transitions between various flow patterns in vortex tubes carrying water. Typically, the flow patterns increase in complexity with increasing flow rate, starting with unidirectional axial flow, developing a reversed flow along the axis, and finally exhibiting an annular reversed flow. These transitions appear to be confined to the low speed range.

Some of the more instructive data from the tests are presented in Figures 5 to 21. The scatter and repeatability of the results can be judged from the plotted points. Many of the curves are based on two sets of readings since measurements were taken across the whole tube.

3.2.3. Interpretation of Results

In this section some of the more obvious implications of the experimental data are pointed out.

It is possible to interpret the measured data to give information about a number of points which cannot easily be investigated directly---the nature of radial flows, the sort of flow occurring near the ends of the tube. The policy adopted is to accept the measured data as representing the essential features of the undisturbed flow within the vortex chamber; that is, we assume that the effects of probe disturbance are qualitatively negligible. It should be noted that violent turbulent mixing is superposed on the mean motions to which the instruments used here are sensitive. The details of the turbulence can be neglected

in a simple discussion of flow mechanics, although it must be borne in mind that associated shearing forces can significantly affect the mean motion.

Series I. (Figures 5, 6, 7)

The most striking feature of the swirl distribution is that the same radial profile exists through most of the tube---from somewhere between Stations 2 and 8 to the far end. (The known profiles that have not been given are very like that at Station 21.)

A simple annular reversed flow exists the length of the tube, save very near the hot end orifice, where a small central reversal is also indicated. The air forming the reversal is drawn from that moving down the walls, the reversed flow being continually augmented as it moves up the tube. It seems unlikely that the main reversal contains any airflow from outside the tube as its area diminishes rapidly towards the end of the tube at which the orifice is fitted. Comparison of volume flows suggests that the core flow is drawn wholely from the annulus of reversal. The flow in the core remains fairly constant for much of the length of the tube.

The pressure distribution shows the gradients associated with these axial flows; the pressure commonly falls in the direction of local axial motion. The surfaces of constant pressure are nearly cylindrical in the core region.

Series II. (Figures 8, 9, 10)

Here the annular reversed flow is much more vigorous,

while the core flow is weaker; presumably the annular flow escapes at the cold end. The core flow seems to be constant the length of the tube, while the annular flow increases as it moves up the tube towards the inlet end orifice.

The narrower core is associated with steeper swirl gradients than those of Series I. Somewhat greater variations in swirl distribution are to be noted here. The "hump" in the distribution in the region of reversed flow indicates a radial inflow feeding the reversal. Once again the central surfaces of constant pressure are very nearly cylindrical.

For this configuration the flow external to the tube was investigated by observing the deflections of small objects. This study was made difficult by the high velocities of the flows from the tube, but the following points were noted. At the hot end only outflow was found (despite the small reversal indicated by the profiles within the tube), but at the cold end a core of inflow seemed to extend about 5" outwards from the orifice. Both the jets diverged with about $35^{\circ}$ semi-angle.

Series III. (Figure 11)

The inflow through the orifice does not seem to be induced by mixing effects but instead by the low core pressures within the vortex chamber. Angular momentum is not transferred into the core rapidly, perhaps because the air there is not initially turbulent. A large loss in angular momentum is indicated by the swirl distributions

(especially when density changes are considered too).

Series IV. (Figures 12, 13)

Here, seemingly, an eddy loop occupies the core near the inlet end. The swirl distributions indicate that the reversed flow is moving outwards as it penetrates into the tube; the main flow down the tube is, of course, expanding inwards as the pressure falls. The flow in the core can be thought of as two impinging jets.

Series V. (Figures 14, 15)

Here the flow down the tube away from the inlets gradually feeds into the reverse flow in the core. However, a considerable amount of the inflow does seem to turn back right at the solid end plate. Again an orifice eddy is indicated.

Series VI. (Figures 16, 17)

The situation near the inlet-end orifice is very like that of the previous series. However, the complex blockage at the far end has modified the situation there. It seems likely that the strong reverse flow in the core is formed by air entering through the central hole. The two outer rings of holes both carry outflow, while the action of the innermost ring is doubtful. The idea that the air near the axis is newly entered is re-inforced by noting the not-very-steep swirl gradient there. That the outer reversal is not fed from outside is indicated by the swirl distribution near the far end.

Series VII. (Figures 18, 19)

Here the flow pattern is intermediate between those of the twp previous series. The annular eddy loop noted in Series VI seems not then to be the result of the inner ring of holes.

Series VIII. (Figures 20, 21)

Again there is a strong inflow through the central holes.

3.3. Discussion of Flow Mechanics

The following features are found in most of the situations investigated:

a) The pressure at the walls is higher than atmospheric and that in the core, lower.

b) The pressure drops off rapidly down the tube near the walls but remains nearly constant in the core.

c) The air entering the tube has little immediate tendency to move inwards (and out the inlet-end orifice, if present) but invariably spirals down the tube along the walls.

d) The radius of maximum swirl moves further in at successive stations down the tube.

e) The core is occupied by a complex flow system involving flows up and down the tube.

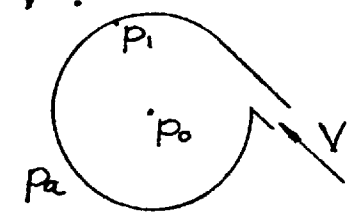
Certain dissimilarities may also be noted:

f) In some situations there appear to be large losses in angular momentum at successive stations down the tube (III, IV), while in others it remains constant (I).

An attempt will now be made to justify these general observations; that is, to sort out the chicken/egg type problem posed by the inter-related pressure and velocity fields. As before, we assume that the measured data do represent the undisturbed flow reasonably well.

At first sight the idea that sub-atmospheric pressures can exist within a device supplied with air at high pressure and exhausting to the atmosphere seems contradictory to elementary notions of fluid motion. But this situation can be rationalized by the following crude analysis.

We assume that the velocity field within the vortex can be characterized by a single velocity, $V$.




Then $p_1 - p_a \propto V^k$

where $p_1$ is the inlet or wall pressure,

$p_a$ is the atmospheric pressure,

so that $p_1 - p_a$ is the pressure drop from inlet to atmosphere. From our test data we find that $K$ is about 1.8

Further $$p_1 - p_o \propto \int_o^{wall} \frac{V^2}{r} dr \propto V^2$$

gives the pressure difference between wall and core (where the pressure is $p_o$). Hence,

$$p_a - p_o = K_2 V^2 - K_1 V^k$$

where $K_1$ and $K_2$ are positive constants. For $V$ sufficiently high, $p_a - p_o > 0$ for $K < 2$.

This analysis is based on the plausible ideas that the absolute level of the interior pressures is set by the ambient pressure, but that the pressure differentials

through the system are fixed solely by the velocity distribution. The model, although itself empirically based and thus offering essentially a correlation of different bits of test data, does indicate the necessity of sub-atmospheric core pressures unless the two pressure differences are related in a rather special way.

Having dealt briefly with the radial pressure distribution, we turn to the axial variation. There are several indications of large shearing forces acting near the walls of the tube: large wall pressure drops down the tube without significant axial acceleration, certain swirl velocity profiles indicating large losses in angular momentum down the tube, and the inwards movement of fluid after passing down the tube. (Unless some significant change occurs in the fluid there seems to be no reason for it to move inwards there rather than immediately after entering the tube. However, some inwards movement is produced by expansion as the pressure drops.)

Several configurations (particularly Series I and II) show little variation in angular momentum down the tube. Yet large wall pressure drops occur axially, indicating significant shear at the wall. The resolution of this apparent contradiction lies in the several reversals in the axial flow direction which occur across the tube. The strong axial flows average out the effects of frictional torques. Fluid which has traversed the length of the tube several times is to be found at the same section as fluid

which has just entered. It seems likely that Series III, lacking such axial mixing completely, gives the truest picture of the effects of shearing forces. On this view, the identical swirl profiles at successive stations observed in Series I and II are reckoned to have been set up by a happy coincidence, rather than by some fundamental mechanism.

The near constancy of pressure along the core is at first puzzling. Perhaps the most useful parallel to call to mind is that of the air cores formed in vortex tubes carrying water.

The depression of a free surface normal to a vortex is easily understood in terms of gravity and centripetal forces, and the air core can be thought of as a more spectacular form of this sort of phenomenon. In a case where the vortex fluid and the ambient fluid are the same, the idea of an air core seems inappropriate. But if the pressures along the axis are low, and the radial gradients in the core high, the density distribution in the air flow is not very unlike that in water. Further, the existence of nearly cylindrical surfaces of constant pressure is dependent merely upon high radial pressure gradients.

Thus the air core in water is an indicator of a general phenomenon rather than its cause. The concept of the core as a region filled with low density fluid which does not take a direct part in the main flow justifies the constancy of pressure along the axis.

The only striking features of the flows investigated

that have not yet been touched on are the complex core flows. These are determined by the simultaneous tendencies for air to escape and to enter at the ends of the tube, caused by the existence of both super- and sub-atmospheric pressures in the interior, and by the tendency for relatively slow-moving eddies to form in regions of the core not involved in the main motions.

It will clarify this complex situation if we introduce terminology to distinguish among the several different phenomena occurring here. We shall attempt to distinguish between eddies, induced flows, and main reversal flows. Turbulent mixing is, of course, superposed on these mean streamline patterns.

The complex core flows found in the inlet end in Series IV and in the far end of the tube in Series VII are termed eddies as they appear to involve merely the recirculation of fluid. The localized central flows encountered several times near orifices are also of this type.

The strong inflows produced by low core pressures will be termed induced flows. Such flows are to be found in Series III and IV and, accompanied by eddies, in Series VII and VIII.

Finally, we distinguish a main flow reversal as part of the main flow through the vortex chamber to the atmosphere. This situation is to be found pre-eminently in Series V and also in VII.

The three categories of flows have been introduced in

the order of their typical intensities. The divisions are not clear-cut; the core flows of Series I and II provide obvious difficulties of classification.

The real complexity of the core flows comes from the interactions of the various types of flow. Series IV and VII provide examples of interaction of eddies and induced flows, while Series VI shows interaction between all three.

### 3.4. Temperature Distributions

#### 3.4.1. Method of Obtaining Data

The thermocouple probe described previously was used in all tests, the thermoelectric emf being measured using a Cambridge Workshop Potentiometer. This combination of instruments allows readings to be made easily with a precision of 1/20 C deg.

The potentiometer and a polarity reversing switch forming the effective cold junction were enclosed in a large cardboard box to maintain them at a fairly even temperature. The box was open at the top, but the instruments were covered with a transparent film to isolate them from draughts. The cold junction temperature was measured by a thermometer under this film; it seldom varied $\frac{1}{2}$ C deg during a half-hour run.

Whenever a potentiometer reading $e$ was made the corresponding inlet pressure, inlet temperature, cold junction temperature, $T_c$, and ambient temperature, $T_a$, were noted. Since the inlet temperature varied more rapidly than the other quantities, it was noted before and

after the other readings, the two readings being averaged to estimate the effective inlet temperature, $T_i$ .

The difference between recovery temperature and inlet temperature is representative of the energy distribution within the tube for reasonably small variations in $T_i$ . This quantity can be computed directly from the measured data: $T_r - T_i = T_c + e/p - T_i$

The thermoelectric power $P$ was taken to be 0.0405 mV/C deg.

The total and static temperatures ( $T_o$ and $T$ ) can be estimated if the local Mach number is known:

$$T_o - T_i = (T_r - T_i) + T_r'\left(\frac{T_o'}{T_r'} - 1\right)$$

$$T - T_i = (T_o - T_i) - T_r'\left(1 - \frac{T'}{T_o'}\right)\frac{T_o'}{T_r'}$$

where the primes indicate absolute temperatures. $T_o'/T_r'$ is determined as a function of Mach number by the calibration curve of Figure 4a; $T'/T_o'$ was obtained from isentropic flow tables ( $\gamma = 7/5$).

3.4.2. Details of Tests

Lateral traverses were made for tube configurations corresponding to four of the pressure test series: II, III, IV and V. Series II is the configuration originally designed for maximum temperature drop; the others are investigated because of the relative simplicity of their flow patterns.

Details of the tests are found in Table IV. Traverses were usually made from the wall outwards. The ambient

temperature fell steadily throughout each run. The inlet temperature commonly fell during the early part of a run, remaining fairly constant through the second half.

It will be noted that temperature traverses were made, for the most part, at stations where pressure measurements had been made and that an attempt has been made to reproduce the conditions of the pressure tests by maintaining the same inlet pressures. The varying disturbance of the thermocouple probe will, of course, frustrate this attempt.

The data from these tests are presented in Figures 22 to 25, plotted against the distance from the wall of the tube. The relationship between scale reading and probe position was obtained by direct measurement at Station 1. An error of 0.01" or 0.02" (depending on the station) will be introduced into this co-ordinate by manufacturing imperfections; a systematic error of perhaps 0.02" will be introduced by the finite size of the thermojunction. An attempt has been made to correct for the latter error. The readings made very near to the wall and in the core are subject to large conduction errors due to the large temperature gradients there.

The interference effects of the probe (and perhaps conduction errors) are indicated by the deviation of the position of minimum temperature from the centre-line of the vortex chamber. This deviation makes the estimation of local Mach number very doubtful, as it is difficult to correlate the various distributions. However, the static

and total distributions have been calculated for a few cases; they are shown in Figure 26. Little information is added to that available in the recovery temperature plots.

3.4.3. Interpretation of Results

For want of a better policy, we shall once again interpret the measured data as representing, in the main, the situation within the vortex chamber at some instant, neglecting the admittedly large probe disturbance.

Series II. (Figure 22)

The temperature differences across the vortex are much larger for this series than for the others investigated. (Note that several scales are used in plotting the temperature data.) The mean temperature across a section rises progressively down the tube, being somewhat lower than the inlet value at the cold end and somewhat above inlet at the hot.

Series III. (Figure 23)

Here the average temperature across a section remains fairly constant down the tube. The high temperatures in the core near the inlet are due to inflow there of warmer atmospheric air. ($T_a - T_i \simeq 13$ C deg for these tests.) The speed with which temperature differences are smoothed out is remarkable. By Station 1 (3" from inlet) a drop of some 6 C deg has already been effected at the axis; the next 3" (From Station 1 to 3) bring a drop of another 4 or 5 C deg. A very rapid redistribution of energy occurs

in the flow near the wall. Comparison of the Station 1 and Station 3 profiles suggests that the thermal energy transferred from the core is very rapidly distributed throughout the surrounding annular region.

Although the temperature differences for this configuration are not large, they are of special interest as they occur in a simple flow in which all the fluid moves down the tube at about the same speed. Axial convection effects need not be taken into account.

Series IV. (Figure 24)

In this case the temperatures through most of the vortex tube are below the inlet level. An eddying mass of cold gas fills the inlet end of the tube. The low temperatures in the inflowing core at the far end suggest that this inflow is made up of gas which has just left the tube; that is, that another eddy extends out of the far end of the tube.

Series V. (Figure 25)

The whole of the air in the tube is above the inlet temperature level. There are several places in the tube where the recovery temperature does not increase monotonically outwards as it invariably has in the other configurations. The reduction in temperature near the wall at Station 21 is probably a result of probe conduction errors and the temperature drop through a boundary layer to a cooled wall. Although no attempt has been made to study the flow near

the wall, a boundary layer is apparent in the corresponding velocity profiles. The inversion in the core near the inlet is not understood. It might be partially due to an interference effect; Figure 4b gives some support for this view.

3.5. Discussion of Energy Flows

The temperature distributions just considered indicate three salient features of the thermodynamics of vortex tube flows:

a) The temperature almost invariably increases monotonically outwards along a radius.

b) Very rapid radial energy transfers are possible.

c) It is possible to maintain all or part of the air in the vortex chamber above (or below) the inlet and ambient temperatures.

The omnipresence of outwards temperature increases in the variety of flows considered (with and without reversed flows, with core and annular reversals, with one or several outlets) suggests that the temperature distribution is related to the radial pressure distribution, as this appears, at this stage in the investigation, to be the only similarly monotonic distribution associated with all the flows. Further, some operation of turbulence is surely necessary to effect the rapid radial transfers noted here.

The most widely accepted hypothesis for the energy separation does, in fact, relate the temperature and

pressure distributions through the mechanism of turbulent mixing. The motion of lumps between radial layers is conceived as being adiabatic; work is done on those moving outwards by compressing them; work is done by those moving inwards on expanding. The mixing of lumps with their new environments tends to shift the static temperature distribution towards that defined by an adiabatic law applied to the static pressure distribution.

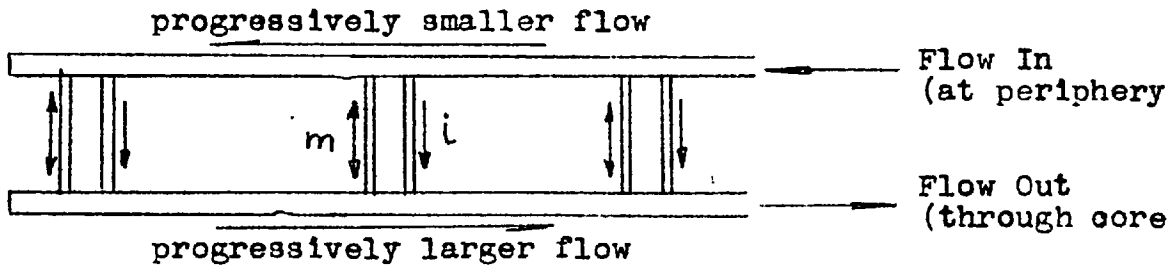
This mechanism seems capable of explaining the energy separations studied here. We note that the larger temperature gradients do correspond to the larger pressure gradients and that the radial temperature gradient in no case exceeds that predicted by the adiabatic law. (Actually, the temperature gradient does exceed this limit near the wall in the far end of the tube for Series II. But the steeper pressure gradients in the inlet end could have given rise to this gradient.)

However, a systematic analysis of the energy fluxes in vortical flows indicates considerably more complex relationships between energy transfer and the dynamical aspects of the flow. It seems that work fluxes may play as large a part as the pressure gradient effect discussed above in achieving energy separation. The main work flux is generally opposed in direction to the radial mass flow and is thus commonly outwards in vortex tube flows in which fluid is injected at the periphery.

Although the radial temperature gradients are always less than those predicted by the adiabatic law, there are temperature differences between different parts of the device which exceed those calculated from the overall pressure ratio using the adiabatic law. We can show that this is not inimical to the suggested mechanism and at the same time explain how large parts of the device can be maintained above or below inlet temperature.

To do this we visualize the processes within the tube in terms of analagous hydraulic systems. As an example we examine a simple exchange mechanism representing the essential features of the configuration of Series V: two main tubes carrying the peripheral inflow and the core outflow and connected by a number of subsidiary tubes.

Mass flow pattern:

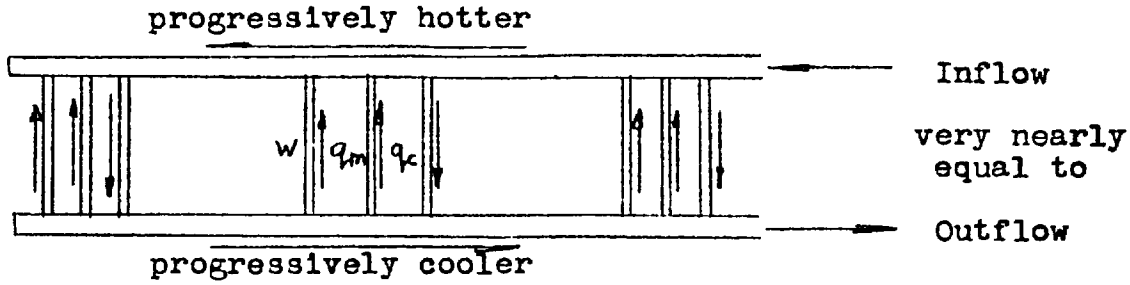



where $i_{in}$ is inwards flow from periphery to core,

$m_{ix}$ is interchange between core and periphery, followed by mixing.

We shall assume that a pressure difference is maintained between the tubes to complete the analogy.

Energy flow pattern:




where $q_c$ is the energy convected inwards by $i$ ,

$w$ is outwards work flux,

$q_m$ is the outwards flux of energy due to the mixing interchange, $m$ . The temperature gradients produced by these fluxes are shown.

Since the mass outflow is from the coolest part of the tube the temperature of the gas leaving will be somewhat lower than the average over the whole tube. But, since conduction effects will be small, the exit temperature can be only a little lower than inlet temperature. Thus we see that the gas throughout most of the tube will be at a temperature above the inlet value (and, coincidentally, the ambient temperature).

At first sight it may appear that conduction is an important factor in setting the temperature level within the tube. But this is probably not the case. As the tube temperature rises upon starting, the outlet level will rise with it, until the inlet value is reached. Thenceforth, the only energy left behind in the tube by the steady throughput is that required to restore the small conduction losses.

That a stable equilibrium is thus set up is shown by the following considerations. If the temperature level were to rise beyond the postulated equilibrium, the outlet temperature must rise too, thus reducing the net energy within the tube and restoring the system to its former condition.

Mass and energy flow models similar to these for Series V can be constructed to justify the sustained temperature levels of the other test series.

3.6. Comparison with Other Test Data

Two investigations of the internal flow of vortex tubes can be compared directly with this: those of Lay and of Hartnett and Eckert. The former used a 2" diameter tube, the others a 3" tube; both investigations were made with pressure ratios which bracketed those used here. In both cases the inlets were very like those of the present apparatus.

These investigators studied the flow within the tube with the inlet-end completely blocked and the far end throttled using a cone valve which moved axially; the air escaped around the periphery of the tube. The results are then most nearly comparable to those of the present Series VII (near the far end) and I and IV (near the inlet end). They show that, as might be expected for configurations in which only small inflows into the core are likely, the velocity attains a maximum value at a position nearer the tube wall than for any of the present series of tests,

excepting Series III. The rises in pressure and temperature from the core are also less abrupt than in most of the configurations studied here.

None of the investigators felt confident enough in his results in the core region to present them. In both cases the core readings are referred to as "erratic," perhaps implying unsteadiness in the pressure readings. Presumably the damping in the pressure measuring system of the present investigation was sufficiently high to obviate this difficulty.

Finally: their results tie in well with those reported here, as do the less detailed data (for a 1" tube) given by Scheller and Brown and by Vulis and Ustimenko for a large (38 cm diameter) cyclone furnace model.

### 3.7. Conclusions

It is possible to rationalize most of the dynamical features of the vortex flows investigated in terms of mass and momentum conservation. Even the strikingly diverse and complex core flows can be justified in general terms by distinguishing between several classes.

The temperature measurements show that there is a flux of energy from the core of the vortex into the peripheral region. The temperature fields can be explained in terms of the mass flows within the vortex chamber and an additional radial energy flux for which turbulence is the efficient mechanism.

## 4. Experiments with Water

Water tests were made with a vortex tube exactly similar to that used in the air tests with the hope of gaining further insight into the complex vortex flows by direct observation of the rotating fluid. Only the gross features of the flows were investigated, the chief method of study being observation of the water surface. Despite this limitation it was possible to find much of interest in the flows considered. Of particular interest were a variety of transitions between supercritical ("shooting") and subcritical ("streaming") flow. Measurements were not made within the vortex chamber since they would have been very time-consuming and since similar data can be more easily obtained from air tests. The flow speeds were usually too high to allow visualization using dye injection.

### 4.1. Apparatus and Installation

The modifications to the basic apparatus were simple: a Perspex vortex chamber replaced the original brass one, brass flanges fixed to the new tube by annular key rings filled with Araldite permitting it to be fitted to the original intake and supports. The new tube had the same interior dimensions as the old and was supplied by identical inlet slots.

The tests were carried out in the Hydrodynamics Laboratory of the Department of Aeronautics. Water leaving

the tube was allowed to fall directly into the sump of this laboratory. Two tube positions were considered: vertical (entry at top) and horizontal. The table on which the original apparatus had been mounted was simply stood on end and laid on its side to support the tube. Water from the high pressure supply (up to sixty feet of head) was carried through flexible tubing to the length of copper tubing which formerly rose at $45^{\circ}$ from the intake. Thus the orifice meter remained in position and provided a means of specifying the operating condition of the apparatus.

The plates used at the end of the tube distant from the inlets in the experiments on air were used once again. Perspex plates were made for the inlet end. The various blockages are detailed in Table II.

### 4.2. Tube Vertical

In these tests the water entered through the inlet slots near the top of the tube and flowed out through various throttling devices at the bottom. For convenience, water was prevented from emerging at the top of the tube by fixing the solid plate there during the high flow rate tests.

#### 4.2.1. Far End Unrestricted

When the tube was completely unblocked at the bottom the fluid ran smoothly down the walls as a thin film. Direct observation of the thickness of the film was not

possible due to the optical distortion of the curved walls of the tube. But the thickness at the top could be seen to be about 1/4" (the width of the inlet slots) through the end plate. There were striations on the surface which seemed to indicate the flow direction, as well as could be told by observing the wake behind a wire breaking the surface. They grew progressively steeper down the tube. Presumably this steepening is primarily due to a vertical acceleration produced by gravity, but loss of angular momentum to friction will also contribute to it.

4.2.2. Five Hole End Plate

We now consider the opposite extreme to the case just dealt with---the case of almost complete blockage at the bottom, produced by fitting one blockage plate on top of another.

As might be expected, a pool of almost stagnant water formed at the bottom of the tube. The appearance of the region above the pool was exactly as for the completely unblocked condition---flow adhering smoothly to the walls, accelerating vertically. This inlet flow slid smoothly into the pool producing little disturbance. As the flow rate increased the pool deepened until it finally filled the whole tube. At the higher flow rates a slight dimpling of the surface of the elongated pool was observed.

The height of the pool surface from the orifice was measured at the wall for various flow rates up to that at which the tube filled completely. The heights are plotted

in Figure 27 against pressure drop across the orifice meter, together with similar data for other blockages. For this case the heights fall very nearly on a straight line except for the highest flow rates, for which the pool depth increases more rapidly. The nearly linear form is to be expected as the plot simply relates the pressure drops across two blockages through which the same mass flow passes. The deviation from linearity at the upper end corresponds to the depression of the surface noted for high swirl. The head acting across the holes at the bottom is thus reduced below the value measured at the wall.

4.2.3. Single Orifice Plate

The cases intermediate to the unblocked and highly blocked produced more complex results. We shall consider the central outlet orifice first.

Once again a "pool" formed at the bottom of the tube, but in this case the air above was connected to the atmosphere through the bottom orifice: an air core was formed for all but the lowest flow rates when a disordered splashing region was found at the bottom. The diameter of the core at the orifice did not vary greatly as the tube filled, remaining throughout about one-half the orifice diameter. The core tapered upwards, having a bell-shape at the top.

Figure 28 shows the air core for several flow rates. The water-film striations previously referred to are visible. It should be noted that the image of the core

is magnified by the cylindrical tube. The surface of the air core was smooth under most conditions, especially in the lower parts. However, stationary circular deformations were observed near the top.

The transition between the "water film" and "air core" was effected smoothly near the top of the tube. An abrupt change in flow direction (as indicated by surface striations) was noted at this transition. Once again, the flow above the jump was identical to that of the no-constriction case. A surface disturbance there was accompanied by the development of helical grooves in the air core surface below the transition.

When the transition took place lower in the tube it was accompanied by considerable foaming. It seems likely that this air entrainment is the result of higher kinetic energy in fluid approaching the jump lower in the tube. However, the core formed smoothly beneath this disordered region. Disturbances were propagated through the foaming region and showed themselves on the air core, just as for the case of smooth transition.

For high enough flow rates the air core extended right to the top of the tube, ending on the plate there. By increasing the inlet pressure it was possible to decrease the taper of the core until it became as nearly as could be seen parallel, with diameter about 1/2". Further increases in throughput reduced the diameter slightly

(to, say, 3/8"). The core was intermittent at the top for this condition and wavered slightly on the end plate.

It should be noted that estimates of the core diameter are likely to be inaccurate as it was necessary to allow for the magnifying effect of the cylindrical tube. Where possible, measurements were made directly through a transparent end plate.

4.2.4. Twenty-one Hole Plate

The behaviour of the fluid for this blockage differed only in detail from that observed for the single-hole plate. The air core passed through the central hole, having a diameter about one-half that of the hole; this influenced the diameter of the core throughout its length. The region of air entrainment was more extensive in this case and the thinner air core more disturbed beneath it. Figure 29 shows three views of the core for this configuration. Note the circular disturbance at the top in (c), the striations and foaming in (a).

The tube filled completely at a somewhat lower flow rate, as might be expected for the smaller, dispersed outlet area. As the flow rate was increased the core narrowed at the top, at first remaining of constant diameter at the bottom (1/8"), then widening slightly. Under some conditions the core was intermittent at the bottom or top, or moved about on the upper plate. The taper never quite disappeared in the range of inlet pressure considered.

Blocking the central hole with a finger caused the core to move to another. This effect is discussed at some length by Bouasse.

4.2.5. Sixteen Hole Plate

The situation for the sixteen hole end plate was quite different from the cases just considered, where the end plate possessed a central hole. As for the previous cases the smooth water film ended in an abrupt transition. But here an air core tapering to the bottom of the tube was not formed. When transition occurred near the top of the tube a relatively short (8" maximum) hollow was formed, below which the tube was completely filled save for a rapidly wavering trail of tiny bubbles on the centre-line. When the jump occurred lower in the tube the depression (if any) was lost in the foaming region.

For this case in which free interchange of air between the tube interior and the atmosphere is impossible through the bottom, the history will obviously be quite different depending on whether the top is sealed or not. The situation described above relates to the case in which air could enter or leave freely at the top.

Two views of the phenomena described are shown in Figure 30.

4.2.6. Sixty Hole Plate

Performance was similar to that described for the twenty-one hole plate. An air core extended up from

the central orifice, its diameter being about one-half that of the hole. Higher flow rates were achieved through the larger exit area provided here.

4.2.7. General

The transition between the "water film" and "air core" type flows is a form of hydraulic jump. This sort of transition can be described in physical terms as a change from shooting to streaming flow, or in mathematical terms as a change from supercritical flow in a hyperbolic regime to subcritical flow in an elliptic regime. This interpretation is supported by the observed inability of surface disturbances to propagate upstream in the water-film regime. A continuous transition from subcritical to supercritical flow presumably takes place in the inlet nozzles.

An interesting dynamic distinction can be made between the supercritical and subcritical flows by comparing their very different responses to gravity. The former merely accelerates vertically, the swirl component playing no part in the response; while for the latter regime a complex interaction between gravity and the dynamic effects associated with rotation takes place, the most obvious consequence of which is the tapering air core. For the subcritical regime, very large swirl completely dominates gravitational forces.

Although the tests described here were performed by going from one equilibrium stage to another, it seemed on starting the flow quickly that essentially similar stages

were passed through as the tube filled with water and the flow moved towards an equilibrium.

The jump here is analagous to the normal shock (or equivalent system) in a supersonic duct; the shock can also be moved by altering downstream conditions or flow rate. The phenomenon is also analagous to an oblique shock: the axial momentum changes abruptly at the transition while the angular momentum apparently remains constant.

But the detailed analysis for this case is likely to prove more difficult than the extension from normal to oblique shock in a compressible fluid. The conservation of angular rather than linear momentum makes it impossible to use the simplifying artifice of referring the motion to a set of axes which eliminate the velocity component along the discontinuity---except, of course, in the trivial case of a very thin water film. The complex flow downstream will also introduce difficulties.

The concept of the jump and the ideas of supercritical and subcritical flow associated with it are useful in forming a causal interpretation of the effect of blockage on swirling flows. Here we see the effect of the blockage extending upstream as the flow rate increases. And the extension upstream is simply a swirl-modified form of the almost stagnant pool which formed at low flow rates. We can see that the effect of swirl is to extend the influence farther upstream, at least in the case of central orifices.

Measurements were made for the configurations just

discussed relating the position of the jump in the tube to the pressure drop across the orifice meter in the inlet line. The data are presented in Figure 27. When considerable air entrainment took place it was not possible to say just where the jump occurred. Hence, for each configuration the transitions are represented by two curves, the upper showing the position of the fairly abrupt entry into the foaming region, the lower, and estimate of its lower boundary.

It is remarkable that the curves characterizing the first four blockages all tend for high flow rates to straight lines of very nearly the same slope. It seems implausible to ascribe this wholly to chance.

One feature of the air core (also noted on the surface of the truncated depression formed for the sixteen hole plate) was a horizontal band which appeared white against the rest of the core. Close examination showed that many tiny bubbles circulating around the core gave the region its characteristic appearance. Small changes in the slope of the core also marked the region. The bubbles appeared to move in nearly horizontal paths, while the flow further down and further up the core seemed to be descending. It seems plausible that this band marked the end of an annular region in which the flow is upwards.

4.3. Tube Horizontal---the Jump

For the cases to be considered in this section the flow was the same whether the solid or orifice plate was introduced at the inlet end. Only for very low flow rates did any water emerge through the orifice plate near the inlets. For higher flows the water adhered to the walls near the entry and swirled away down the tube. To obtain sufficiently small blockages at the far end of the tube, the plates used previously were held about half-an-inch away from the end of the tube by four pillars of nuts and washers.

4.3.1. Tube Unblocked at Far End

Once again a jump phenomenon was observed, this time moving along and out of the tube as the flow rate was increased. The change in velocity did not seem to be as abrupt in this case but was extended over one or two diameters. When the transition region was ejected from the tube at sufficiently high flow rates, the jet formed at the end adopted a more orderly and symmetrical aspect. The final movement out of the tube (more than a foot) took place for a very slight change in inlet conditions. The jump is shown in several positions in the tube in Figure 31.

Prior to the jump the surface of the film was fairly smooth, although marked by striations. The thickness (1/2" to 3/4") seemed to increase for the first foot or so after the inlet, then remain

essentially constant until the jump was encountered. No variation of thickness with flow rate could be discerned.

As can be seen in the photographs, the air-water interface downstream of the jump was disordered. For low flow rates the flow in this region separated from the upper side of the tube and flowed out along the bottom.

Judging from the striations, the flow angle changed along the tube. Just after the jump had moved out of the tube the following striation angles were noted: $30^{\circ}$ near the inlet, $45^{\circ}$ in the middle of the tube, $60^{\circ}$ at the far end. Increasing the flow rate further produced maximum and minimum angles of $45^{\circ}$ and $25^{\circ}$. The acceleration which seems to be indicated by these angles is not incompatible with the constant-thickness film observed as thickening of the boundary layer against the wall could compensate for surface acceleration.

4.3.2. Sixty Hole Plate, held away from End

The movements of the transition were similar to those described above, but a slightly higher flow rate was required to maintain the jump at any particular position. The jump moved completely from the tube at high flow rates. Once again the final movement occurred suddenly, upon a very slight increase in flow rate. The flow angles given by the striations were as above. The appearance of the water film was the same.

4.3.3. Twenty-one Hole Plate, held away from End

Here an even higher flow rate was necessary for each jump position. The jump stabilized in one position near the end of the tube but finally moved out for sufficient increase in flow rate. A hysteresis was noted near the end of the tube; having once moved out, the jump did not return so far up the tube.

4.3.4. Solid Plate, held away from End

In this case a considerably greater flow was needed to put the jump at any place. The jump never moved fully out of the tube. A short disturbed region remained even at high flow rates. The appearance of the film was as in the other cases: thickening for the first 6", then of constant width, finally (18" or 2' from the end) thickening again; striations as usual.

The disturbed region which remained in the tube is probably a bore resulting from the impingement of the flow on the solid end plate. Whether the reduced outlet area could of itself have caused this bore, or whether the unperforated end plate is responsible, is not known. Tests were made to see whether the transitions upstream were simply extensions of this bore phenomenon. On rapid starting, the transition moved steadily down the tube (inlet to far end) and took up its equilibrium position. It was not sent out from the end plate. There was indeed a reflection from the end plate on starting in the form of weak surface waves; these passed through the jump and

moved upstream to the inlet.

4.3.5. General

It seems likely that the transition described here is the result of the combined effects of wall friction and the upstream blockage and that it is analogous to the standing shocks found in duct flows of a compressible fluid. The fact that the surface wave generated on rapid starting passed through the interface and travelled on through the supposedly supercritical region upstream is not inconsistent with this interpretation. It merely indicates that the axial component of the upstream velocity was subcritical. In this case there seems to be no necessity for the normal component of the upstream velocity to exceed the wave speed.

Since the effect of the downstream blockage is not due to the upstream propagation of surface waves (even though this is possible), it seems that it must be due to a pressure gradient in the body of the water. This pressure gradient, combined with the wall friction, produces the jump. Thus, the greater the constriction, the greater the effect on the point of transition. The mechanism of pressure propagation upstream is quite apparent for low flow rates. Here the flow separates from the upper wall and forms a pool in the bottom of the tube, the depth of the pool being determined by the constriction at the end.

Figure 32 shows the measured jump positions plotted against pressure drop across the inlet orifice. The

curves indicate the various effects described above--- the rapid final movement from the tube, the hesitation before moving out, the continuing bore, the hysteresis.

4.4. The Tube Horizontal---the Air Core

It was felt that the study of the air core in a vertical tube was confused by the effects of gravity and hoped that investigation of the air core in the horizontal tube might clarify ideas on this phenomenon.

4.4.1. Single Hole Plate at Far End

Slightly different phenomena were observed for the solid inlet-end plate and for the inlet-end orifice plate.

For the solid plate at the inlet end a constant diameter core was found at high flow rates (3/8" diameter). This core narrowed (to 1/4") on reduction of the flow rate and vibrations were noted, especially near the inlet. Another slight reduction in flow rate initiated the break-up of the core and further reduction caused it to form into discrete bubbles. These gradually moved out through the orifice, the tube being left entirely filled with water. It is not possible to obtain this condition on starting up as some air is trapped at the end of the tube until an air core is formed.

For the orifice plate at the inlet end the core was at no time seen to be parallel (for high flow rate 1/2" at entry end, 5/8" at the other). Lowering the flow rate brought a slight reduction in diameter and, once again,

tremulations. Further reduction in flow resulted in the break-up of the core. But bubbles of air continued to enter at the inlet end and to move along the axis and out at the far end. Finally, the point was reached where a slight reduction allowed air to enter at the far end and the symmetry of the flow broke down.

4.4.2. Twenty-one Hole Plate

An even more striking difference in behaviour was produced by the different plates at the inlet end when the twenty-one hole plate was in position at the far end.

For the solid plate near the inlet, the air core was parallel and about 1/8" in diameter for high flow rates. It vibrated slightly near the inlet. Reduction in flow rate narrowed the core slightly and increased the vibration. The core then began to withdraw from the tube through the far end, the diameter being about 1/10" when half-way withdrawn.

But with the orifice plate at the entry end, a 1/2" diameter core (slightly thinner near inlet) was found in the tube for high flow rates and persisted for large reductions in flow rate. Finally it grew thinner near the inlets, then intermittent there. The final stage before air entered at the far end was a line of dancing bubbles (3/8" diameter, some elongated) moving from the far end towards the inlet end.

4.4.3. Sixteen Hole Plate

The performance with this plate at the far end and the solid plate at the inlet end is complicated by the trapping of air on starting. By starting rapidly, it was found possible to obtain a large tapering core (1-1/4" at inlet end, 3/4" at far end with high flow). However, progressive bleeding off of air produced narrower cores tapering the other way (petering out, in fact, short of the inlet end) for the same high flow rate.

But for smaller flows the smaller amounts of trapped air were concentrated near the inlet end. Intermediate flow rates produced bubbles distributed along the axis. In short, the situation arising with air trapped within the tube was most complicated and is probably not worth sorting out.

When the orifice plate was used at the inlet end the situation was much simplified. For high flow rates an air core (1/2" diameter, perhaps 5/8" near the far end) extended throughout the tube. It vibrated and undulated slightly. This situation pertained for large reductions in flow rate. Finally, the core grew thinner near the inlet, then narrowed to 1/8" throughout, and shortly thereafter became intermittent. The final stage was a row of dancing bubbles along the axis, moving out for further reductions in flow rate.

4.4.4. Sixty Hole Plate

With the solid plate fitted at the inlet end the core diameter was about 3/8", slightly thinner and intermittent near inlet. The intermittency extended up the tube from the inlet as the flow rate was reduced until 3/8" diameter bubbles were to be found at the far end and smaller bubbles near the inlet. Further reductions in flow produced a wavering, misty core of bubbles. Finally the bubbles moved out of the tube leaving a misty core.

For the orifice plate at the inlet end a wider core (3/4" throughout at high flow, then 5/8") existed. This broke up into bubbles, starting near the inlet. They moved out through the inlet end and finally air entered at the far end.

4.4.5. Far End Completely Blocked

Here only the case of the orifice plate fitted at the inlet end is of interest. Rapid starting led to the formation of a parallel core some 1/8" in diameter throughout the tube, vibrating violently in the half nearer the inlet. The flow pattern associated with this core seemed to be quite permanent. The core persisted over a wide range of flow rate but thinned and moved out for very low flows.

If the flow rate were then increased, another core configuration was adopted---the core extending only a foot or so up the tube, then bending over to the wall, the bent portion whirling around with the fluid. This phenomenon is shown in Figure 33. The diameter was 1/4" to 3/8".

Whether this second configuration was permanent or not is not certain. On several occasions it appeared settled, then suddenly began to move down the tube (still whirling) until the continuous core was formed. The transition between regimes took several minutes from the time when movement was first noticed. On no occasion was a complete core seen to change to the second, whirling configuration without suitable manipulation of the flow rate. During the process of rapid starting the whirling core was seen moving up the tube to form the continuous core.

When the whirling core occupied the region near the inlet the velocities near the far end were low, judging by the motions of solid particles in the water. However, the velocities increased rapidly up the tube. Reversed flows could be seen near the axis. It did not seem to be the case that the whirling core marked the total extent of the penetration of the inlet flow into the tube, the rest of the tube being relatively stagnant and only activated by viscous forces. Nevertheless, the existence of an air core right through the tube in the other configuration does seem to indicate a more vigorous penetration of the swirling fluid.

The termination of the core (which presumably marks the centre of a strong vortex) on the wall can be justified if it is supposed that the fluid mass beyond the whirling core is relatively stagnant by recalling the theorem

of Helmholtz that a vortex cannot terminate within the fluid. This line of thought was suggested by Professor Squire.

But the real significance of the two configurations found here does not lie in the details of the flow patterns, but rather in their very existence. It appears that more than one flow pattern can exist for the same inlet and boundary conditions, depending on the past history of the flow, the several patterns being permanent or at least changing only very slowly. As stated here, this is no more startling than the several flows set up by trapping varying amounts of air within the tube. But there is a rather more surprising phenomenon here---the asymmetry of the one configuration. The tendency towards axisymmetry in flows forced to rotate by cylindrical boundaries is strong due to the stabilizing effects of large centripetal pressure gradients. Yet here we find an air core extending to the tube wall, indicating a highly asymmetric pressure distribution and flow.

Although we have here learned of the existence of the asymmetric flow by observing an air-water interface, there seems to be no reason to suppose that this interface is necessary for the establishment of such an asymmetric configuration. It seems quite likely that a similar pattern might form in a flow field occupied by a single fluid.

Since these observations were made, reference to the

whirling core in a similar situation has been found in the work of Sprenger (1951). He has also found a like whirling core (the rotation being weaker, however) in the far end of the tube. His sketch shows the two cores ending at the same section of the tube.

Sprenger discusses the effect of bleeding fluid away at the far end of the tube. The lesser core is first displaced and then ejected at the far end as the outflow is slowly increased. Although he mentions the existence of straight cores in some situations, there is no suggestion of transition between the two patterns.

4.4.6. General

In the tests just described the effects of gravity were negligible except at very low flow rates, judging from the symmetry of the flow as evidenced by the air cores. For some configurations symmetrically placed air cores were maintained even for very low flow rates. On stopping the flow they broke up and floated to the top of the tube.

No very clear-cut pattern emerges from the observations of air cores. Once again the behaviour of the three intermediate blockages is similar while the extreme cases of fully blocked far end and the least blockage there (the sixty hole plate) offer divergent behaviour. For extremely small blockage (discussed in the previous section, 4.3.) we have already seen that a true air core does not form.

At high flow rates the air core diameter seems to be

determined primarily by the orifice near the inlet. With the orifice plate in position there, a 1/2" core (slightly wider near the far end) was found for the three intermediate throttling plates over a wide range of flow rate. A 3/4" to 5/8" core resulted from the fourth throttling plate. The extreme cases are obviously exceptions.

In the absence of an orifice plate at the inlet end a central orifice at the far end seems to determine the core diameter. The sixty hole plate is an exception to this rule.

In short, when the cores are vented to the atmosphere they are generally of nearly constant diameter---that diameter being set seemingly by the vena contracta at the controlling orifice.

The break-up of cores at low speeds is usually presaged by tremulations. Then the core becomes intermittent at a few places. A further reduction in the flow rate brings the formation of bubbles in place of the core. Finally, these move out of the tube. No pattern has emerged as to which end they will leave by. A possible penultimate stage is a stream of bubbles from one end to the other, both directions of flow being possible.

4.5. General Observations

a) The Air Core

It has been observed that for high swirl the air cores formed are not dependent on gravity for most configurations; that is, they are independent of the inclination

of the tube to the horizontal. In both horizontal and vertical tubes the high-swirl air cores are very nearly parallel.

The existence of parallel air cores in a vertical tube is rather surprising at first sight. One expects a downwards tapering core in the axial gravitational field. However, a simple calculation (taking $\frac{\partial p}{\partial r} = \rho \frac{v^2}{r}$, $\frac{\partial p}{\partial z} = -\rho g$ , $rv =$ inlet value) does suggest that a core of diameter 0.76" at the top and 0.72" at the bottom could exist in the present installation. In the actual flow the angular momentum is not constant throughtout the tube; the air cores found are of smaller diameter. However, the calculation serves to show that a large diameter (say, 1/2") air core with relatively slight taper can be set up in this apparatus.

We have observed a marked correlation between core diameter and the diameter of the central hole of the blockage, noting also that in the absence of such a hole an air core does not form. It appears that even a small central hole profoundly affects the flow throughout the tube or, more precisely, all along the axis. It seems probable that the orifice draws fluid away from the core, setting up an axial flow there and introducing more rapidly swirling fluid. If there is no central orifice the core of the vortex is relatively stagnant. The larger the orifice, the higher the rate at which new fluid is drawn into the vortex core, and the larger the air core established. This

line of thought explains the observed dependence of the air core on the central orifice, qualitatively, at least.

b) The Effect of Blockage

Another point of interest which has emerged from these investigations is some clarification of the ways in which blockages spread their influence upstream.

First, we might note that there seem to be three ways in which we can think of a body of fluid being influenced by another body of fluid or by a solid body: by bodily contact, as when a jet impinges on a pool of stagnant water, or conversely, when a pool of water intercepts a jet; by a steady pressure gradient acting through an intermediate mass of fluid; by propagation of surface or acoustic waves between the bodies.

Consider first the vertical tube with the water film merging with the core region. The thin films seemed to be quite independent of upstream conditions until they actually collided with the "pool." It appears that they are only very poor mechanisms for propagating blockage disturbances. The real mechanism for extending the blockage influence is the "pool" formed at the bottom. The backing up of the fluid is necessary to produce the pressure difference to pass the flow through the blockage. It is to be expected that the entry of a rapidly-moving film at the periphery of the pool will give rise to a reverse flow nearer the axis: as it moves downwards the film will entrain fluid; the reversed flow supplies the entrained

fluid.

So far our remarks apply equally well to fluid without swirl. But the pool is profoundly influenced by any angular momentum of the fluid forming it, the swirl extending the blockage disturbance farther upstream. Thus the flow reversals will also extend upstream. But they are not the mechanisms by which blockage influences the flow, only a side effect of that mechanism.

The processes acting to set up the flow in a partially filled tube can thus be grasped in simple terms. This understanding will perhaps make the tube-filled case (no water-film at the top), and even the flows in air, more comprehensible.

The influence of the blockage with tube horizontal is not so easily grasped. For here the jump is from one water film to another only slightly thicker. Seemingly a pressure gradient set up by the blockage extends upstream through these relatively thin films.

Finally, we note that surface waves did not seem to play an important part in spreading blockage influence through the fluid. This observation is consistent with the basic similarity of the flows set up by swirling air and water.

## 5. Theoretical Treatment

In view of the complexity of the problem of the vortex tube and the Ranque effect it is not surprising that its theoretical treatment has progressed only slowly, especially during the period prior to detailed experimental study. The problem posed by three-dimensional vortical flow is already a difficult one for laminar motions of a viscous incompressible fluid. And here we have the additional complications of compressibility coupled with violent turbulence. We cannot expect to give at this time a completely convincing analysis of the phenomena within the vortex chamber.

Two approaches to this difficult problem seem possible. We can make radical simplifying assumptions in order to build up a model of the separation mechanism immediately. Or we can deal more rigorously with simpler problems with the hope of finding techniques through which more difficult tasks may be performed and of gaining insight into the mechanisms operative so that clarifying assumptions may be introduced on a more rational basis. Both techniques have been used in the past; both will again be used here.

We begin our theoretical considerations by reviewing the trends which the analysis of the Ranque tube has taken in the past. Then a frontal attack will be made on the turbulent vortex in a compressible fluid, an attack giving considerable insight into the problem, but not pressed far enough to give explicit solutions. Finally, the

simpler problem of laminar vortical motion is considered and some detailed solutions are found.

## 5.1. A Survey of Previous Work

For some twenty years after the discovery of the Ranque effect theoretical workers were preoccupied with the qualitative discussion of the basic mechanism by which the observed energy separation might be effected. Their progress was delayed by lack of knowledge about what actually took place within the vortex chamber. We shall deal first with the evolution of ideas on energy separation and then move on to consider subsequent attempts to construct a model capable of predicting the observed energy separation.

### 5.1.1. Qualitative Theories of the Ranque Effect

a) Main Stream: Turbulent Mixing

The suggestion first put forward by Ranque in explanation of the effect he had discovered was that the gas which moves into the core of the vortex loses energy (presumably in the form of work) to the outer fluid simply by its movement through the radial pressure field. The theory does not refer to heat transfer or turbulent mixing; the steady laminar flow of a compressible, inviscid fluid is held to be sufficient to produce the energy separation. But this theory cannot, in fact, explain the establishing of a total temperature difference in a steady flow without transport properties. In such a flow energy

cannot be transferred across streamlines. Further, successive fluid particles will have exactly the same history, interactions with neighbouring particles being always in equilibrium. Hence, the total energy of each particle will remain constant.

An attempt to introduce the effects of viscosity and conductivity in a laminar motion was made by Scheper. He considered the effect of viscous dissipation on an initially constant energy field. In the vortex core kinetic energy is converted into thermal energy by viscous effects, while further out the kinetic energy remains relatively unchanged. Hence energy will flow away from the core by thermal conduction and the total temperature there will be reduced. But these ideas seem implausible on several grounds: the time spent in the tube is not sufficient for laminar conduction to have an important effect, and the model proposed is based tacitly on an unrealistic flow pattern. Deissler and Perlmutter analyzed a simple laminar flow model and found that, indeed, the separation effects due to laminar conduction were too small to produce separations of the observed magnitude.

A later theory of Ranque which was also supported by Hilsch was that the outwards migration of energy was due to a radial work transfer. They pictured an initial "free" vortex being converted into a "forced" vortex by viscous shearing forces and a consequent outwards movement of kinetic energy. Their ideas are thus linked to a particular

flow pattern, one which is not often approximated in reality.

Fulton carried forward these ideas of vortex conversion by noting that inwards conduction of heat would counteract the outwards work flow. He found that a net outwards flux of energy occurred in laminar flow but estimated that it was not of sufficient magnitude to produce the observed energy separations.

All the ideas reviewed above are based on considerations of laminar motion. But it gradually became apparent that it was unlikely that molecular transport properties could account for the significant energy redistribution which had to be justified. It seemed reasonable that the more rapid mixing of turbulence must be considered; this conclusion still seems valid today. The recent calculations of Deissler and Perlmutter, based on simple laminar and turbulent models, support the idea that account must be taken of turbulence to obtain energy separations of the required magnitude. The present writer has put forward the view (in a yet unpublished note in the Journal of Aero/Space Sciences) that turbulent mixing is the prime agent in a variety of aerodynamic cooling and heating processes.

At first the role of turbulence in the vortex tube was thought of as being qualitatively the same as that of molecular transport, although giving rise to very much greater energy flows. The first discussion noting that the effects of turbulent mixing across a large radial

pressure gradient might be essentially different from those of molecular diffusion is that of Knoernschild. His contribution was to note that it is not correct to think of the mixing of a compressible fluid across a pressure gradient in terms of the simple model used for an incompressible fluid---a fluid lump shifted unchanged to a new position and there mixing with the ambient fluid. A lump of compressible fluid will not be transported unchanged and without interactions with the fluid through which it moves. A work interaction with the surroundings will occur during such a movement, the particle being compressed on moving outwards to a region of high pressure or expanding on moving inwards. This work interaction with the matrix of fluid through which mixing takes place results in the cooling of the inwards-moving particles and heating of the outwards-moving. It seems plausible that the effects on the matrix fluid of the inwards and outwards-moving lumps will cancel. But if we return to the simple mixing ideas and envisage the heated and cooled lumps mixing in their new environments, we see that a radial transfer of energy can nvertheless take place.

It is generally assumed that the convecting particles do not interact with their surroundings except by expanding and contracting. That is, it is held that they are very nearly adiabatic while in motion. Deissler and Perlmutter mention work supportingthe idea of adiabatic movements of fluid lumps in the field of meteorology and in pipe flow

studies. In any case, the utility of the theory does not require strictly adiabatic lump movements.

According to this simple theory the radial transfer will be zero if the temperature field is related to the pressure field by an adiabatic law, since in that case particles will adjust to the local ambient temperature while moving. This conclusion follows even if lump motion is not adiabatic. It is towards this adiabatic distribution that the temperature distribution will end as mixing progresses following this simple pattern.

Knoernschild's concept seems to be the most widely favoured explanation of the Ranque effect at present. The advantages of this proposal were several: the possible temperature changes were easily large enough to account for the Ranque effect; it seemed capable of acting with sufficient speed to produce the observed temperature changes since the motion within the vortex chamber is violently turbulent; it was not dependent on a particular flow pattern within the vortex chamber.

But some workers feel that other effects are important too. Knoernschild himself thought that radial work flux was significant; Kreith in his recent discussion of Lay's papers supported this view. Yudine in discussing Hinze's paper mentioned an Archimedean effect in atmospheric mixing that may have a counterpart in the vortex tube. Both of these alternative mechanisms are associated with turbulent mixing and thus could be comparable to that linked to the

pressure gradient. But in neither case has a convincing exposition been given.

The idea that the radial energy transfer due to turbulent mixing is influenced by the pressure gradient was developed independently by Prins. It was put in analytic form by van Deemter and again by Deissler and Perlmutter using the arguments given above to justify their results. Hinze has recently given a somewhat more detailed derivation.

The ideas just discussed form the main stream of thought concerning the Ranque effect. We shall later discuss several detailed analyses which arise from this evolution of ideas. But first we consider several alternative explanations which do not fit into the main evolutionary pattern.

b) Alternatives: Unsteady Processes

We shall consider two suggestions concerning the mechanism of energy separation in the vortex tube which differ radically from the ideas put forward above and, indeed, from one another.

The first is the suggestion of Goetz (made in discussing a paper by Webster) that the phenomenon can be attributed to a "molecular shifting." This idea has been effectively countered by Webster who noted that the radical departure from equilibrium conditions required for Goetz' theory was very unlikely in the vortex tube as the time interval characterizing a typical flow was very

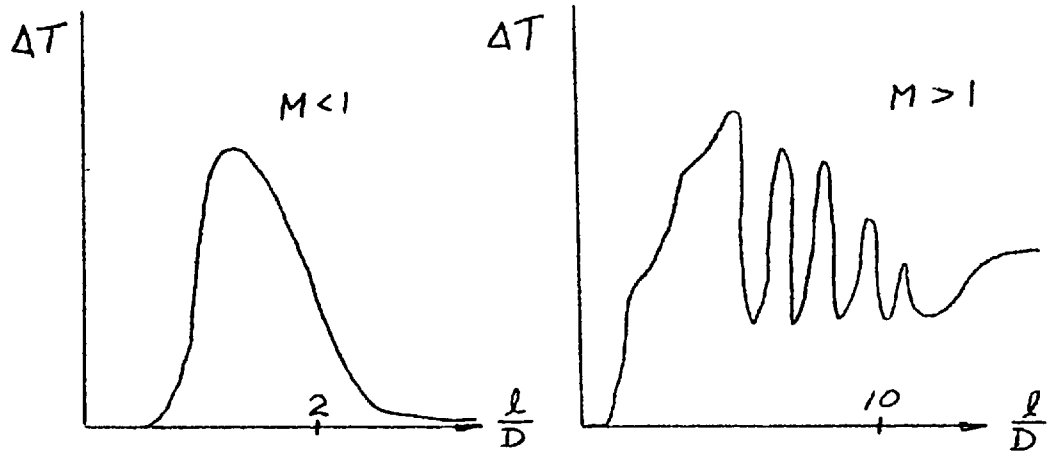
large compared to the mean time between molecular interactions.

The second suggestion, due apparently to Ackeret and espoused by his co-worker Sprenger, is not so easily dealt with. They felt that organized unsteady processes (as distinct from turbulence) play an important role in energy separation. Sound waves were originally thought to be the mechanism, attention has more recently been given to travelling shocks. As these ideas appear to offer the only serious competition to the turbulent mixing concept, we shall deal with them at some length.

Sprenger (1954) presents many experimental data for a resonance tube in the form of a Hartmann generator and tries to show a close connection between this device and the Ranque-Hilsch vortex tube. The phenomena he studied were produced by directing a jet of air into a resonance tube. The nozzle and tube were co-axial and of the same diameter, $D$ , the tube usually closed at the far end. The sound level produced by this device and the pressure and temperature within the generator were measured for both subcritical and supercritical nozzle pressure ratios as the distance, $\ell$ , between nozzle and resonance tube was varied.

The relevant findings of his main tests are:

1) The temperatures in the tube are dependent on $\ell$ , typically as indicated in the sketches below.




Peak temperature increments are equivalent to four or five times the dynamic head for both subcritical and supercritical cases.

2) Significant temperature increments (as illustrated) did not occur for subcritical jets unless turbulence was induced in them. A fine thread was stretched across the nozzle to produce turbulence. The introduction of a turbulence wire also augmented the temperature increments for the supercritical case; the periodic peaks remained and were magnified by factors as large as four.

3) The positions of the peaks in temperature were not dependent on the resonator length (nor, as a result, on frequency) but were markedly influenced by jet speed variations. A maximum temperature increment did occur for a particular tube length. However, details of these measurements are not given, so the relevance of this point is not clear.

4) Peaks in sound level and tube pressure corresponded to those in temperature.

5) Temperatures along the wall of the resonance tube

increased monotonically from mouth to end.

Sprenger reached the conclusion that the resonant oscillation within the tube produced the heating effect. But the evidence he presents does not support this view at all strongly. It seems more likely that the heating effect is produced by turbulent mixing, complicated in the supercritical case by the cellular shock pattern in the jet.

One bit of evidence which does not fit into this pattern and which does support Sprenger's theory is the close linking of noise and temperature. Several investigators of the Ranque-Hilsch vortex tube (including the present writer) have noted that maximum energy separation seemed to be associated with maximum noise level. Another puzzling feature of the data is the large gradient in temperature along the resonance tube. Such a gradient would seem to lend support to Sprenger's idea of dissipation within the tube, rather than to that of separation processes without.

Finally, Sprenger compared the performance of a vortex tube with a resonance tube (bleeding away hot air at the end distant from the jet) by plotting outlet temperatures against cold and hot air fractions. The devices were similar in construction and were tested at the same pressure ratio. The performance curves for the two devices are not unlike, either in shape of magnitude. This coincidence does suggest that the energy separation mechanisms for the

two are similar. But we have seen that the resonance tube phenomena are highly dependent upon turbulence, so this conclusion does not mitigate the turbulent mixing theory of energy separation.

More recent experimental investigations have revealed the nature of the unsteady flow associated with the resonance tube. Hall and Berry present photographs of pressure pulses travelling into and out of the tube, noting that the pulses are associated with alternating periods of swallowing and spilling of the jet. Several attempts have been made to analyze the heating effect of a succession of steepening pressure pulses passing through the tube; no account is taken of turbulent mixing.

The case of unsteady energy separation in the Ranque tube is dependent on its efficacy in the resonance tube. And even for the latter device its importance seems doubtful. It seems safe to assume that organized unsteady effects do not play a large part in producing the Ranque effect.

5.1.2. Theoretical Models of the Vortex Tube

The problem of modeling the vortex tube flow and energy separation processes has been found too difficult to be approached directly. Two methods of attack have been used: the study of simple solutions of equations potentially capable of representing the phenomena, and the study of flows with the required geometric complexity

but satisfying simpler equations. The contributions to be discussed are applicable to the Ranque-Hilsch vortex tube only in the light of these two approaches. Each contribution represents a compromise between conflicting demands of reality; as the fluid properties are specified more realistically, the geometric verisimilitude must be correspondingly reduced.

Lay gives an extensive discussion of spiral flows of an inviscid compressible fluid. But he fails to show that these models can be used to gain insight into the more complex phenomena within the Ranque tube. Not only are the necessary energy separation mechanisms absent, but it is impossible to apply meaningful boundary conditions to these flows. Some of the studies of perfect fluids by Long and others provide greater insight into vortex flows. In particular, the study by Long of a point sink on the axis of a pipe filled with rotating fluid is enlightening in that it indicates reversed flows within the tube when the swirl is sufficiently high relative to the sink flow.

Dornbrand and Pengelley consider a viscous fluid, but restrict themselves to plane flows. While they are able to give some consideration to energy flows, immediate application to vortices with important three-dimensional effects is not possible. Their analysis has been extended in Part A of this thesis. Rott studies a simple three-dimensional vortex flow of a viscous fluid. His laminar flow model fails to predict energy separation of the observed magnitude.

Vulis and Ustimenko consider an incompressible fluid but include the effects of turbulence in their theoretical models. They simplify the equations of motion by dropping less important terms and by assuming a particular distribution of eddy viscosity. However, their work is based on incorrect derivation of Reynolds' equations, so the progress made is for the most part illusory.

Finally, we consider two serious attempts to set up models of the internal flow and hence of the energy separation mechanism of the vortex tube. These are due to van Deemter and to Deissler and Perlmutter. They consider the turbulent motion of a compressible fluid, but assume highly simplified models of the flow pattern. The effective mechanism of separation in their models is mixing across the pressure gradient set up by the vortex. They obtain predictions of the outlet temperatures as functions of cold mass flow ratio; the functional relationships are similar to those determined experimentally; reasonable numerical agreement can be obtained by suitably specifying undetermined parameters.

## 5.2. The Dynamics of Turbulent Vortical Flow

Turbulent mixing will profoundly influence high velocity vortex flows such as those in the Ranque-Hilsch vortex tube---even laying aside the seemingly important role of turbulence in thermal energy separation. The analysis of such flows must then be approached through Reynolds' equations.

Initially we shall consider an incompressible fluid of constant viscosity, for which the applicable form of Reynolds' equations are obtained from the simple Navier-Stokes equations on taking mean values with respect to time and specializing to steady and axisymmetric mean flow:

$$\frac{1}{r}\frac{\partial}{\partial r}(r\overline{u^2}) + \frac{\partial}{\partial z}(\overline{uw}) - \frac{\overline{v^2}}{r} = -\frac{\partial}{\partial r}\left(\frac{P}{\rho}\right) + \nu\left(\nabla^2 U - \frac{U}{r^2}\right) \quad (1)$$

$$\frac{1}{r}\frac{\partial}{\partial r}(r\overline{uv}) + \frac{\partial}{\partial z}(\overline{vw}) + \frac{\overline{uv}}{r} = \nu\left(\nabla^2 V - \frac{V}{r^2}\right) \quad (2)$$

$$\frac{1}{r}\frac{\partial}{\partial r}(r\overline{uw}) + \frac{\partial}{\partial z}(\overline{w^2}) = -\frac{\partial}{\partial z}\left(\frac{P}{\rho}\right) + \nu\nabla^2 w \quad (3)$$

and for which the mean-value continuity equation is

$$\frac{1}{r}\frac{\partial}{\partial r}(rU) + \frac{\partial W}{\partial z} = 0 \quad (4)$$

The linear terms are already in terms of the mean values: $P$, the mean pressure; $U$, $V$, $W$ the mean velocity components; $\rho$ and $\nu$ the constant density and kinematic viscosity. The non-linear terms can be resolved into mean accelerations and Reynolds' apparent stresses due to turbulent mixing. Taking $u = U + u'$, etc., we have

$$\overline{u^2} = U^2 + \overline{u'^2}, \quad \overline{uv} = UV + \overline{u'v'}, \quad \text{etc.}$$

The introduction of time-mean values has brought

order into the system, but at a great price. For we now have ten dependent variables related by only four equations. The situation is succinctly described by Townsend (p. 23): "The number of mean-value functions always exceeds the number of equations, which makes the problem mathematically indeterminate, but the restrictions imposed are useful in discriminating between alternative physical hypotheses." He goes on to outline the plan of attack that will be used here: "The application of the equations of motion to turbulent shear flow is conveniently made in two stages, the first stage being the derivation and use of the exact relations and the second the use of approximations to reduce the complexities of these exact relations."

5.2.1. Exact Results

Several exact first integrals can be obtained for constant density and viscosity if axial variations are restricted.

Assuming that all mean values are independent of $z$, we get:

From (4), $$rU - \nu C \tag{5}$$

From (3), $$\nu\frac{\partial W}{\partial r} - \overline{uw} = \frac{K}{r} = \frac{\tau_{rz}}{\rho} - UW \tag{6}$$

where $\tau_{rz}$ is the time-mean axial shear stress, and the constant $K$ is a measure of the momentum transferred across a cylindrical surface. Using (5),

$$\nu r^2\frac{\partial}{\partial r}\left(\frac{W}{r^2}\right) - \overline{uw} = \frac{K}{r}$$

From (2), $$\nu r\frac{\partial}{\partial r}\left(\frac{V}{r}\right) - \overline{uv} = \frac{G}{r^2} = \frac{\tau_{r\theta}}{\rho} - UV \tag{7}$$

where $\tau_{r\theta}$ is the time-mean tangential shear stress and the constant $G$ is a measure of the moment on a cylindrical surface or of the torque applied to the fluid. Using (5) we may write $\nu r^{1+c}\frac{\partial}{\partial r}\left(\frac{V}{r^{1+c}}\right) - \overline{u'v'} = \frac{G}{r^2}$.

An immediate integral of equation (1) cannot be obtained unless we specify $\overline{u^2} - \overline{v^2}$. For example, $\overline{u^2} = \overline{v^2}$ gives

$$\frac{P}{\rho} + \overline{u^2} = \frac{P_0}{\rho} + \frac{\nu}{r}\frac{\partial}{\partial r}(rU) \qquad (8)$$

The viscosity-dependent term is seen to be zero here.

At first sight it seems possible to generalize this model by taking $P = f(r)z$, the other variables being still $z$-invariant. This assumption corresponds to axially constant losses and is consistent with equation (3). However, the assumptions can only be consistent with equation (1) for $f$ = constant, and then only if $\frac{\partial}{\partial r}(r\overline{u^2}) = \overline{v^2}$.

The generalized axial momentum relation is

$$\nu\frac{\partial W}{\partial r} - \overline{uw} = \frac{\alpha}{2}r + \frac{k}{r} \qquad (9)$$

where $\alpha$ is a measure of the axial pressure drop.

The results obtained here are generalization of well-known relations for zero radial flow. Once again we have found (as in Part A of this thesis) that generalization by admitting source-type radial flow does not inhibit analytic development.

Equations (5) and (7) govern plane, basically axi-symmetric turbulent flow. The generalization (6) has no obvious exact application but will apply approximately to

the axial translation of an isolated rotating cylinder, especially in cases where suction is specified so as to reduce boundary layer growth in the axial direction.

Similarly, equations (8) and (9) are exactly applicable only when very special conditions are satisfied. But these conditions are approximately satisfied when the flow is very nearly in the axial direction. Thus these results have their utility in problems of only slightly swirling flow through tubes and annuli.

5.2.2. Approximate Results

In the last section we obtained some results applicable to plane axisymmetric flows and other relationships which are very nearly true for realistic axially-directed flows. In working away from these firm bases we can consider either swirl perturbations to the axial flows or axial perturbations to the planar ones. The former approach is that adopted in the extensive literature on swirling pipe flow; the latter seems more appropriate here.

We shall henceforth drop the viscous terms from Reynolds' equations; however, account will be taken of compressibility, in order that the results be directly applicable to the Ranque tube. The results of this analysis will then be valid only in the turbulent body of the flow.

From continuity and Euler's equations we obtain, on taking time means and requiring the mean motion to be steady and axisymmetric:

$$\frac{1}{r}\frac{\partial}{\partial r}(r\overline{\rho u}) + \frac{\partial}{\partial z}(\overline{\rho w}) = 0 \qquad (10)$$

$$\frac{1}{r}\frac{\partial}{\partial r}(r\overline{\rho u^2}) + \frac{\partial}{\partial z}(\overline{\rho u w}) - \frac{\overline{\rho v^2}}{r} = -\frac{\partial P}{\partial r} \qquad (11)$$

$$\frac{1}{r}\frac{\partial}{\partial r}(r\overline{\rho u v}) + \frac{\partial}{\partial z}(\overline{\rho v w}) + \frac{\overline{\rho u v}}{r} = 0 \qquad (12)$$

$$\frac{1}{r}\frac{\partial}{\partial r}(r\overline{\rho u w}) + \frac{\partial}{\partial z}(\overline{\rho w^2}) = -\frac{\partial P}{\partial z} \qquad (13)$$

Taking $u = U + u'$, $\rho = R + \rho'$, etc., we have

$$\overline{\rho u^2} = R\overline{u^2} + \overline{\rho' u'(2U + u')}$$

$$\overline{\rho u w} = R\overline{u w} + \overline{\rho'(U w' + V u' + u' w')}, \text{ etc.}$$

We shall now proceed to derive approximate forms of these equations for several cases of large swirl.

a) Axial Perturbations to Radial/Swirling Flow

That the results derived for swirling flow in a plane remain approximately true for small axial perturbations can be shown by an order-of-magnitude analysis. We take

$$U, V \sim O(1), \quad W \sim O(\varepsilon)$$

$$\frac{\partial}{\partial r} \sim O(1), \quad \frac{\partial}{\partial z} \sim O(\delta)$$

to represent the perturbed flow, and

$$i^2\left(\sim \overline{u'^2}, \overline{v'^2}, \overline{w'^2}\right) \sim O(\eta), \quad \rho' \sim O(\mu)$$

to represent the turbulence.

We choose units of measurement so that $r$, $U$, $V$, $\Delta P \sim O(1)$. Then $R \sim O(1)$ also for consistency of these assumptions with the equation governing tangential momentum. This result will be more clearly seen a posteriori.

The quantities $\varepsilon$ , $\delta$ , $\eta$ , $\mu$ are, of course, assumed to be small compared with unity so that terms of higher order in them will be negligible.

If the fluid is homogeneous (that is, such that it would be homogeneous on being brought to rest) the density fluctuations, $\rho'$, will be dependent upon the turbulent intensity, $i$ . It seems plausible that these density differences are maintained by the centripetal pressure fields of the eddies making up the turbulent velocity field. The pressure difference from core to periphery of a typical eddy is $p' \sim R i^2 \sim O(\eta)$ ; we know that $\rho'/p' \simeq K$ , the compressibility of the fluid.

Hence, $\mu \sim K\eta$

Introducing these orders into equations (10) - (13), we find:

The continuity relation,

$$rRU = C_1 + O(\varepsilon\delta, \mu\eta^{1/2})$$

The radial momentum relation,

$$\frac{\partial P}{\partial r} + \frac{1}{r}\frac{\partial}{\partial r}(rRU^2) = \frac{RV^2}{r} + O(\eta)$$

The tangential momentum relation,

$$r^2 R\overline{uw} = O(\varepsilon\delta, \delta\eta, \mu\eta^{1/2}) + G$$

The axial momentum relation,

$$\frac{\partial P}{\partial z} + \frac{1}{r}\frac{\partial}{\partial r}(rR\overline{uw}) = O(\delta\eta, \mu\eta^{1/2})$$

$O(\delta)$ $\qquad$ $O(\varepsilon, \eta)$

where only the lowest order terms are indicated and those not marked are $\sim O(1)$.

The axial momentum relation appears to be the least accurate of the simplified equations. Note that the "exact" relations of the previous section retain a residual error due to non-zero compressibility even with $\epsilon, \delta \to 0$.

Integration of the continuity and tangential relations has still been possible. A result of some interest can be derived from the integrated forms. We have

$$r^2 R \overline{u'v'} = -G_0 \quad \text{for} \quad \sqcup V = 0.$$

If the variation of Reynolds' stress does not change decisively with $\sqcup$, we can write $R \sqcup V = -\frac{G}{r^2} + \frac{G_0}{r^2}$

$$\text{or} \quad V = \left(\frac{G_0 - G}{C_1}\right)\frac{1}{r}$$

Then it appears that $V \propto \frac{1}{r}$ for small or vanishing $\sqcup$. This law is found to be obeyed in the fully turbulent region between two rotating cylinders, adjustments to particular boundary conditions taking place in boundary layers. But its justification is not simple unless the more general radial distribution is considered.

It is interesting to note that the exact result (7) is consistent with the functional forms

$$\sqcup \propto \frac{1}{r}, \; V \propto \frac{1}{r}, \; \overline{u'v'} \propto \frac{1}{r^2}.$$

b) Radial Perturbation to Swirling Flow

The real interest of this investigation is in vigorously swirling flow through a tube, for which the appropriate specializations are

$$V \sim O(1), \quad U \sim O(\varepsilon)$$
$$\frac{\partial}{\partial r} \sim O(1), \quad \frac{\partial}{\partial z} \sim O(\delta)$$
$$i^2 \sim O(\eta), \quad \rho' \sim O(\mu)$$

Units are again chosen so that $r$ , $V$ , $\Delta P \sim O(1)$ ; $R \sim O(1)$ for consistency.

Some justification of these specifications is perhaps necessary. That small values of $U$ are appropriate is suggested by the requirements that the radial velocity vanish at the axis and the wall of the tube. The relative magnitudes of the rates of change are suggested by the case studied previously, by the elongated cylindrical vortex chambers in which we are often interested, and finally by examination of the flow patterns in a variety of vortices.

Introducing these orders into the continuity equation we find that $W \sim O(\varepsilon/\delta)$, at most, so that

$$\underset{O(\varepsilon)}{\frac{1}{r}\frac{\partial}{\partial r}(rRU)} + \underset{O(\varepsilon)}{\frac{\partial}{\partial z}(RW)} = O(\mu\eta^{1/2})$$

Radial momentum gives

$$\frac{\partial P}{\partial r} = R\frac{V^2}{r} + O(\eta)$$

Tangential momentum,

$$\underset{O(\varepsilon)}{\frac{\partial}{\partial z}(RVW)} + \underset{O(\varepsilon,\eta)}{\frac{1}{r^2}\frac{\partial}{\partial r}(r^2 R\overline{uw})} = O(\eta\delta, \mu\eta^{1/2})$$

Axial momentum,

$$\underset{O(\delta)}{\frac{\partial P}{\partial z}} + \underset{O(\eta)}{\frac{1}{r}\frac{\partial}{\partial r}(rR\overline{uw})} = O(\varepsilon^2/\delta, \eta\delta, \frac{\varepsilon}{\delta}\mu\eta^{1/2})$$

These results should be applicable in the body of the vortex tube, although not in the ends nor very near the

walls. The accuracy of the simplified relations suggested by this analysis does not seem to be as high as for those of the previous model. However, we can estimate the applicability of these results to flows such as that in the Ranque-Hilsch vortex tube using data from the test results given earlier.

In the turbulent body of the flow we find, typically, $\frac{W}{V} \sim O(\frac{1}{4})$ suggesting that $\varepsilon \sim \frac{\delta}{4}$.

Considering the pressure distributions we find, typically,

$$\frac{\Delta P}{\Delta z} \Big/ \frac{\Delta P}{\Delta r} \sim \frac{10}{40} \Big/ \frac{20}{1.5} \sim \frac{1}{50}$$

suggesting that $\delta \sim \frac{1}{50}$, so that $\varepsilon \sim \frac{1}{200}$

For balance of the tangential and axial momentum equations we must have $\eta$ of order of both $\delta$ and $\varepsilon$. Say

$$\eta \sim 2\varepsilon \sim \frac{\delta}{2} \sim \frac{1}{100}$$

This implies that the intensity of turbulence in the body of the flow will be $\sim 10\%$. As this is of the order expected it offers a slight check on these estimates.

We can easily estimate $K$, the compressibility, in the units adopted here. We have taken $\Delta P \sim o(1)$ and $R \sim O(1)$ But in these high-velocity air flows we have also $\Delta R \sim O(1)$. Then $K \sim \Delta R / \Delta P \sim O(1)$ so that $\mu\eta^{1/2} \sim K\eta^{3/2} \sim \frac{1}{1000}$

Finally, we obtain estimates of the error terms as percentages of those retained:

$$\frac{1}{r}\frac{\partial}{\partial r}(rRU)+\frac{\partial}{\partial z}(RW) = O(20\%) \qquad \text{1 term}$$

$$\frac{\partial P}{\partial r} = R\frac{V^2}{r} + O(1\%) \qquad \text{2 terms}$$

$$\frac{\partial}{\partial z}(RVW) + \frac{1}{r^2}\frac{\partial}{\partial r}(r^2 R\overline{u'w'}) = O(15\%) \qquad \text{1 term}$$

$$\frac{\partial P}{\partial z} + \frac{1}{r}\frac{\partial}{\partial r}(rR\overline{u'w'}) = O(10\%) \qquad \text{2 terms}$$

The number of the larger rejected terms is indicated.

Although it is not possible to obtain first integrals for this case, some of the gross features of the flows in the central part of the vortex tube can be grasped using these approximate relations.

A rather surprising feature of these not-very-high-speed flows (~ 400 feet per second) is the apparent importance of the compressibility-turbulence interaction. Both the continuity and tangential momentum relations are significantly influenced by radial mixing of the compressible fluid. Their more accurate forms are

$$\frac{1}{r}\frac{\partial}{\partial r}(rRU) + \frac{\partial}{\partial z}(RW) + \frac{1}{r}\frac{\partial}{\partial r}(r\overline{\rho' u'}) = O(\delta\mu\eta'^{1/2})$$

$$\frac{1}{r^2}\frac{\partial}{\partial r}(r^2 R\overline{u'w'}) + \frac{\partial}{\partial z}(RVW) + \frac{1}{r^2}\frac{\partial}{\partial r}(r^2 V\overline{\rho' u'}) = O(\delta\varepsilon, \delta\eta)$$

The largest error terms are seen to be those involving $\overline{\rho' u'}$. It should be noted, however, that estimates of the turbulent mixing terms were made on the basis of 100% correlation. For example, we have taken $\overline{\rho' u'} \sim O(\mu\eta'^{1/2})$. Thus the errors estimated here are more likely to be high than low.

The correlation $\overline{\rho' u'}$ will again be found of interest in the discussion of energy flows. It seems likely that $\overline{\rho' u'} > 0$ since lighter lumps will move inwards due to Archimedean buoyancy forces.

The tangential momentum relation is no longer a simple balancing of Reynolds' stress against convection of mean vorticity; the effects of axial convection are not negligible here:

$$RU\left(\frac{\partial V}{\partial r} + \frac{V}{r}\right) + RW\frac{\partial V}{\partial z} = -\frac{1}{r^2}\frac{\partial}{\partial r}\left(r^2 R\overline{u'v'}\right) \qquad (14)$$

(Note that the simple continuity relations are sufficiently accurate in both systems of approximation to allow the mean motion acceleration terms to be written in their more usual forms without altering the orders of the errors.)

The simple radial equilibrium relation:

$$dP = R\frac{V^2}{r}dr$$

retains its applicability in this type of flow.

Although the simplified axial momentum equation seems to be the least accurate of the set---the errors here being due to the neglect of mean motion convection terms---it is sufficient to show that the axial pressure changes are chiefly accountable to Reynolds' stresses. This result is in accord with conclusions reached upon examination of the experimental results in Section 3.

c) General Flow with High Swirl

The two sets of simplified equations derived in the preceding sub-sections contain, for the most part, the same terms. That is, most of the terms of Reynolds' equations are negligible for both categories of flow, only a few becoming important or losing their importance as we shift from one sort of flow to the other.

It seems plausible that by combining the two sets, retaining the dominant terms of both classes, we will obtain equations valid for a less restricted group of vortical flows, a group containing not only the two specified classes, but also the whole range of flows intermediate to them.

The combined set is

$$\frac{1}{r}\frac{\partial}{\partial r}(rRU) + \frac{\partial}{\partial z}(RW) = 0$$

$$\frac{\partial P}{\partial r} = R\frac{V^2}{r} - RU\frac{\partial U}{\partial r}$$

$$\frac{\partial}{\partial z}(RVW) + \frac{1}{r^2}\frac{\partial}{\partial r}(r^2R\overline{uv}) = 0$$

$$\frac{\partial P}{\partial z} + \frac{1}{r}\frac{\partial}{\partial r}(rR\overline{uw}) = 0$$

We know that these equations are valid for high swirl so long as one of the other velocity components is small. But are they also valid when all the velocity components are of the same order? This is easily checked.

Taking $U, V, W \sim O(1)$; $\frac{\partial}{\partial r} \sim O(1)$, $\frac{\partial}{\partial z} \sim O(\delta)$, $\zeta^2 \sim O(\eta)$ we obtain the approximate forms

$$rRU = C_1 + O(\delta)$$

$$\frac{\partial P}{\partial r} = R\frac{V^2}{r} - \frac{1}{r}\frac{\partial}{\partial r}(rRU^2) + O(\delta, \eta)$$

$$r^2RUV = G + O(\delta, \eta)$$

$$rRUW = F + O(\delta, \eta)$$

These results are contained in the general set given above. For this degenerate case all the Reynolds' stresses are found to be negligible and explicit solutions are possible.

The accuracy of the more general equations should be generally higher than is indicated by the calculations of sub-section (b). Compressibility errors are relatively large for small radial flows.

d) The Vortex Shape Hypothesis

Now that the restrictions on the velocity components have been relaxed, it is possible to see that the key feature in the simplifying analysis is the hypothesis (not unlike that associated with the boundary layer) that changes in the axial direction are much more gradual than those in the radial direction. It seems appropriate to term this a vortex shape hypothesis. The considerable simplifications in the governing equations for high-swirl flow are only possible when this concept is introduced.

The introduction of this vortex shape hypothesis needs little justification for the problem of present

interest, swirling flow through cylindrical chambers. But it is also a useful approximation for many other vortex problems.

On considering the swirling flow of water through a contracting conical chamber Binnie and Teare found a cylindrical air core indicating the validity of the hypothesis away from the tapering sides of the chamber. The study of swirling flow through a convergent-divergent nozzle (Binnie, Hookings, and Kamel) revealed a cylindrical air core in the contracting, subcritical flow above the throat. However, the supercritical flow below the throat did not form a cylindrical core along the axis, but fanned out along the diverging walls. A supercritical flow will not necessarily violate the assumption that radial changes are very much more rapid than axial. If the supercritical flow is retained within a cylinder, as in the water tests reported in this thesis, the hypothesis may still be valid.

A somewhat similar situation is found in the vortices shed from lifting surfaces. Commonly they tighten in on the axis and the elongation hypothesis represents the pattern well. But a vortex burst phenomenon is sometimes encountered, the tight core breaking up and the swirling fluid moving away from the axis. Another case of interest is the emergence of a swirling jet from a pipe or orifice into the atmosphere. Commonly the vortex spreads out, often leaving the core free for reversed flow.

Finally: there are cases for which the vortex shape hypothesis is not useful, but it does adequately represent the situation in the vortex core for a variety of problems, not only flows confined within nozzles and tubes, but also some cases of unrestrained flow in the atmosphere.

The reasons for its wide applicability and the limitations to its applicability are not hard to see. In the first place, the radial and swirl components must be zero on the vortex axis. Therefore their gradients must be related as suggested by the elongation hypothesis. If, further, we have swirling fluid close to the axis (that is, a high angular velocity) the radial pressure gradient will be high in the core. This in turn leads to steep radial density gradients whether by air core formation or by the normal effect of compressibility.

Thus we see that the kinematic requirement of axisymmetry, together with the dynamical requirement of radial equilibrium for rapidly rotating fluid, must specify a flow in which radial gradients are large compared to axial gradients.

## 5.3. Energy Flows in a Turbulent Vortex

Having gained some insight into the mechanics of vortex flows by specializing Reynolds' momentum equations to appropriate approximate forms, we now turn to the energy equation to see whether the same sort of analysis will be fruitful there.

### 5.3.1. Basic Analysis

As before, we neglect molecular transport properties and body forces, the simple form of the energy equation being

$$\rho \frac{Dh_o}{Dt} = \frac{\partial p}{\partial t}$$

where $h_o = h + \frac{1}{2}\underline{u}^2$ is the total enthalpy of the fluid, the sum of the enthalpy and the kinetic energy per unit mass. Using continuity we can obtain the alternative form

$$\frac{\partial}{\partial t}(\rho h_o) + \nabla\cdot(\rho h_o \underline{u}) = \frac{\partial p}{\partial t}$$

Taking mean values with respect to time we have $\nabla\cdot(\overline{\rho h_o \underline{u}}) = 0$

which gives $$\frac{1}{r}\frac{\partial}{\partial r}(r\overline{\rho u h_o}) + \frac{\partial}{\partial z}(\overline{\rho w h_o}) = 0$$

for axisymmetric mean flow.

We can write $\overline{\rho u h_o} = \overline{(R+\rho')(U+u')(H_o+h_o')}$

$$= RUH_o + R\overline{u'h_o'} + U\overline{\rho' h_o'} + H_o\overline{\rho' u'} + \overline{\rho' u' h_o'}$$

But $h_o = h + \frac{1}{2}\underline{u}^2 = H + h' + \frac{1}{2}(u^2+v^2+w^2)$

so that $H_o = H + \frac{1}{2}[U^2+V^2+W^2+\overline{u'^2}+\overline{v'^2}+\overline{w'^2}]$

and $h_o' = h' + u'U + v'V + w'W$

We shall specialize the energy equation using the scheme of orders-of-magnitude of Section 5.2.2. (b):

C

$V \sim o(1)$, $U \sim o(\epsilon)$ leading to $W \sim o(\epsilon/\delta)$

$\frac{\partial}{\partial r} \sim o(1)$, $\frac{\partial}{\partial z} \sim o(\delta)$

$i^2 \sim o(\eta)$, $\rho' \sim o(\mu)$

adding $h' \sim o(\alpha)$

We choose units to that $r$, $V \sim o(1)$, knowing that $R \sim o(1)$ from the previous analysis. We also take $\Delta H_o \sim o(1)$, knowing that energy separations are typically a few times the dynamic head. This assumption will be seen to be consistent with the others a posteriori.

This scheme is appropriate to swirling flow through a tube. A few more terms must be retained in an equation valid for more general vortical flows.

The approximate energy equation for this case is

$$\underset{o(\epsilon)}{\frac{1}{r}\frac{\partial}{\partial r}(rRUH_o)} + \underset{o(\epsilon)}{\frac{\partial}{\partial z}(RWH_o)} + \underset{o(\mu\eta^{1/2})}{\frac{1}{r}\frac{\partial}{\partial r}(r H_o \overline{\rho' u'})}$$

$$+ \underset{o(\alpha\eta^{1/2})}{\frac{1}{r}\frac{\partial}{\partial r}(rR\overline{u'h'})} + \underset{o(\eta)}{\frac{1}{r}\frac{\partial}{\partial r}(rRV\overline{u'v'})} + \underset{o(\frac{\epsilon}{\delta}\eta)}{\frac{1}{r}\frac{\partial}{\partial r}(rRW\overline{u'w'})}$$

$$= O(\delta\eta, \epsilon\eta, \delta\alpha\eta^{1/2})$$

Only the leading error terms have been indicated.

This result relates the several important energy fluxes into an elemental volume. It can be cast into another form without altering the orders of the errors if we use the more accurate form of continuity.

Thus,

$$R\frac{DH_o}{Dt} = -\frac{1}{r}\frac{\partial}{\partial r}(rR\overline{u'h'}) - \rho\overline{u'w'}\frac{\partial H_o}{\partial r}$$

$$-\frac{1}{r}\frac{\partial}{\partial r}(rVR\overline{u'v'}) - \frac{1}{r}\frac{\partial}{\partial r}(rWR\overline{u'w'})$$

where $\frac{D}{Dt}$ indicates the rate of change following the mean motion. Here we have a relation between the radial energy fluxes and the energy input to a constant mass moving through the system.

From these two results we see that the changes in the total energy of fluid spiraling through the tube are produced by three effects:

a) the transport by radial mixing of lumps of fluid with higher and lower thermal energy,

b) the transfer of energy (thermal and kinetic) by mixing across a radial energy gradient, and

c) the work done by the two significant Reynolds' stresses.

Each of these effects has been mentioned before. But an explicit statement of their combined role has not been made. Note that (b) does not act in an incompressible fluid.

We shall consider the nature of each of the several contributions in vortex motion before attempting to estimate their overall effect. Naturally none of the organized unsteady effects suggested by Sprenger appear here. We have ruled them out by specializing the analysis to steady mean motion.

5.3.2. The Energy Fluxes

a) Mixing across a Pressure Gradient

The correlation function $\overline{u'h'}$ appears innocuous at first sight, seemingly merely a turbulent analogue of molecular thermal conduction. It is not till Knoernschild's train of thought regarding the movements of compressible lumps through a pressure gradient is brought to mind that the full significance of this mixing term is realized. But the effectiveness of this mechanism even in the absence of a pressure gradient is shown in the results of Series III.

Several workers (van Deemter, Deissler and Perlmutter, Hinze) have shown that the mathematical expression of the mixing model outlined in Section 5.1.1. leads, for a perfect gas and with other idealizations, to a representation of the correlation in the form

$$\frac{1}{c_p}\overline{u'h'} = -\epsilon_T\left(\frac{\partial T}{\partial r} - \frac{\gamma-1}{\gamma}\frac{T}{P}\frac{\partial P}{\partial r}\right)$$

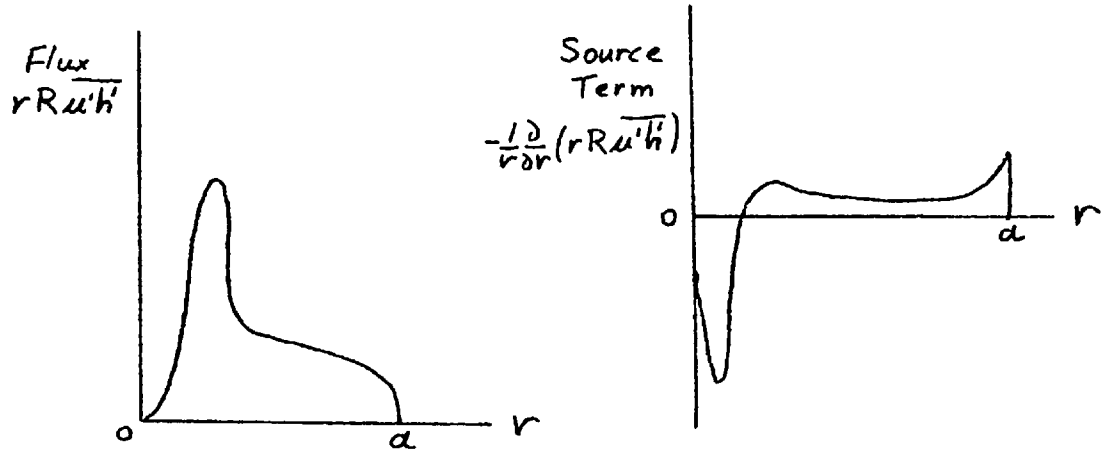
where $T$ is the time-mean temperature,

$\epsilon_T$ is an eddy-diffusion coefficient.

An alternative form can be given using the radial equilibrium condition and the equation of state for a perfect gas: $\overline{u'h'} = -\epsilon_T\left(\frac{\partial H}{\partial r} - \frac{V^2}{r}\right)$

When the radial temperature distribution is less steep that that defined by the adiabatic law applied to the pressure distribution (as is the case in the flows examined in this investigation) the heat flux due to this

effect is everywhere outwards, although falling to zero at axis and wall (neglecting conduction to the wall). In the absence of data concerning directly the distribution of turbulent activity in the vortex chamber it is not possible to estimate the flux distribution with any conviction. However, it may be expected to rise rapidly in the region of large pressure gradients commonly found near the axis. Then




may be taken as suggesting typical distributions.

Finally, the effect of mixing across the radial pressure gradient will be, in most practical cases, to remove energy from the fluid in the vortex core and redistribute it in the outer fluid.

b) **The Archimedean Effect**

The existence of this contribution was suggested by Yudine's remarks on Hinze's paper. We are led to expect a heat flux associated with Archimedean forces by analogy with turbulent mixing through the pressure gradient in the earth's atmosphere.

As was pointed out in the discussion of flow dynamics, the correlation $\overline{\rho' u'}$ may be expected to be positive in a vortex in a compressible fluid. Then the associated energy flux, $H_o \overline{\rho' u'}$, will be everywhere radially outward. Surprisingly, the overall effect of this outwards flux, as indicated by the term $-\overline{\rho' u'} \frac{\partial H_o}{\partial r}$, seems to be to cool the fluid throughout the tube, except in a region very near the wall. In most practical situations $\frac{\partial H_o}{\partial r} > 0$, except near the wall.

This conundrum can be resolved as follows. The overall effect of the energy flux $H_o \overline{\rho' u'}$ is to redistribute energy in the various <u>regions</u> of the tube. But when continuity requirements are taken into account, this results in a reduction in energy per <u>unit mass</u> of the whole of the moving fluid.

Consider a simple example: purely radial flow. Continuity is $\frac{\partial}{\partial r}(r \overline{\rho u}) = 0$, whence, for zero net source flow, we get $RU = -\overline{\rho' u'}$

We shall take $\overline{\rho' u'}$ to be positive. Then the requirement of continuity is an inwards mean velocity, $U = -\frac{\overline{\rho' u'}}{R}$

The energy equation derived from continuity is

$$RU \frac{\partial H_o}{\partial r} = R \frac{DH_o}{Dt} = -\overline{\rho' u'} \frac{\partial H_o}{\partial r}$$

Thus we see that the rate of change following the mean motion is, in fact, the rate of change as a particle moves inwards in the direction opposite to the energy flux.

The energy equation can, of course, be integrated

immediately for this case of restricted axial variation, giving $r\overline{\rho u h_0} = C$.

We shall attempt to show the influence of the mean flow on the correlation $\overline{\rho' u'}$ as has previously been done for $\overline{u'h'}$. Let us clarify the situation be relating the turbulent velocity fluctuation at a point to the perturbation velocity of a lump at that point. We write

$$u' = u'_1 + u'_2$$

where $u'$ is the deviation from the time-mean value at a point; $u'_1$ is the velocity of the coincident particles due to the Archimedean buoyancy force per unit volume, $\rho' \frac{V^2}{r}$; and $u'_2$ is the part of the local motion induced by surrounding turbulence. The term $u'_1$ is random with respect to the fixed point but not so far as the passing eddy is concerned. Then $\overline{\rho' u'} = \overline{\rho' u'_1}$

Our next task is to relate the velocity $u'_1$ to the buoyancy force producing it. It seems plausible to compare the inwards-moving lighter lumps to microscopic particles whose net drift through a gas is superposed upon Brownian motions. In the present case, the turbulence of the fluid supplies the random disturbance to the drift due to the Archimedean force.

In his theory of Brownian motion Einstein has assumed that the drift speed is linearly related to the force on a particle, that is, that the drift motion obeys Stokes' law. The results of his theory have been verified

experimentally. Similarly in electricity: a linear resistance law---Ohm's law---is found to apply when the electrons' drift speed is small compared with the speed characterizing their random thermal motion.

We shall assume that a similar relationship governs the lump movements, taking $u_1' \propto \rho' \frac{V^2}{r}$

Hence, the Archimedean correlation is of form

$$\overline{\rho' u'} = \varepsilon_A \frac{V^2}{r} = \varepsilon_A \frac{1}{R} \frac{\partial P}{\partial r}$$

where $\varepsilon_A$ is dependent on the scale and structure of the turbulence and, more especially, on the compressibility of the fluid.

c) Work Flux due to Tangential Stress

It is difficult to make general statements about the work fluxes in vortex flows. They are not primarily dependent on the ubiquitous radial pressure gradient but on the multifarious flow patterns. The equation (14) relating the tangential stress to the mean velocity suggests this difficulty: it is too complicated in its general form to be immediately useful.

An obvious simplification of this relation is that of specifying the swirl distribution to be independent of axial position. Fortunately, this idealization has close counterparts in the vortex flows studied experimentally, especially those of Series I and II. Subject to this restriction we have

$$(rRU)\frac{\partial}{\partial r}(rV) = -\frac{\partial}{\partial r}(r^2R\overline{u'v'})$$

We shall study this relationship by considering simple examples, beginning with the case of constant radial flow:

$$rRU = C$$

For this case the torque is found to be $r^2R\overline{u'v'} = -CrV$ on requiring that both velocity and mixing stress be zero at the axis. The work flux is $rVR\overline{u'v'} = -CV^2$ inwards for $C > 0$, outwards for $C < 0$; that is, opposed in direction to the radial mass flow. The source term is

$$-\frac{1}{r}\frac{\partial}{\partial r}(rVR\overline{u'v'}) = \frac{2C}{r}V\frac{\partial V}{\partial r}$$

Local heating occurs for inflow combined with swirl decreasing outwards and for outflow combined with swirl increasing outwards. The other combinations result in cooling. Practically, this means that radial inflow will result in the cooling of fluid in the core and the heating of the fluid farther out.

Having considered the effect of swirl on the work flux for a particular radial flow, we now take the other point of view. We take $V = Kr^{-1/2}$ and consider a variety of radial flows. This form of swirl distribution is suggested by the test results. Except in the core and near the wall, it models the experimentally determined distributions quite well, especially those of Series I and II to which this simple analysis is particularly applicable. We table the results for some simple examples:

| | Radial Flow $rRU$ | Work Flux $rVR\overline{u'v'}$ | Source Term $-\frac{1}{r}\frac{\partial}{\partial r}(rVR\overline{u'v'})$ |
|---|---|---|---|
| 1) | $Cr^2$ | $-\frac{CK^2}{5}r$ | $\frac{CK^2}{5}\frac{1}{r}$ |
| 2) | $Cr$ | $-\frac{CK^2}{3}$ | $0$ |
| 3) | $C$ | $-CK^2\frac{1}{r}$ | $-\frac{CK^2}{r^3}$ |
| 4) | $C(a-r)$, $r \le a$ | $-CK^2\left(\frac{a}{r}-\frac{1}{3}\right)$ | $-\frac{aCK^2}{r^3}$ |
| 5) | $Cr^2(a-r)$, $r \le a$ | $-CK^2\left(\frac{a}{5}-\frac{r}{7}\right)r$ | $-CK^2\left(\frac{2}{7}-\frac{a}{5r}\right)$ |

Case (1) models flow in the core; cases (2) and (3), that in the body of the flow; case (4), that near the wall. Case (5) covers the whole radius from axis to wall. Again we have chosen solutions such that the torque approaches zero in the core.

These examples follow the pattern that emerged previously. Similar results are found for the more general swirl distribution $V = Kr^n$ where $n > -1$; stability considerations suggest that cases for which $n < -1$ are not of physical interest. We conclude that the radial work flux is usually in the direction opposed to the radial mass flux.

Since inwards radial flows are more often encountered in the vortex tube than outwards (as is to be expected, since the air commonly enters at the periphery) we can expect that the core will commonly be cooled and the peripheral fluid heated by action of the tangential stresses.

d) Work Flux due to Axial Stresses

The effect of the other important Reynolds' stress is not simple. We have

$$\frac{1}{r}\frac{\partial}{\partial r}(r R \overline{u'w'}) = -\frac{\partial P}{\partial z}$$

as the approximate relation for axial forces in the body of the tube. Requiring that the stress be bounded at the axis, we find the work flux to be

$$rWR\overline{u'w'} = -W\int_0^r r\frac{\partial P}{\partial z}\,dr$$

In order to investigate the properties of this function we consider a simple example:

$$W = -\frac{\partial P}{\partial z} = r - 1 \qquad \text{for} \quad r < 3$$

incorporating the property that $W$ and $\frac{\partial P}{\partial z}$ are usually of opposite sign in the vortex flows studied. The work flux is $rRW\overline{u'w'} = \frac{1}{3}r^2(r-1)(r-\frac{3}{2})$

$$> 0 \quad \text{for} \quad r < 1, \quad r > 3/2$$

$$< 0 \quad \text{for} \quad 3/2 > r > 1$$

This example illustrates the trends of more complex examples. Usually $W$ and $\int_0^r r\left(-\frac{\partial P}{\partial z}\right)dr$ have the same sign in an outer annulus, indicating an outwards flux there. Most of the fluid in this outer annulus will be cooled; only that very near the wall is heated. The core will be occupied by complex fluxes which will probably not play an important part in overall energy separation.

5.3.3. The Efficient Mechanisms of Energy Separation

To sum up: it seems likely that each of the effects considered will usually produce a flow of energy from the vortex core to the peripheral region.

Our final task is to estimate the magnitudes of the several contributions to the energy separation. We use the values suggested by the test data to determine the relative magnitudes of the contributions:

$$\underset{O(-\frac{1}{200})}{\frac{1}{r}\frac{\partial}{\partial r}(r R U H_0)} + \underset{O(-\frac{1}{200})}{\frac{\partial}{\partial z}(R W H_0)} + \underset{O(\frac{1}{1000})}{\frac{1}{r}\frac{\partial}{\partial r}(r H_0 \overline{\rho u'})}$$

$$+ \underset{O(\frac{\alpha}{10})}{\frac{1}{r}\frac{\partial}{\partial r}(r R \overline{u'h'})} + \underset{O(\frac{1}{100})}{\frac{1}{r}\frac{\partial}{\partial r}(r R V \overline{u'w'})} + \underset{O(\frac{1}{400})}{\frac{1}{r}\frac{\partial}{\partial r}(r R W \overline{u'w'})}$$

$$= O\left(\frac{1}{5000}, \frac{\alpha}{500}\right)$$

The Archimedean effect seems to be of somewhat less importance than the others. The work fluxes are of the same order as the heating/cooling terms. There is no reason to assume that the energy separation due to the Knoernschild effect is more important than that produced by radial flux of work. The quantity $\alpha$ will have to be $\sim$ 1/20 if the thermal convection term is to be important.

Finally, we come to the following conclusions concerning the air flows studied here and probably valid for a wider class:

The efficient mechanism of energy redistribution in the vortex core is thermal transfer by turbulent mixing across the large radial pressure gradients commonly found there.

The further separation in the outer fluid is primarily due to work fluxes associated with turbulent mixing stresses.

## 5.4. A Class of Axisymmetric Solutions of the Navier-Stokes Equations

The analysis of the previous sections stopped short of the prediction of three-dimensional flow patterns. It became apparent that additional restrictions would have to be supplied to specify a meaningful mathematical problem. Relationships between the mean motion and the turbulence seem to be required at this stage, but physical principles on which they might be based have not yet been devised.

In order to get some idea of the vortex solutions that might be expected from Reynolds' equations we shall consider the geometrically similar, but properly set, problem governed by the Navier-Stokes equations. The two sets of equations have the same mean acceleration and pressure terms. They differ only in the way in which shear is established in the fluid.

Reynolds' equations become formally identical to the Navier-Stokes equations on introducing the hypothesis of constant eddy viscosity. It is not intended to offer any very serious attempt to justify this hypothesis for the flows of interest here. However, it does seem to be far from the worst guess that could be made. The direct application of Prandtl's hypothesis

$$\varepsilon \propto b(u_{max} - u_{min})$$

where $\varepsilon$ is the eddy viscosity,

$b$ is the width of the mixing zone, and

$u_{max} - u_{min}$ is the velocity difference at a section through the zone, does suggest that the eddy viscosity does not vary rapidly in the axial direction. On the other hand, we find for the flow between two rotating cylinders the same form for both apparent and viscous shear stresses,

$$\overline{u'v'} \propto \frac{1}{r^2} \qquad \frac{\partial V}{\partial r} - \frac{V}{r} \propto \frac{1}{r^2}$$

consistent with constancy of eddy viscosity along the radius. The strong flow reversals found in many vortex tube flows seem to provide a large-scale mixing tending to even out properties through the vortex chamber.

5.4.1. Basic Analysis

The equations governing the steady axisymmetric flow of an incompressible fluid of constant viscosity can be written

$$\frac{1}{R}\frac{\partial}{\partial R}(Ru) + \frac{\partial w}{\partial Z} = 0 \tag{1}$$

$$u\left(\frac{\partial v}{\partial R} + \frac{v}{R}\right) + w\frac{\partial v}{\partial Z} = \nabla^2 v - \frac{v}{R^2} \tag{2}$$

$$u\frac{\partial u}{\partial R} + w\frac{\partial u}{\partial Z} - \frac{v^2}{R} = -\frac{\partial P}{\partial R} + \nabla^2 u - \frac{u}{R^2} \tag{3}$$

$$u\frac{\partial w}{\partial R} + w\frac{\partial w}{\partial Z} = -\frac{\partial P}{\partial Z} + \nabla^2 w \tag{4}$$

where $\nabla^2 = \frac{\partial^2}{\partial R^2} + \frac{1}{R}\frac{\partial}{\partial R} + \frac{\partial^2}{\partial Z^2}$

and the equations have been simplified by the substitutions:

$$R = \frac{r}{\nu}, \quad Z = \frac{z}{\nu}, \quad P = \frac{p}{\rho}$$

Note that the first two equations are independent of the kinematic pressure, $P$; the analysis to follow springs from this observation.

We consider those flows for which the swirl distribution is the same in every cross-section: $w = w(R)$
Then, from equation (2), $u = u(R)$
and the flow patterns are seen to be necessarily the same in every cross-section.

There are two reasons for interest in this class of flows. They are suggested by the two-dimensional analysis of Part A and by the relatively small changes in swirl distribution found in some experimental situations.

Subject to this restriction on axial variations, equations (1) and (2) can be integrated to give

$$Rv = \beta_0 \int^R R \exp\left[\int^R u\,dR\right] dR + a_0 \qquad (5)$$

$$w = -q(R)\,z + f(R) \qquad (6)$$

where $q(R)$ can be interpreted as a source distribution in a purely two-dimensional flow. A three-dimensional flow pattern is completely specified (save for constants of integration) by supplying $f(R)$ and one of $u$, $v$, $q$. But the only patterns of physical interest are those which satisfy the dynamical condition posed by equations (3) and (4).

From equation (3), we find that $\frac{\partial^2 P}{\partial R \partial z} = 0$
for the class considered here. Then from (4) we get

$$u\frac{\partial w}{\partial R} + w\frac{\partial w}{\partial z} - \frac{\partial^2 w}{\partial R^2} - \frac{1}{R}\frac{\partial w}{\partial R} - \frac{\partial^2 w}{\partial z^2} = g(z) \qquad (4')$$

where $g(z)$ is seen to be $kz + \ell$ ( $k$, $\ell$ constants) using equation (6). An axially directed gravitational force can be absorbed in $\ell$.

It is convenient to introduce $F = Ru$, a variable representing local radial flow. In terms of this variable

$$w = -\frac{1}{R}\frac{\partial F}{\partial R} z + f(R) \qquad (6')$$

On substituting for $u$ and $w$ in the dynamical condition (4'), we obtain ordinary differential equations for $F$ and $f$.

$$R^2F''' - RF'' + F' - RFF'' + RF'F' + FF' = KR^3 \qquad (7)$$

$$Rf'' + f' - Ff' + F'f = -\ell R \qquad (8)$$

where differentiation is with respect to $R$.

The problem of obtaining solutions for this class is thus resolved into solving equation (7) for the radial flow parameter $F$. Once this is done, the axial and swirl components follow from (5), (6'), and (8).

5.4.2. Radial Flow Distributions

The equation (7) for $F$ can be simplified slightly. Introducing a new dependent variable, $G = F + 1$,

$$R^2G''' - RGG'' + GG' + RG'G' = KR^3 \qquad (7')$$

Introducing a new independent variable, $t = \log R$,

$$\dddot{G} - 3\ddot{G} + 2\dot{G} - G\ddot{G} + \dot{G}\dot{G} + 2G\dot{G} = Ke^{4t} \qquad (7'')$$

This equation is not unlike those encountered in other searches for viscous flow solutions, although somewhat more complex. It seemed unlikely that solutions in closed form could be found. Nevertheless, several attempts were made to reduce the equation to an integrable form. For the case $K = 0$, it can be written as a second-order equation with $G$ the independent variable. However, this does not appear to be a useful result. The resulting

equation is not one of the canonical forms discussed by Ince for which solutions can be easily obtained.

We seek a solution in the form of an expansion about the origin in integral powers of $R$ :

$$G = A_n R^n \qquad \text{where } n = 0, 1, 2 \ldots$$

In practice it is easier to work from the form (7"), the appropriate form of solution being

$$G = A_n e^{nt} \qquad \text{where } n = 0, 1, 2 \ldots$$

Substituting we get

$$[n(n-1)(n-2)A_n + q(n+2-2q)A_q A_{n-q}]e^{nt} = k e^{4t}$$

where $n = 0, 1, 2 \ldots$, $q = 0, 1, 2 \ldots\ldots n$

On setting the various coefficients of $e^{nt}$ equal to zero we have

$$A_1 = 0$$
$$A_3(2 - A_0) = -\tfrac{5}{3} A_1 A_2 = 0$$
$$A_4(3 - A_0) = -\tfrac{1}{8}(4A_2^2 - k)$$
$$A_5(4 - A_0) = -\tfrac{3}{5} A_2 A_3$$
$$A_6(5 - A_0) = -\tfrac{1}{3} A_2 A_4 - \tfrac{1}{4} A_3^2, \quad \text{etc.}$$

Solutions of restricted validity exist for $A_0 = 2, 3 \ldots$ But the solution of prime interest is that for which

$$A_1 = A_3 = A_5 = A_7 = \text{etc.} = 0,$$

$A_0$ and $A_2$ being parameters in terms of which all the even coefficients can be expressed.

A group of solutions that can be studied easily and that is of considerable physical interest is that for which $A_0 = 1$. Here $G = 1$, $F = R\mu = 0$ on the axis.

For this case, the series solution can be written (setting $4A_1^2=\alpha^2$, $K=\beta^2$):

$$F=\tfrac{1}{2}(\alpha R^2)-\frac{3}{2\,4}\left[1-(\beta/\alpha)^2\right](\alpha R^2)^2+\frac{3\cdot5}{8\,6}\left[1-(\beta/\alpha)^2\right](\alpha R^2)^3$$
$$-\frac{5\cdot7}{8\,8}\left[1-(\beta/\alpha)^2\right]^2(\alpha R^2)^4+\frac{5\cdot7\cdot9}{32\,10}\left[1-(\beta/\alpha)^2\right]^2(\alpha R^2)^5$$
$$-\frac{7\cdot9\cdot11}{32\,12}\left[1-(\beta/\alpha)^2\right]^2\left[\frac{3}{2}-(\beta/\alpha)^2\right](\alpha R^2)^6$$
$$+\frac{3\cdot7\cdot7\cdot11\cdot13}{8\cdot32\,14}\left[1-(\beta/\alpha)^2\right]^2\left[\frac{11}{14}-(\beta/\alpha)^2\right](\alpha R^2)^7+\ldots. \qquad (9)$$

The form of this solution suggests that the governing equation might be simplified by the introduction of the independent variable $\eta=R^2$. Taking in addition $H=G-3=F-2$ we have

$$2\eta H'''-HH''+H'H'=K \qquad (7''')$$

where differentiation is with respect to $\eta$.

For $(\beta/\alpha)^2=1.0$, the solution given above reduces to the well-known stagnation-point solution $u=\frac{\alpha}{2}R$, $w=-\alpha z$. The more complicated solution can be thought of as a generalized stagnation-point flow. The series solutions that are not bounded at the axis ($A_0\neq1$) are generalizations of $u=\frac{\alpha}{2}R+\frac{c}{R}$, $w=-\alpha z$.

The solutions determined by the first seven terms of the series (9) for various values of $(\beta/\alpha)^2$ are shown in Figures 34 and 35. Judging by the descending magnitude of the terms, the seven-term representation is adequate for

$\alpha R^2\leq 20$ with $(\beta/\alpha)^2=0.35$ to 1.5

$\alpha R^2\leq 15$ with $(\beta/\alpha)^2=0$ to 2.0

The seventh term is less than 0.25 within these limits.

5.4.3. Attempts at Generalization

The solution derived in the last section has only two undetermined parameters. As the third-order equation may be expected to have solutions with three parameters there is some hope of generalizing this result by an extension of the methods used already.

Introducing an arbitrary index in the trial solution,

$$G = A_n R^\gamma R^n = A_n e^{\overline{n+\gamma}\, t}$$

we get $[(n+\gamma)(n+\gamma-1)(n+\gamma-2)\, A_n$

$+(q+\gamma)(n+2-\gamma-2q)\, A_q\, A_{n-q-\gamma}]\, e^{\overline{n+\gamma}\, t} = k e^{4t}$

Thus we see that only integral values of $\gamma$ are possible; no generalization arises.

A third form of solution tried was

$$G = A_{mn} R^n \log^m R = A_{mn}\, t^m e^{nt}$$

for which the equation takes the form

$$[(m+1)(m+2)(m+3) A_{m+3,n} + 3(m+1)(m+2)(n-1) A_{m+2,n}$$

$$+ (m+1)(3n^2 - 6n + 2) A_{m+1,n} + n(n-1)(n-2) A_{mn}$$

$$+ \{p(m+3-2p) A_{m+2-p,n-q} + [(n+2-4q)p + q(m+1)] A_{m+1-p,n-q}$$

$$+ q(n+2-2q) A_{m-p,n-q}\}\, A_{pq}]\, t^m e^{nt} = k e^{4t}$$

where $m = 0, 1, 2, \ldots,$ $n = 0, 1, 2, 3 \ldots,$

$p = 0, 1, 2 \ldots m,$ $q = 0, 1, 2 \ldots n.$

But the set of equations obtained by setting the coefficients equal to zero cannot be solved successively for the coefficients of the assumed solution.

5.4.4. Axial Flows

We shall term the part of the axial velocity distribution which is dependent on $z$ the basic axial velocity, and that given by $f(R)$, the additional axial velocity.

The basic distribution follows easily from equation (6') and the series solution (9) for $F$ since

$$\frac{1}{R}\frac{\partial F}{\partial R} = 2\alpha \frac{\partial F}{\partial(\alpha R^2)}$$

Distributions for various values of $(\beta/\alpha)^2$ are given in Figure 36. Both core and annular reversals are represented.

The additional axial distribution is determined by equation (8). The substitution $t = \log R$ allows it to be written $\ddot{f} - F\dot{f} + \dot{F}f = -\ell e^{2t}$

It has not proves possible to integrate this equation formally so a solution in series is sought:

$$f = B_m e^{mt} \qquad \text{where } m = 0, 1, 2 \ldots$$

On substituting we get

$$\left[ m^2 B_i + (m-2q) A_{m-q} B_q \right] e^{mt} = -\ell e^{2t}$$

where $q = 0, 1, 2 \ldots m$. Equating the coefficients of $e^{mt}$ to zero, we have a series of equations for $B_m$ in terms of $A_m$, the coefficients of the series for $F$. The $B_m$ can be written in terms of the single new parameter $B_o$. Once again the solution is less general than might be expected.

The complete solution can be found for the special case $F = 0$: $f = -\frac{\ell}{4}R^2 + C_1 \log \frac{R}{R_1}$

giving some indication of the nature of the generalized complete solution. (Note that this special case includes Poiseuille flow.) However, the trial solution suggested,

$$f = B_{mn} t^n e^{mt}$$

does not give rise to a suitable set of equations for $B_{mn}$.

5.4.5. Swirl Distributions

The swirl distribution associated with a particular radial flow can be found from (5). The solution contains two parameters, allowing the scale of the swirl to be set and another property of the solution to be specified.

In general, numerical integration of (5) will be necessary. But for the simple case $u = -\frac{\gamma}{2}R + \frac{c}{R}$, $w = \gamma z$ the integration may be carried part way in closed form:

$$Rv = \rho_0 \int^R R^{1+c} \exp\left(-\frac{\gamma}{4}R^2\right) dR + a_0 = \rho_0 I + a_0$$

The integral $I$ can be given in terms of tabulated functions (powers of $R$, the exponential function, the error function, and the exponential integral) for integral values of the parameter $c$.

For $c = 0$, we get $Rv = \rho_0 \exp\left(-\frac{\gamma}{4}R^2\right) + a_0$

The solution which remains bounded at the axis is

$$u = \frac{a_0}{R}\left[1 - \exp\left(-\frac{\gamma}{4}R^2\right)\right]$$

It has been discussed previously by Burgers and by Rott.

The solutions for $c \neq 0$ are generalizations of this result. Those given for $\gamma \geq 0$ seem to be the more

interesting physically. Far away from the axis the radial flow is inwards for this class and the swirl distribution tends towards that for constant angular momentum.

Swirl distributions subject to the condition

$$v = 0 \qquad \text{for} \quad \frac{\gamma}{4} R^2 = 1$$

are shown in Figure 37, and those obeying the condition

$$\tau = 0 \qquad \text{for} \quad \frac{\gamma}{4} R^2 = 1$$

in Figure 38.

5.4.6. Possible Applications; an Example

The solutions obtained have the disadvantage that they are not flexible enough to represent realistic situations. This difficulty manifests itself in unrealistic behaviour far away from the origin of co-ordinates when reasonable conditions are imposed in the region of the origin. However, they hint at the vast variety of solutions of the Navier-Stokes equations. That they can be obtained at all gives some hope that further progress can be made with analysis springing from the exact equations.

The models discussed in the previous sections are simple cases of swirling flows within and about cylinders. If a solution for $F$ involving three parameters can be found, a greater variety will open up. A case that could then be dealt with is re-entrant flow in a cylinder, satisfying the conditions

$$u = 0 \qquad \text{for} \quad R = 0, a$$

$$w = 0 \qquad \text{for} \quad R \leq a, \quad z = 0$$

Solutions of some physical interest can be derived from the results already obtained. The stagnation-point applications have already been noted. Another application is to the flow near the end of an air core.

We take the core radius to be $\sqrt{\frac{4}{\gamma}}$ and choose $C$ such that there is zero penetration; that is, such that

$$u\left(\sqrt{\frac{4}{\gamma}}\right) = -\frac{\gamma}{2}\sqrt{\frac{4}{\gamma}} + C\sqrt{\frac{\gamma}{4}} = 0$$

Then $C = 2$ for any $\gamma > 0$. The swirl distribution for which $u = 0$ and $\frac{\partial v}{\partial r} - \frac{v}{r} = 0$ on the surface $R = \sqrt{\frac{4}{\gamma}}$ is that for $C = 2$ in Figure 38. For the class considered here the shear components other than the tangential are zero throughout the flow.

The final condition to be applied is that of constant pressure within the core. Within the fluid the pressure is given by $P = h(R) + j(z)$ for this class of flows. From (4'), $j(z) = -\frac{1}{2}Kz^2 - \ell z$

For the air core case $\left(\frac{\beta}{\alpha}\right)^2 = \frac{K}{\gamma^2} = 1$; we can take $\ell = 0$. From equation (3), taking into account the developments following from equation (5), we have near the air core

$$h(R) \simeq a_0^2 n(R) \quad \text{where } n(R) \geq 0 \quad \text{for } R > \sqrt{\frac{4}{\gamma}}$$

$$= 0 \quad \text{for } R \leq \sqrt{\frac{4}{\gamma}}$$

Then a surface of zero pressure is given approximately by

$$a_0^2 n(R) = \gamma^2 z^2$$

It lies outside the surface $R = \sqrt{\frac{4}{\gamma}}$. However, for high swirl ( $a_0^2$ large) the equation of the surface tends to

$$n(R) = 0 \qquad \text{or} \qquad R = \sqrt{\frac{4}{\gamma}}$$

Thus we see that the solution for $C = 2$ gives a reasonable representation of a flow near the end of an air core for the high swirl case. It is interesting to note that interest in a parallel core arises only because axial accelerations (including gravity) are often found to be negligible in nature compared with the centripetal.

## 6. Conclusions

Energy separation within the Ranque-Hilsch vortex tube is chiefly effected by two energy fluxes produced by turbulent mixing: an outwards flow of work associated with the tangential shear stress, and an outwards heat flux due to mixing of the compressible fluid across the radial pressure gradient.

The flows within the vortex chamber where the separation takes place are so complex that a well-founded qualitative discussion is not yet possible. The essential problem to be solved is that of expressing precisely the role of turbulent mixing. Nevertheless, it is possible to understand most of the phenomena encountered by combining a careful study of detailed measurements and basic theoretical results.

## 7. References

1. Binnie, A. M., Hookings, G. A. and Kamel, M. Y. M.: "The Flow of Swirling Water through a Convergent-Divergent Nozzle," J. Fl. Mech., 3, p. 261 (1957-8)

2. Binnie, A. M. and Teare, J. D.: "Experiments on the Flow of Swirling Water through a Pressure Nozzle and an Open Trumpet," Proc. Roy. Soc., A235, p. 78 (1956)

3. Bouasse, H.: "Tourbillons," Biblioteque Scientifique de l'Ingenieur et du Physicien, 2 Volumes, Paris (1931, 1932)

4. British Patent Specification 762563, Nov. 28th, 1956

5. Dornbrand, H.: "Theoretical and Experimental Study of Vortex Tubes," A. F. Tech. Rep. 6123, Republic Aviation Corp. (1950)

6. Deissler, R. G. and Perlmutter, M.: "An Analysis of the Energy Separation in Laminar and Turbulent Compressible Vortex Flows," Proc. 1958 Heat Transfer and Fluid Mechanics Institute, Stanford University, Palo Alto, Calif.

7. Fulton, C. D.: "Ranque's Tube," Refrig. Eng., 58, No. 5, p. 473 (1950)

8. Gartshore, I. S.: "Swirling Flow of Water in a Straight Pipe," M. Sc. (Eng.) Thesis, University of London (1960)

9. Hall, I. M. and Berry, C. J.: "On the Heating Effect in a Resonance Tube," J. Ae/Sp. Sci., 26, No. 4, p. 253 (1959)

10. Hartnett, J. P. and Eckert, E. R. G.: "Experimental Study of the Velocity and Temperature Distribution in a High-velocity Vortex-type Flow," Trans. ASME, 79, p. 751 (1957)

11. Hilsch, R.: "Die Expansion von Gasen im Zentrifugalfed als Kälteprozess," Z. für Naturforschung, Band I, Nr. 4, p. 208 (1946)

12. Hinze, J. O.: "The Effect of Compressibility on the Turbulent Transport of Heat in a Stably Stratified Atmosphere," Proc. Symposium at Oxford, Aug. 1958; "Atmospheric Diffusion and Air Pollution," p. 229, Academic Press, New York, London (1959); Ed. F. N. Frenkiel, P. A. Sheppard; Vol. 6 in "Advances in Geophysics"

13. Hughes, R. R.: "Modern Developments in Fluid Mechanics to Aid Chemical Engineering Research--- Vortex Tube Flows," Ind. Eng. Chem., 49, p. 951 (1957)

14. Ince, E. L.: "Ordinary Differential Equations," Dover, New York (1956)

15. Kassner, R. and Knoernschild, E.: "Friction Laws and Energy Transfer in Circular Flow," Tech Rep. No. F-TR-2198-ND, GS-USAF Wright Patterson AF Base, No. 78 (1947)

16. Lay, J. E.: "An Experimental and Analytical Study of Vortex-Flow Temperature Separation by Superposition of Spiral and Axial Flows," Trans ASME, 81, Series C, No. 3, p. 202, p. 213 (1959)

17. Long, R. R.: "Sources and Sinks at the Axis of a Rotating Liquid," Johns Hopkins University, Civil Engineering Department, Tech. Note No. 9 (1957)

18. McGee, R., Jr.: "Fluid action in the vortex tube," Refrig. Eng., 58, p. 974 (1950)

19. Otten, E. H.: "Producing Cold Air---Simplicity of the Vortex-tube Method," Engineering, 186, No. 4821, p. 154 (1958)

20. Pengelley, C. D.: "Flow in a Viscous Vortex," J. Appl. Phys., 28, No. 1, p. 86 (1957)

21. Prins, J. A.: "Brief aan de Redactie," Ned. Tijdschrift voor Natuurkunde," 14, p. 241, (1948)

22. Ranque, G.: French Patent (1931), American Patent (1932)

23. Ranque, G.: "Experiences sur la Detente Giratoire avec Productions Simultanees d'un Echappement d'air Chaud et d'un Echappement d'Air Froid," J. Phys. Rad., Tome IV, Ser. VII, No. 6, p. 2 (1933)

24. Rott, N.: "On the Viscous Core of a Line Vortex," ZAMP, IXb, 5/6, p. 543 (1958); X, 1, p. 73 (1959)

25. Savet, P. H.: "On a Stationary Temperature Separating Device used as a Measuring and Cooling/Heating Apparatus," ASME Preprint 58-AV-28

26. Scheller, W. A. and Brown, G. M.: "The Ranque-Hilsch Vortex Tube," Ind. Eng. Chem., 49, p. 1013 (1957)

27. Scheper, G. W., Jr.: "The Vortex Tube---Internal Flow Data and Heat Transfer Theory," Refrig. Eng., 59, p. 985 (1951)

28. Sprenger, H.: "Beobachtungen an Wirbelrohren," ZAMP, II, No. 4, p. 293 (1951)

29. Sprenger, H.: "Über thermische Effekte in Resonanzrohren," Mitt. Inst. Aerodyn., ETH, Zürich, No. 21, (1954)

30. Townsend, A. A.: "The Structure of Turbulent Shear Flow," Cambridge U. P. (1956)

31. van Deemter, J. J.: "On the Theory of the Ranque-Hilsch cooling effect," App. Sci. Res., A3, No. 3, p. 174 (1952)

32. Vulis, L. A. and Ustimenko, B. P.: "Über die Aerodynamik der Zyklonfeuerungskammern," Energietechnik, 5, No. 6, p. 265 (1955)

33. Webster, D. S.: "An Analysis of the Hilsch Vortex Tube," Refrig. Eng., 58, No. 2, p. 163 (1950)

34. Westley, R.: "A Bibliography and Survey of the Vortex Tube," College of Aeronautics, Cranfield, Note No. 9, (1954)

35. Westley, R.: "Vortex Tube Performance Data Sheets," College of Aeronautics, Cranfield, Note No. 67 (1957)

Table I. End Plate Details

Cold or Inlet End Plates

a) Solid

b) Orifice: 1.25" diameter

Plates used during air tests were brass; those used for water tests, Perspex.

Hot or Far End Plates

a) Solid

b) Orifice: 1.35" diameter

c) 21-$\frac{1}{4}$" holes: 8 at $1\frac{1}{4}$", 8 at 7/8", 4 at 15/32", 1 at centre

d) 16-$\frac{1}{4}$" holes at $1\frac{1}{4}$" radius

e) 60-3/16" holes: 18 at 1-3/8", 18 at 1-1/8", 9 at 7/8", 9 at 5/8", 5 at 5/16", 1 at centre (distributed to give as nearly as possible uniform outlet area distribution)

The following blockages were utilized only in water tests:

f) 5-$\frac{1}{4}$" holes: plates (b) and (c) together

g) Various plates held 17/32" away from end of tube by four pillars built up from 2BA nuts and washers.

All these plates were of 1/8" brass.

Table II. Instrumentation Stations

Distances are measured from the inlet end of the tube.

| Stn. | | | Stn. | |
|---|---|---|---|---|
| 0 | 2" | (pressure tap only) | | |
| 1 | 3" | | | |
| 2 | 4½" | | | |
| 3 | 6" | | | |
| 4 | 7½" | | 14 | 24" |
| 5 | 9" | | 15 | 27" |
| 6 | 10½" | | 16 | 30" |
| 7 | 12" | | 17 | 33" |
| 8 | 13½" | | 18 | 36" |
| 9 | 15" | | 19 | 39" |
| 10 | 16½" | | 20 | 42" |
| 11 | 18" | | 21 | 45" |
| 12 | 19½" | | | |
| 13 | 21" | | | |

Table III. Pressure Test Data

| Series | Cold End Plate | Hot End Plate | Pressure Ratio | Stations Traversed |
|---|---|---|---|---|
| I | a) Solid | b) Orifice | 2.29-2.32 | 2, 8, 14, 18, 21 |
| II | b) Orifice | b) Orifice | 2.30-2.39 | 2, 6, 11, 15, 18, 21 |
| III | b) Orifice | None | 1.99-2.02 | 3, 21 |
| IV | a) Solid | None | 1.98-2.02 | 2, 12, 21 |
| V | b) Orifice | a) Solid | 2.31-2.34 | 2, 15, 21 |
| VI | b) Orifice | c) 21-hole | 2.30-2.36 | 2, 17, 21 |
| VII | b) Orifice | d) 16-hole | 2.30-2.32 | 3, 16, 21 |
| VIII | b) Orifice | d) 60-hole | 2.31-2.33 | 3, 15, 21 |

Blockage details and station positions are given in Tables I and II. Note that all unused pressure taps were blocked during these tests.

Table IV. Temperature Test Data

| Series | Station | Pressure Ratio | Inlet Temperature | Ambient Temperature |
|---|---|---|---|---|
| II | 2 | 2.32-2.33 | 14.0-10.3 | 22.1-21.0 |
| | 15 | 2.33-2.34 | 5.3-4.1 | 18.8-18.3 |
| | 21 | 2.32-2.33 | 14.7-11.5 | 24.7-23.3 |
| III | 1 | 1.99-2.00 | 9.7-7.1 | 23.8-22.7 |
| | 3 | 2.01-2.02 | 9.9-8.6 | 21.6-21.2 |
| | 21 | 1.99-2.00 | 10.3-6.5 | 23.5-23.1 |
| IV | 2 | 2.01-2.02 | 11.6-9.7 | 22.6-22.0 |
| | 12 | 2.01-2.02 | 11.2-10.2 | 22.5-22.0 |
| | 21 | 2.01-2.02 | 11.7-10.8 | 22.4-22.0 |
| V | 2 | 2.31-2.32 | 12.8-11.5 | 25.9-24.8 |
| | 6 | 2.30-2.32 | 15.0-,2.8 | 25.0-24.1 |
| | 15 | 2.31-2.32 | 6.3-5.7 | 20.0-19.3 |
| | 21 | 2.31-2.32 | 12.1-7.0 | 20.4-19.7 |

Temperatures are measured on the Centigrade Scale.

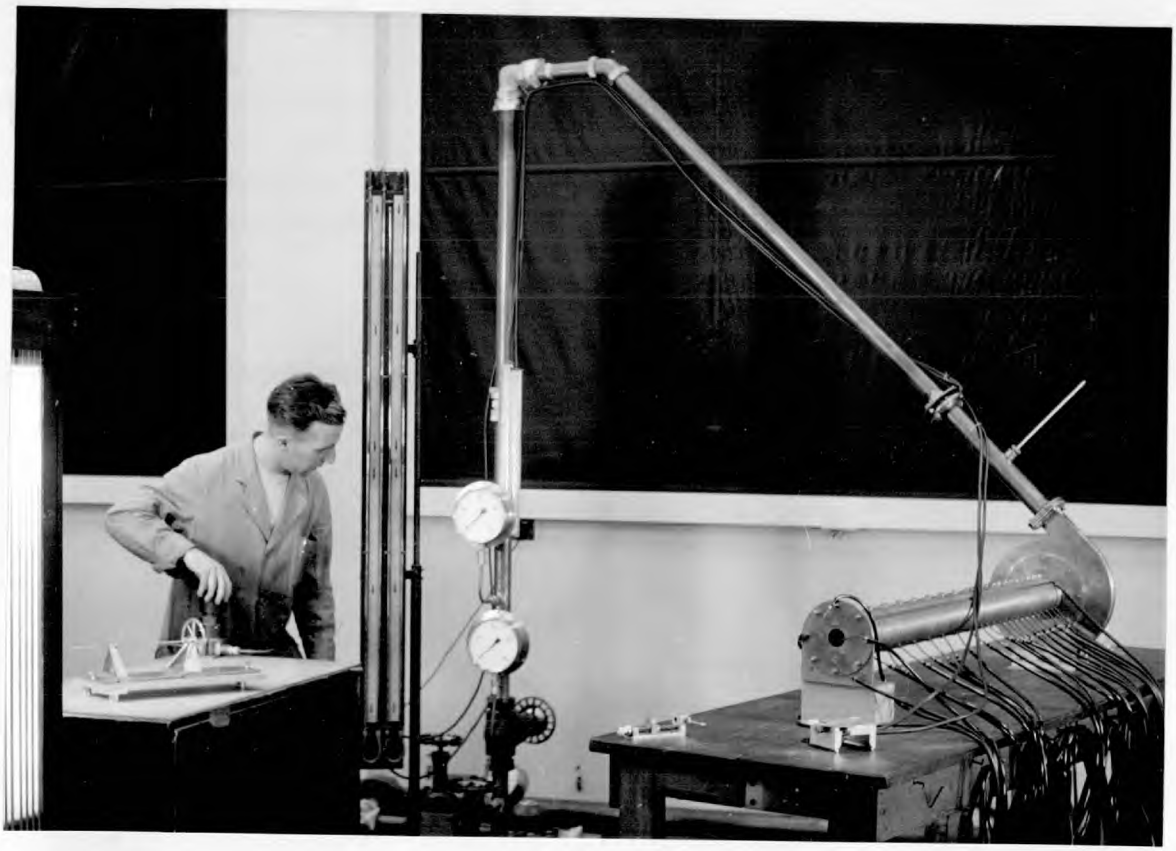


Figure 1. Overall View of Installation

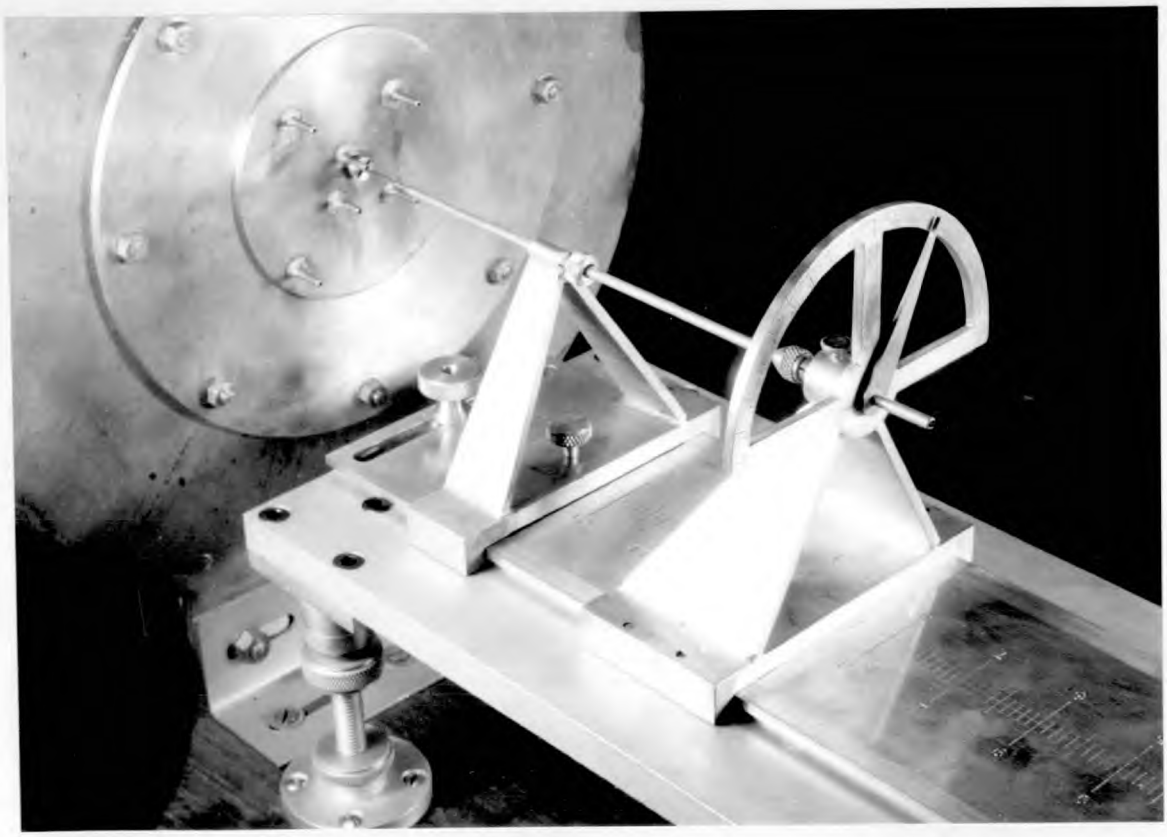


Figure 2. Cold End with Solid End Plate,
Longitudinal Traversing Mechanism

C

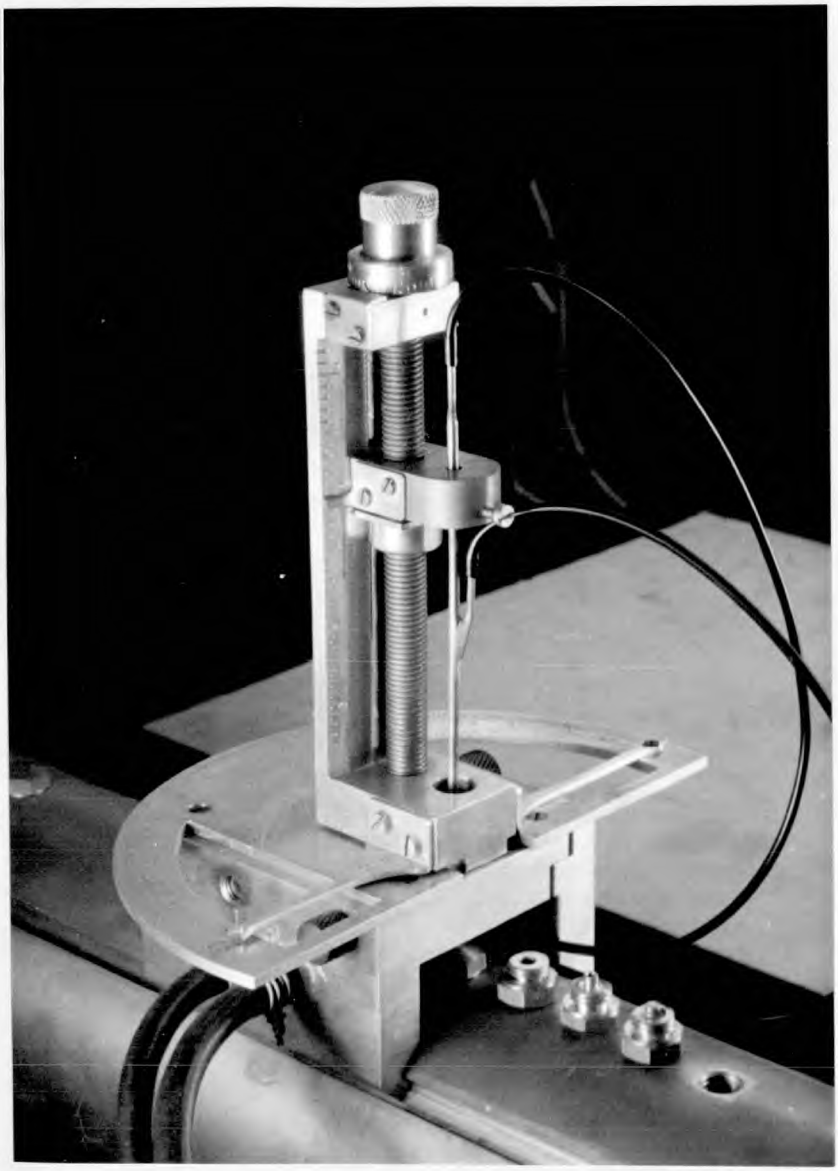


Figure 3. Lateral Traversing Mechanism

Figure 4a. Thermocouple Probe Calibration Curve

(Total and recovery temperatures related to Mach number)

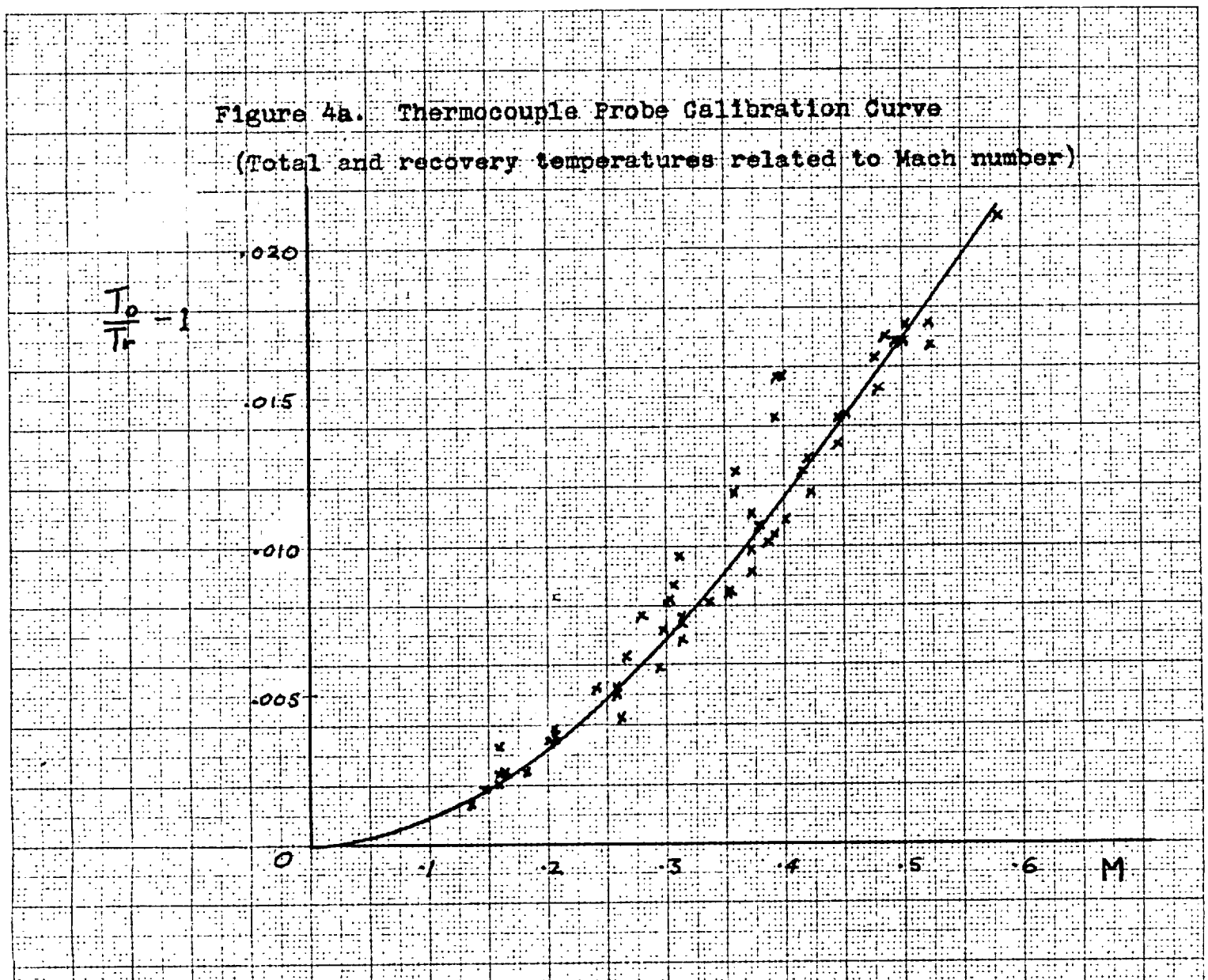



Figure 4b. Temperature Disturbance due to Probe Traversing

(Recovery temperature vs. distance from tube wall)

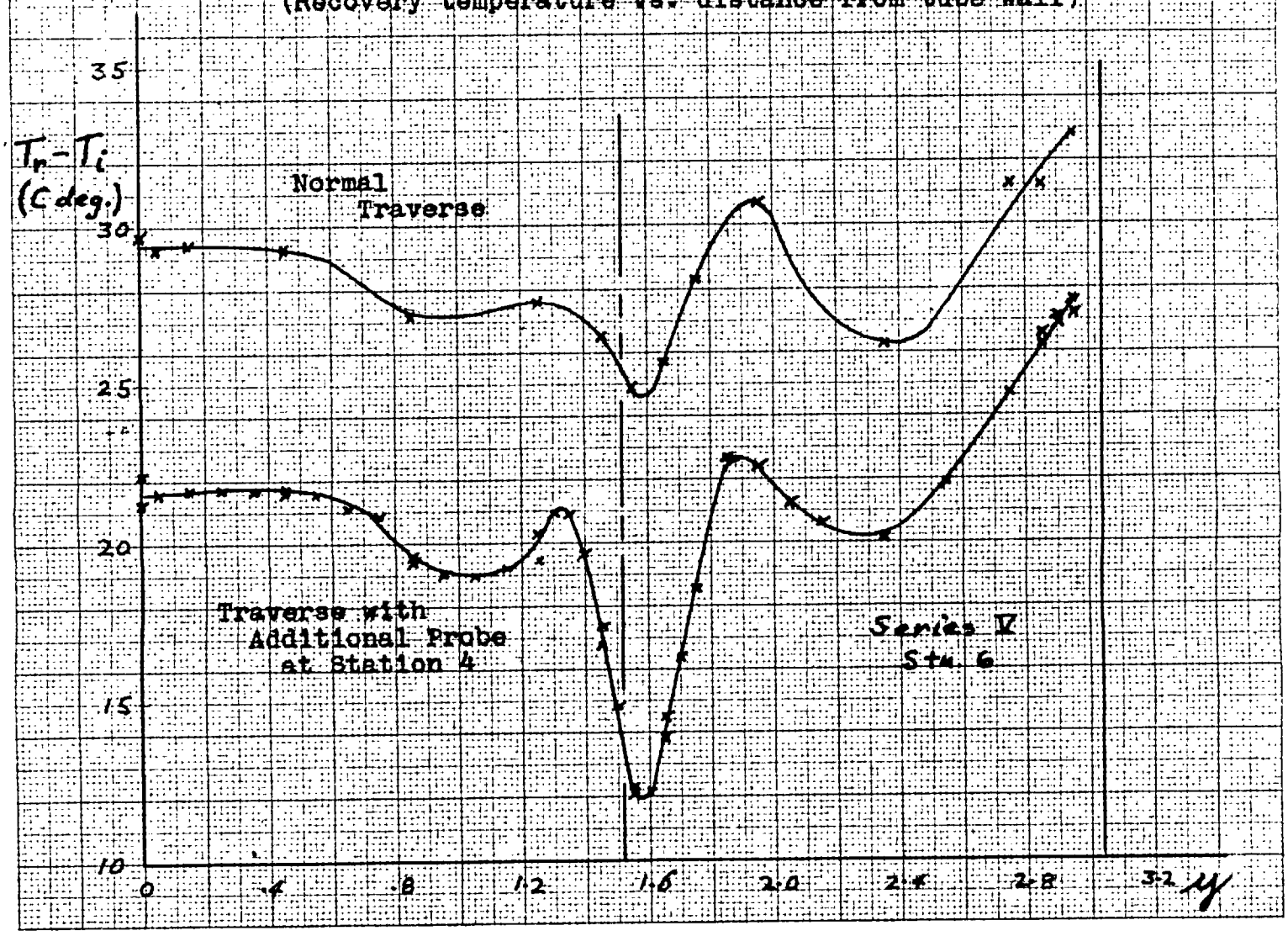
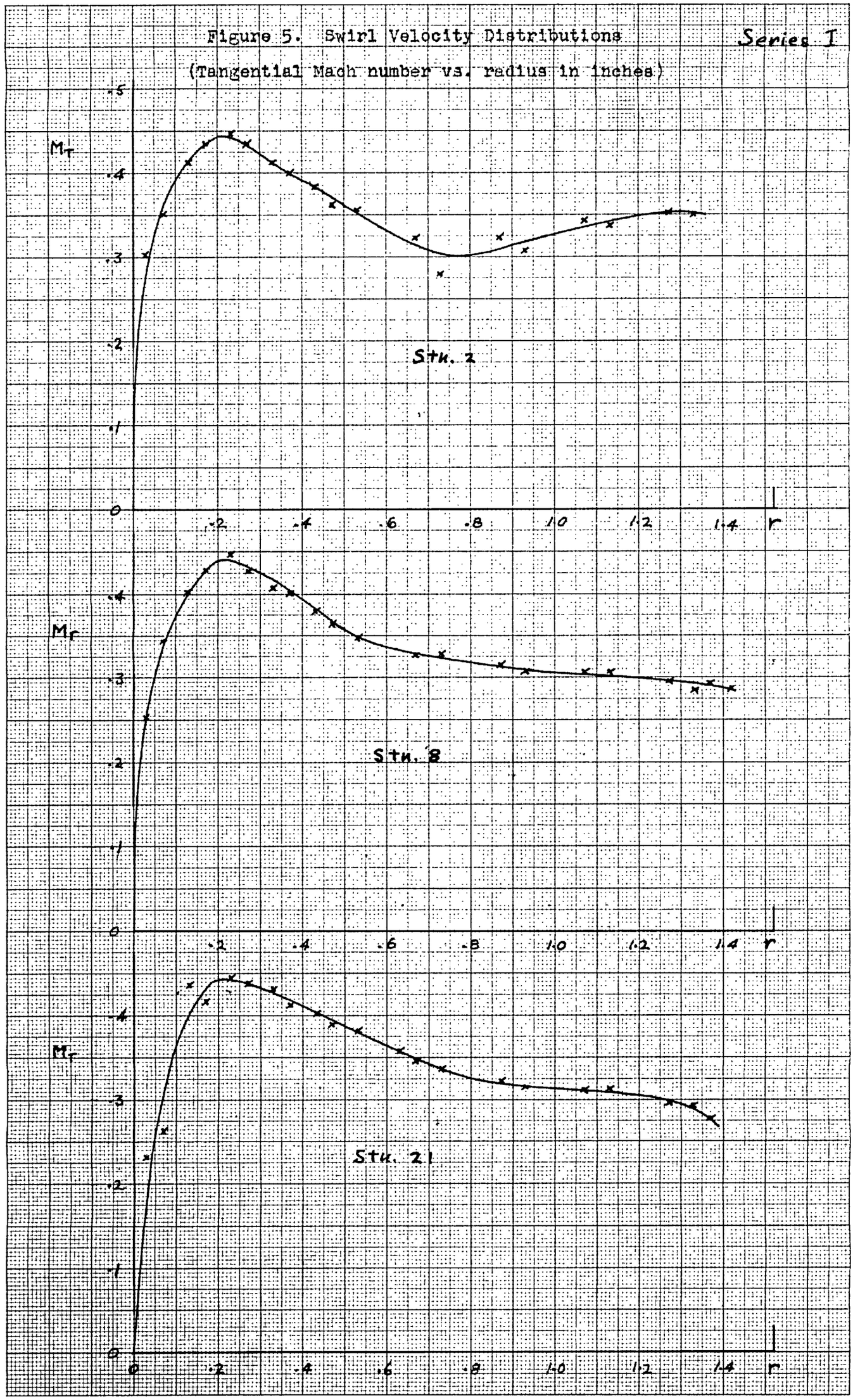


Figure 5. Swirl Velocity Distributions Series I

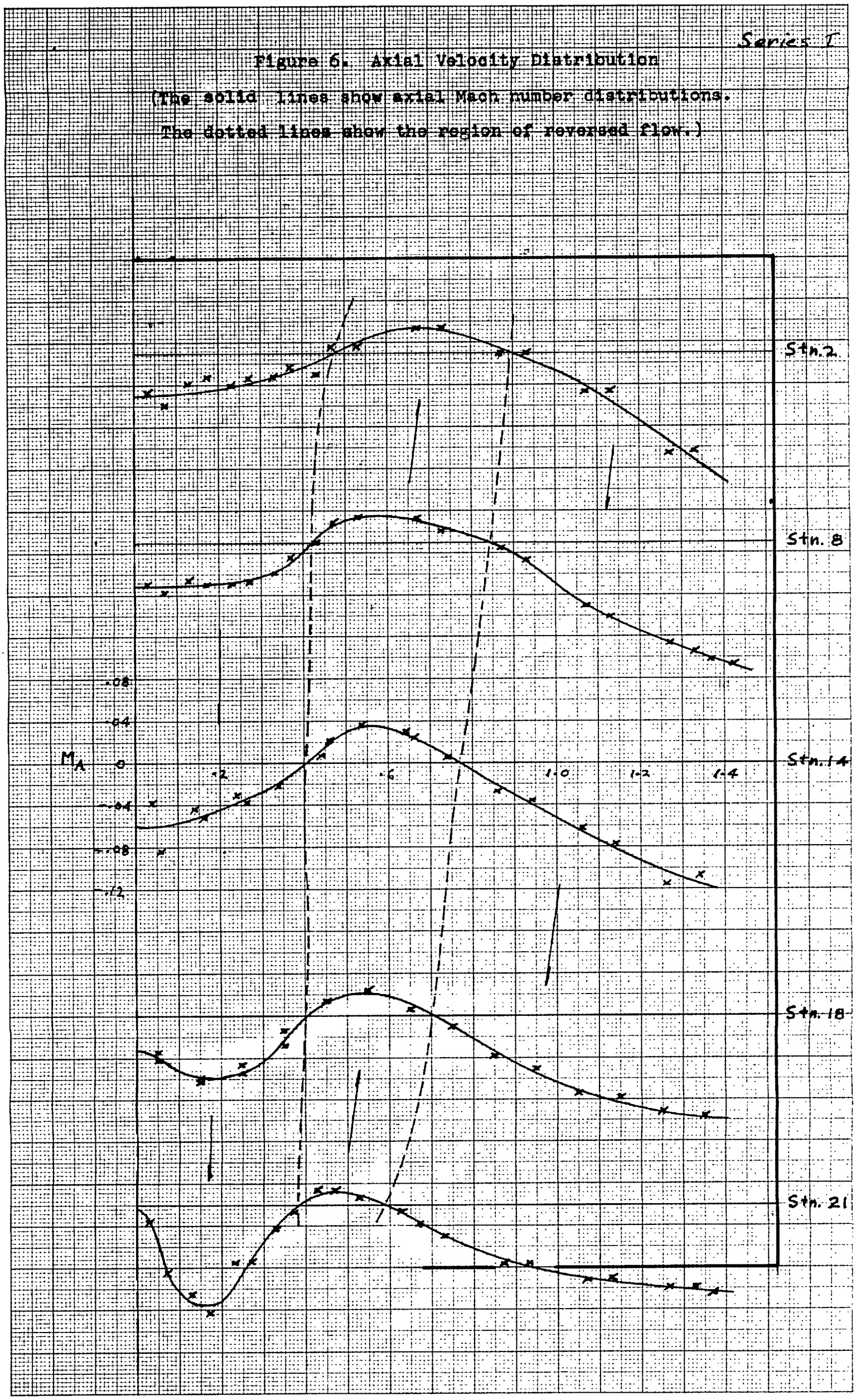
(Tangential Mach number vs. radius in inches)



Series I

Figure 6. Axial Velocity Distribution

(The solid lines show axial Mach number distributions.
The dotted lines show the region of reversed flow.)



Series I

Figure 7. Pressure Distribution

(The solid lines are isobars; gauge pressures in inches of mercury are indicated at their ends. The dotted lines show the region of reversed flow.)

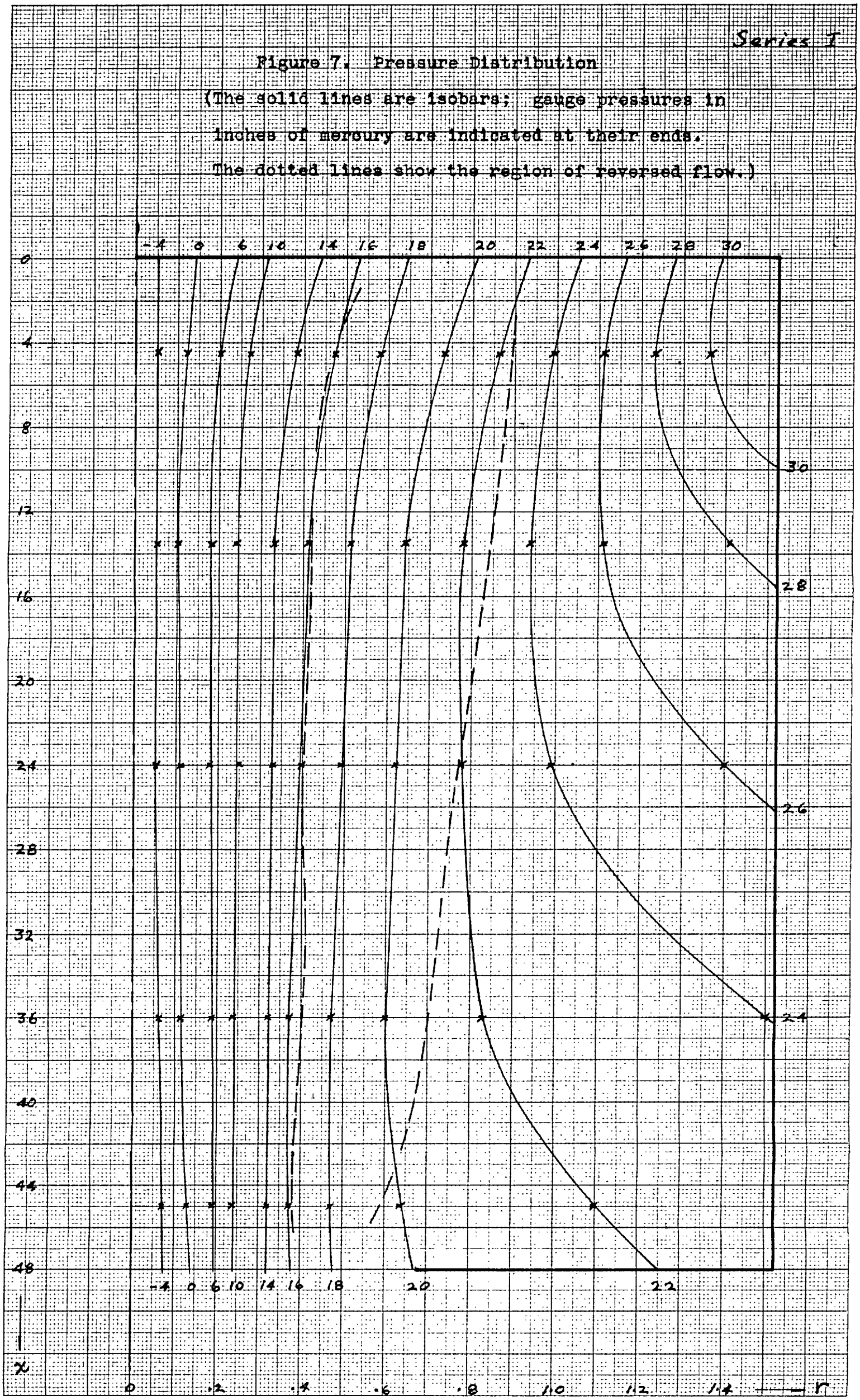
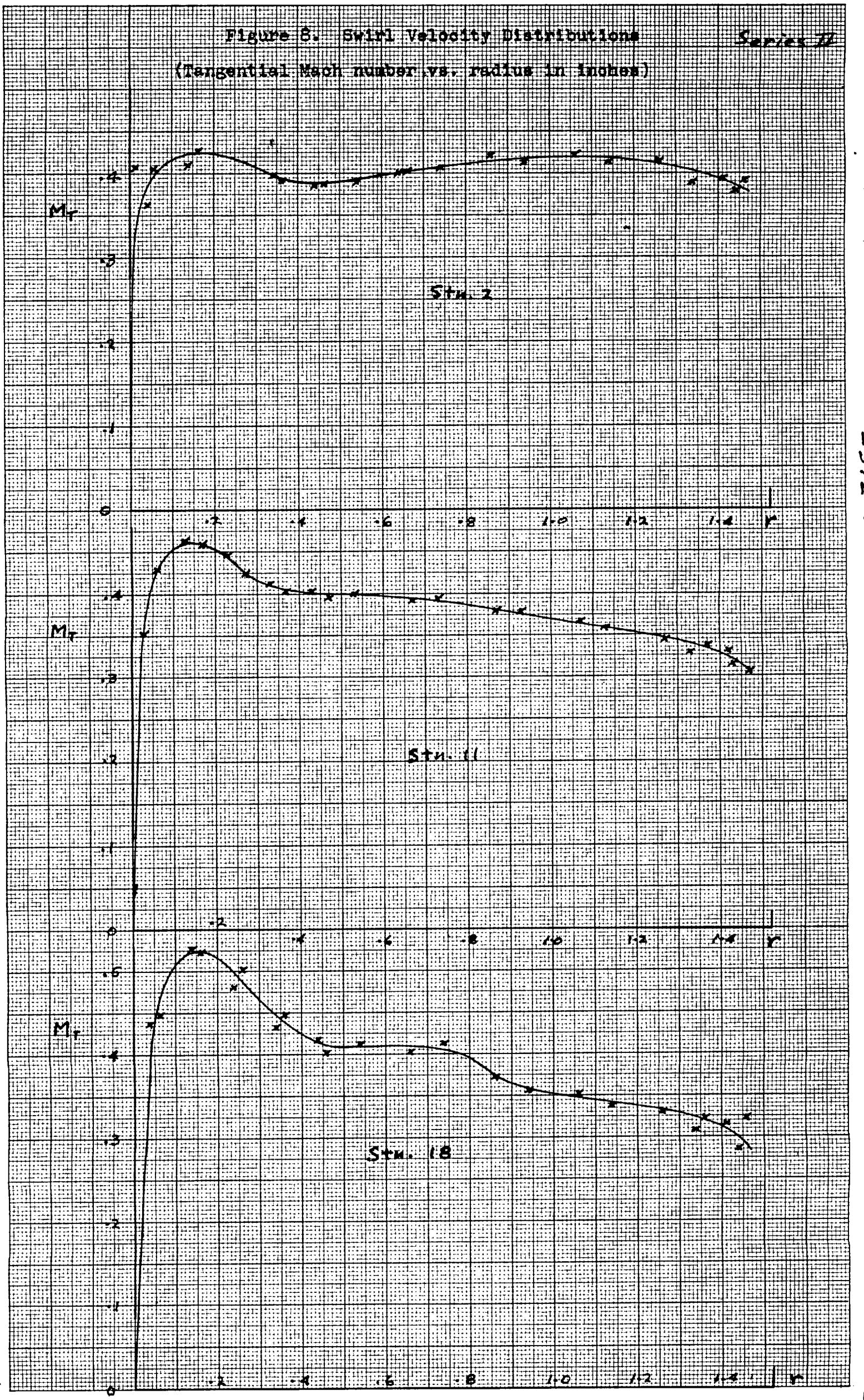


Figure 8. Swirl Velocity Distributions Series II

(Tangential Mach number vs. radius in inches)

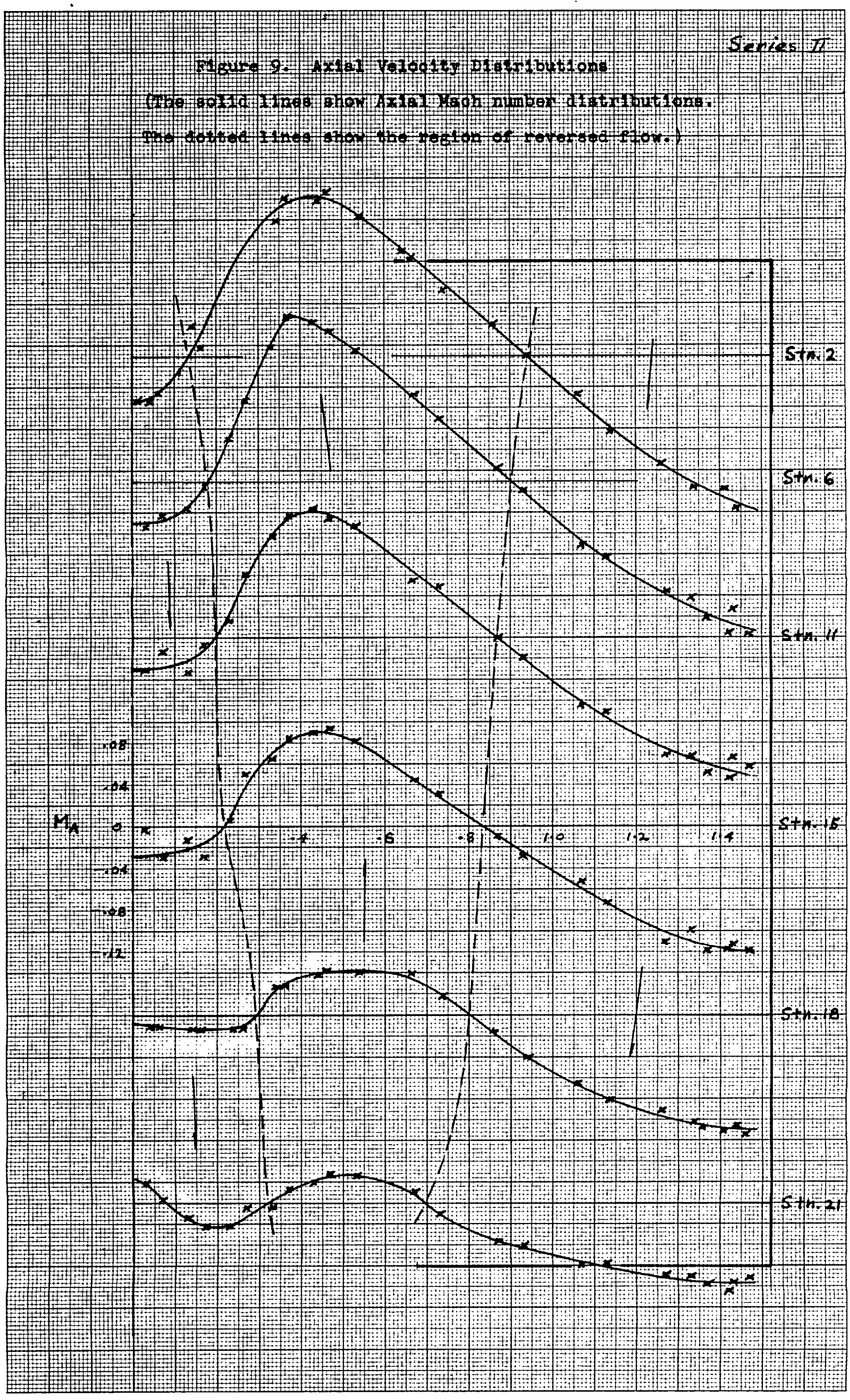


Series II

Figure 9. Axial Velocity Distributions

(The solid lines show Axial Mach number distributions.

The dotted lines show the region of reversed flow.)



Series II

Figure 10. Pressure Distribution

(The solid lines are isobars; at their ends gauge pressures in inches of mercury are indicated. The dotted lines show the region of reversed flow.)

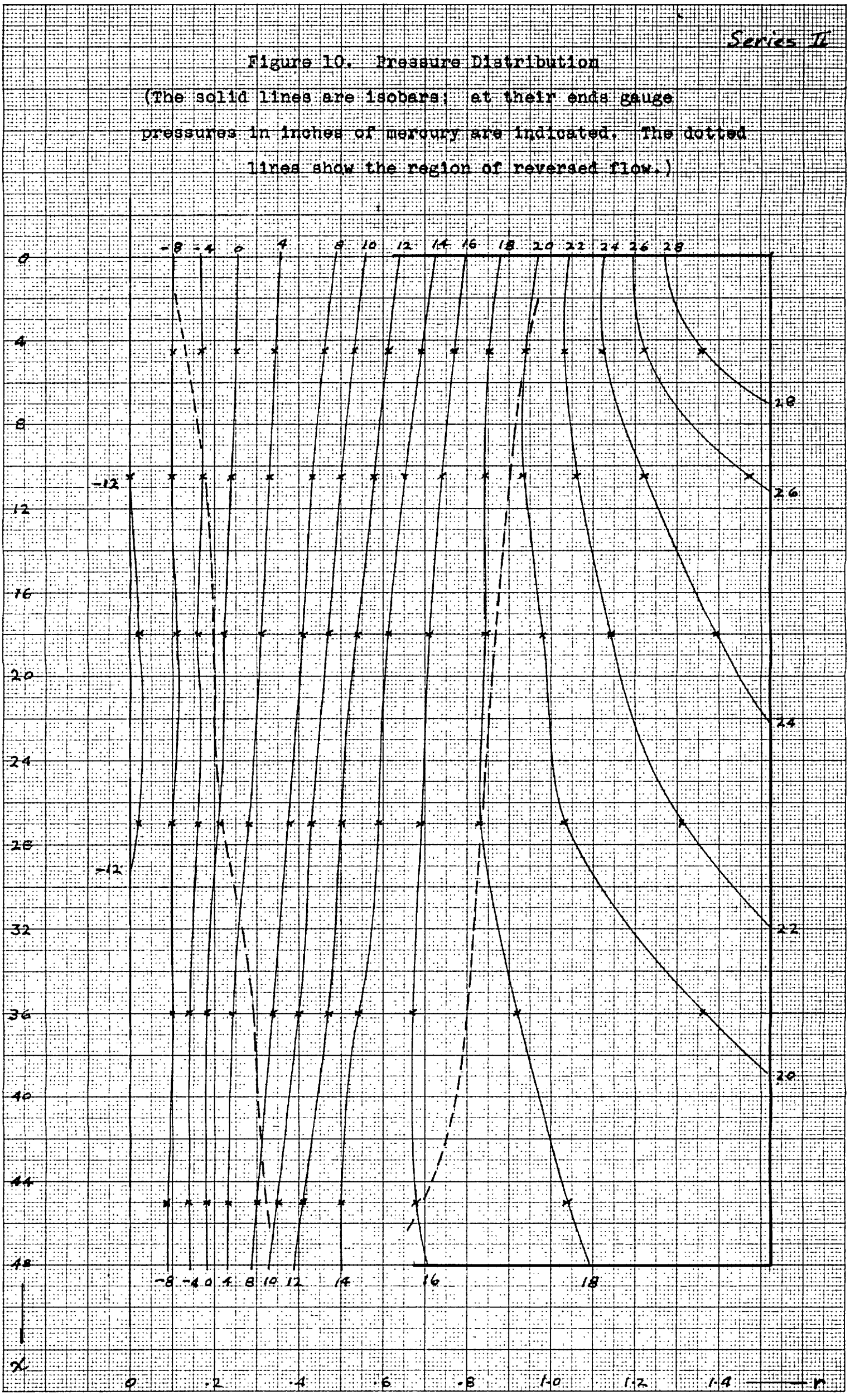


Figure 11a. Velocity Distributions

(Tangential and Axial Mach numbers vs. radius in inches)

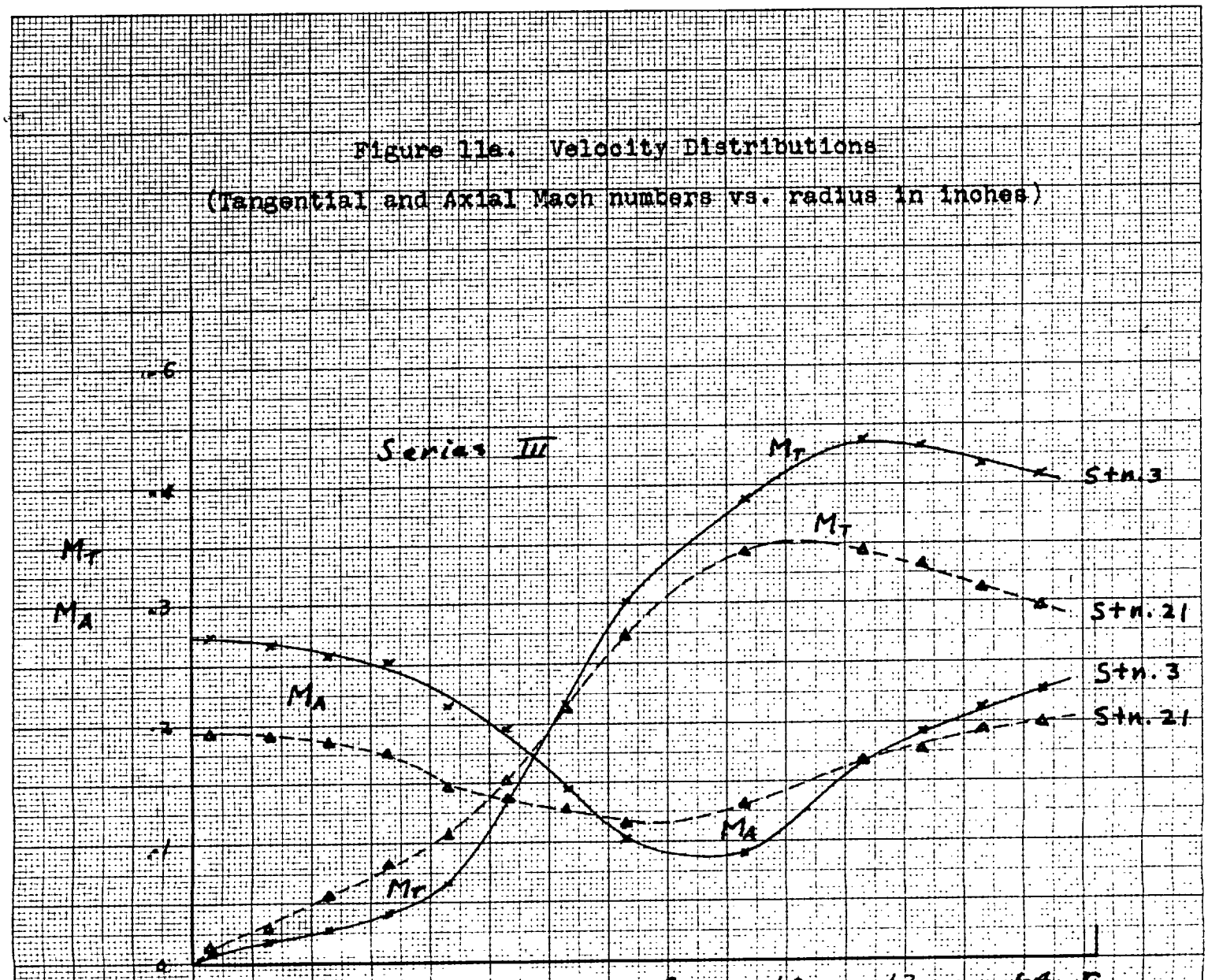
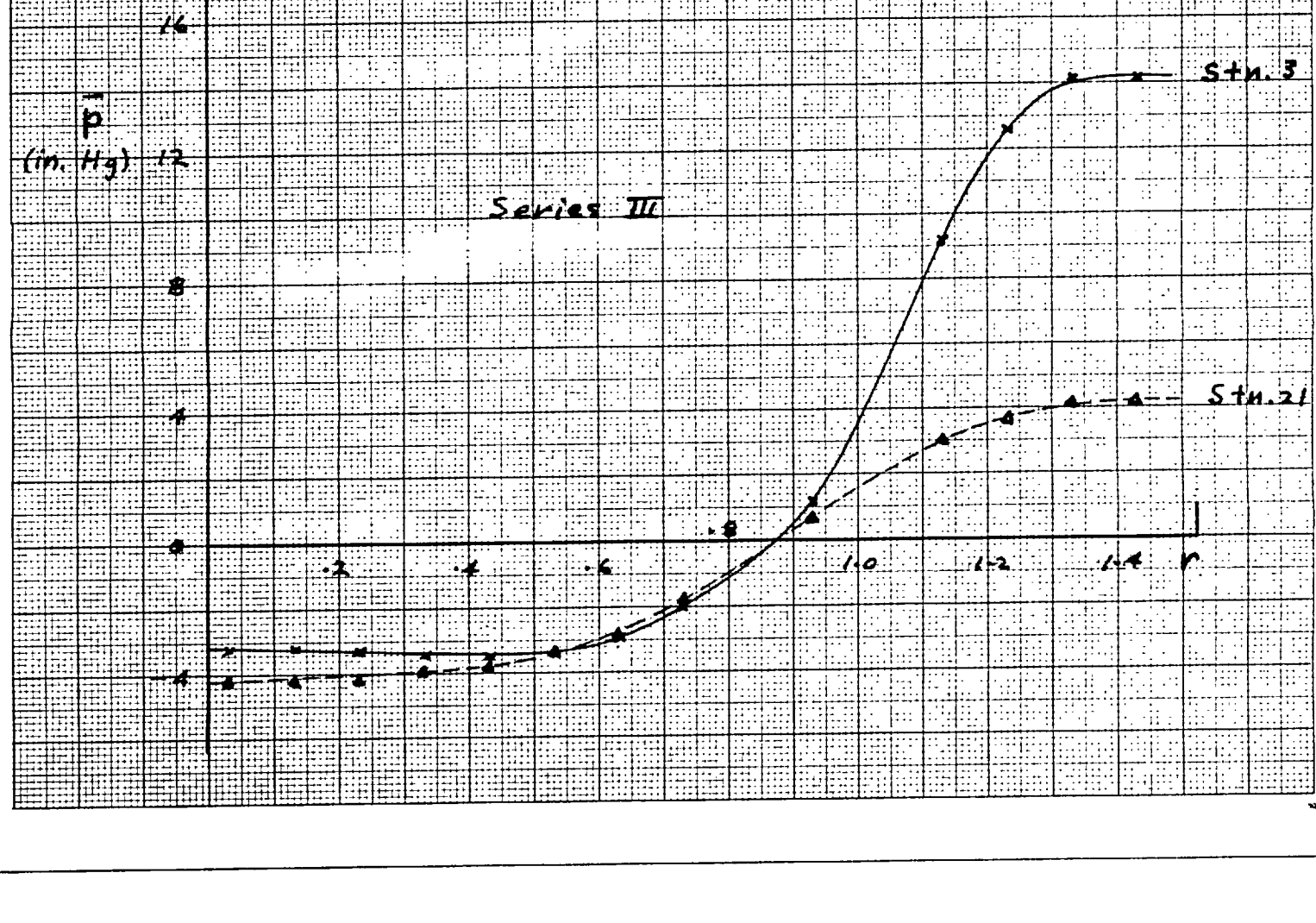



Figure 11b. Pressure Distributions

(Gauge pressure in inches of mercury vs. radius in inches.)



Series IV

Figure 12. Velocity Distributions

(Tangential and axial Mach number distributions vs. radius in inches.)

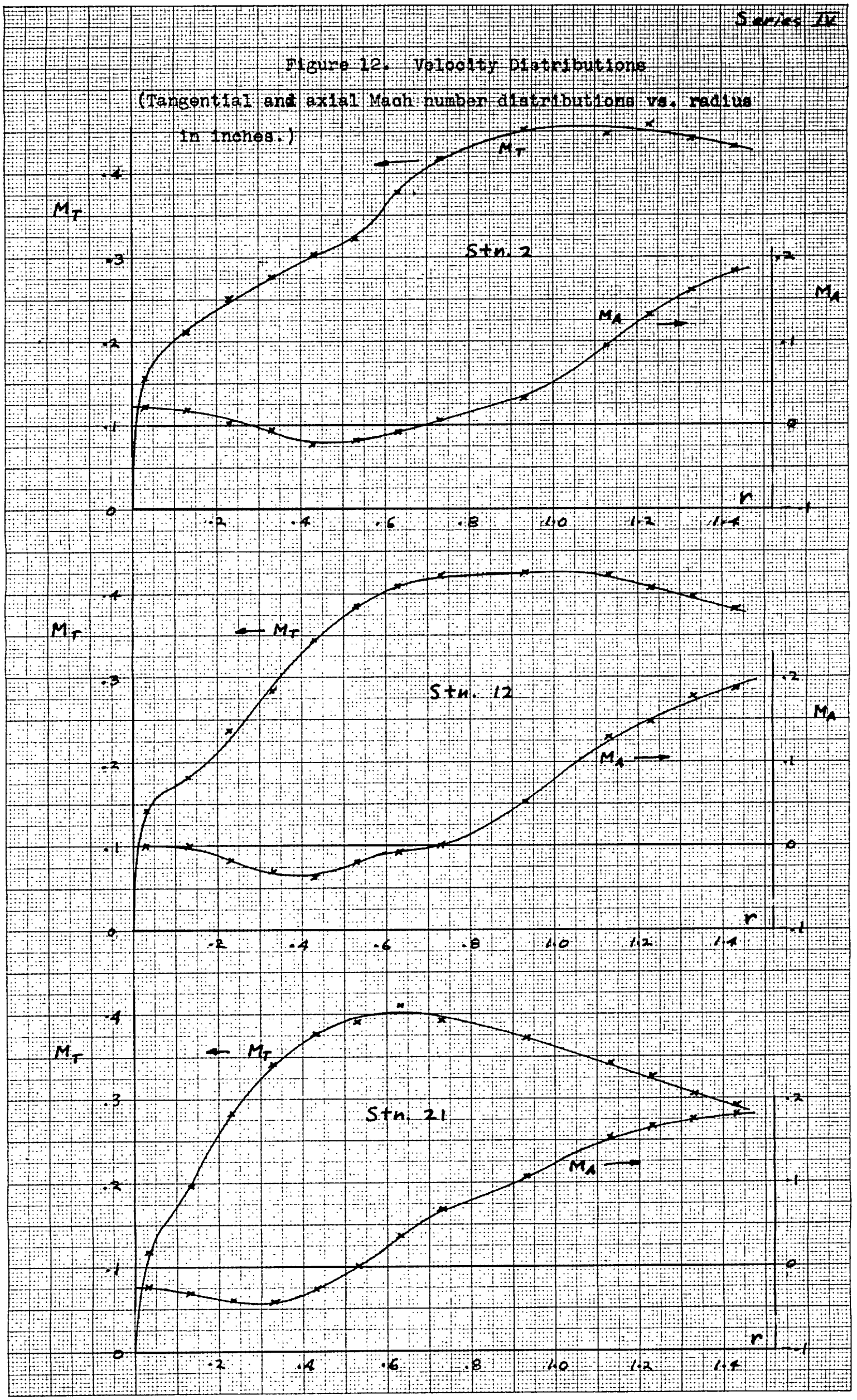
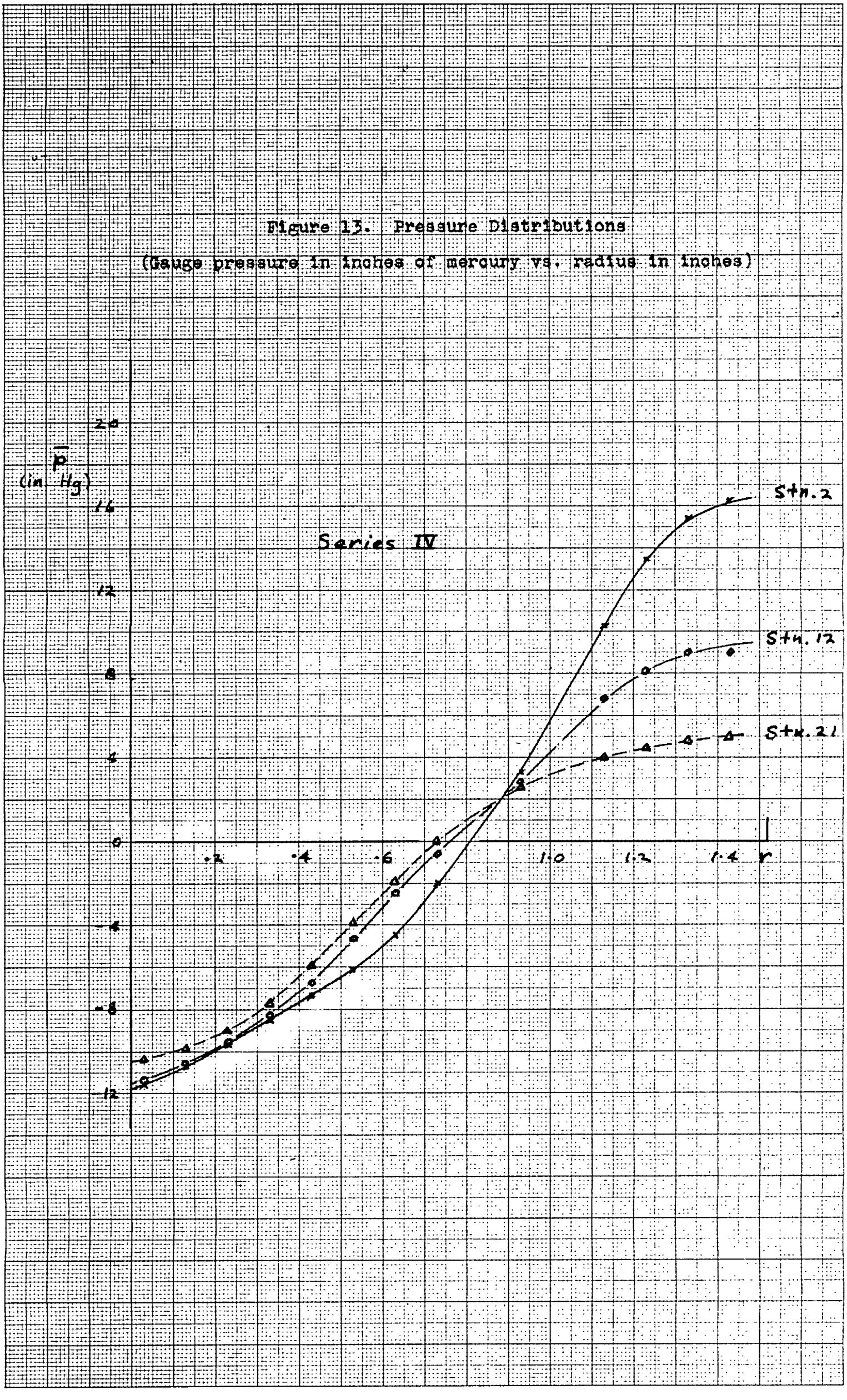


Figure 13. Pressure Distributions

(Gauge pressure in inches of mercury vs. radius in inches)



Series V

Figure 14. Velocity Distributions

(Tangential and Axial Mach number distributions vs. radius in inches)

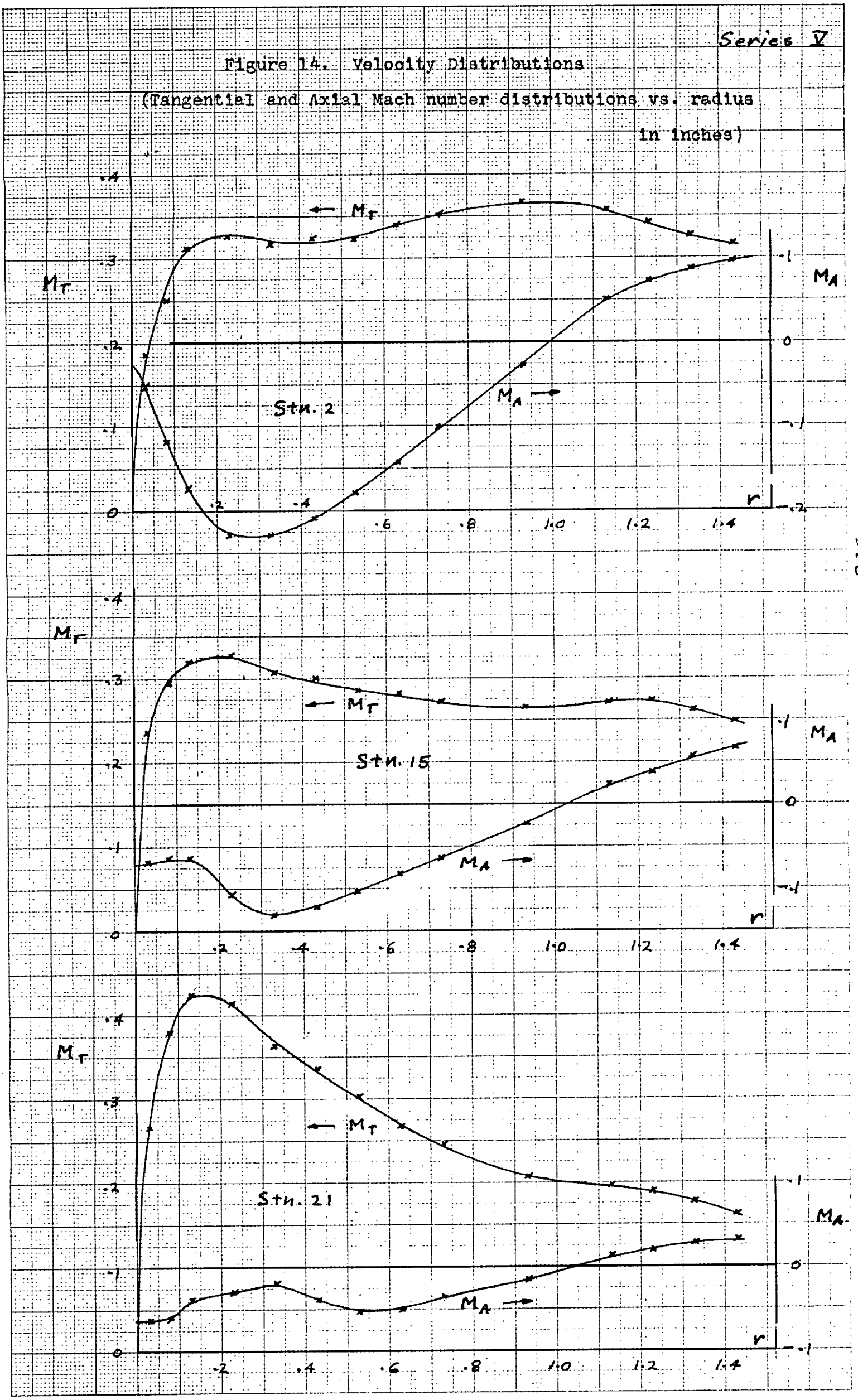
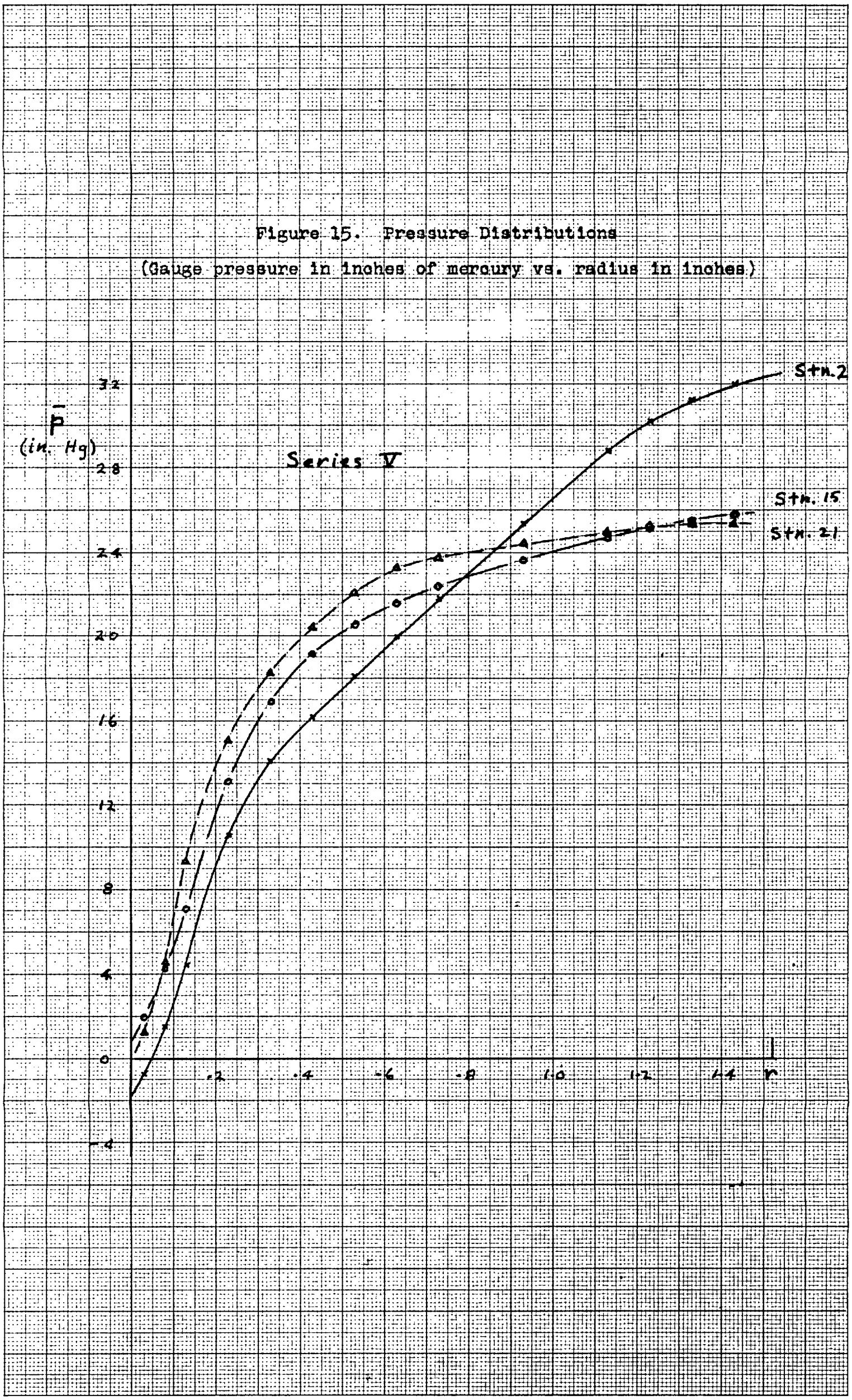


Figure 15. Pressure Distributions

(Gauge pressure in inches of mercury vs. radius in inches)



Series VI

Figure 16. Velocity Distributions

(Tangential and Axial Mach numbers vs. radius in inches)

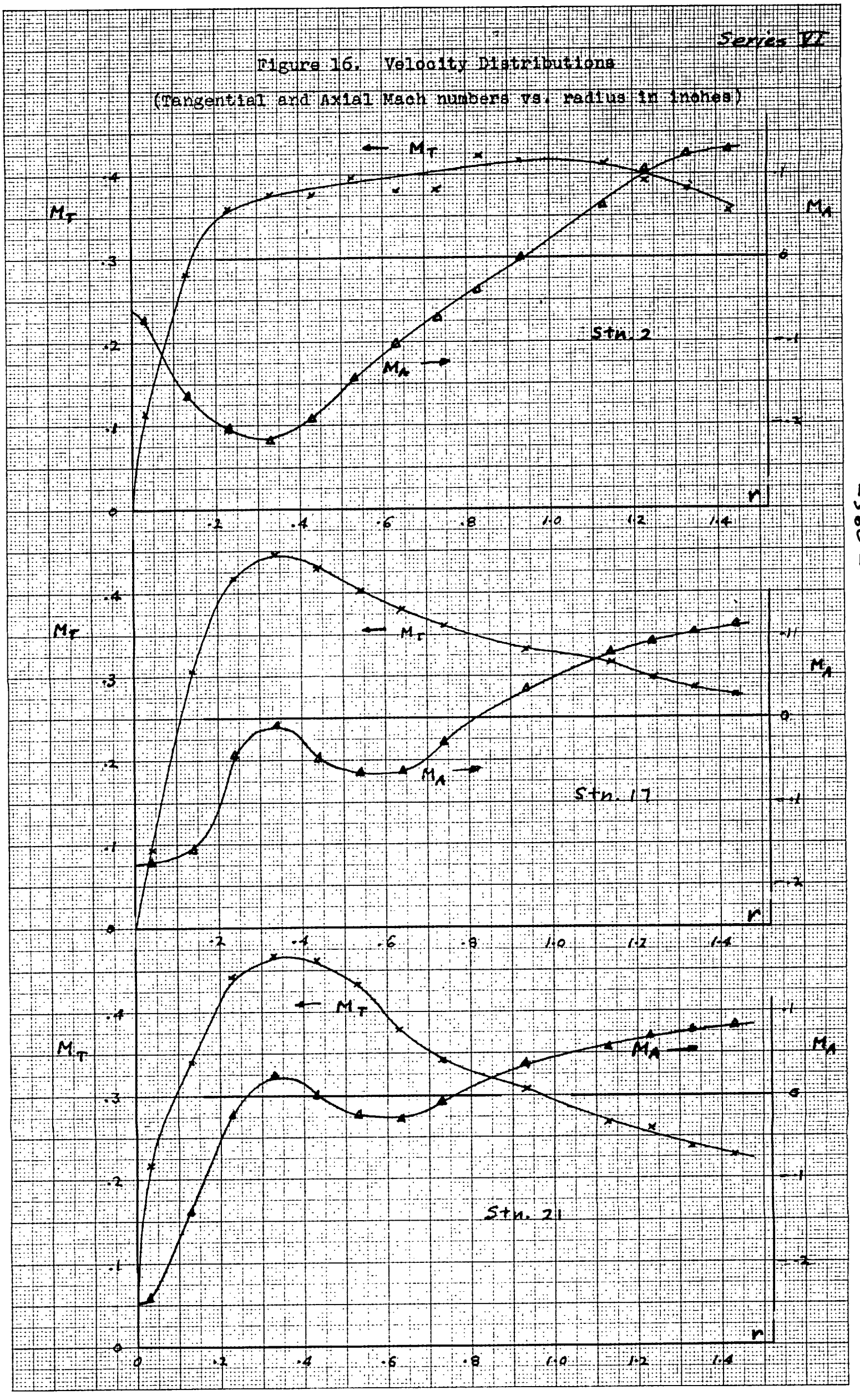
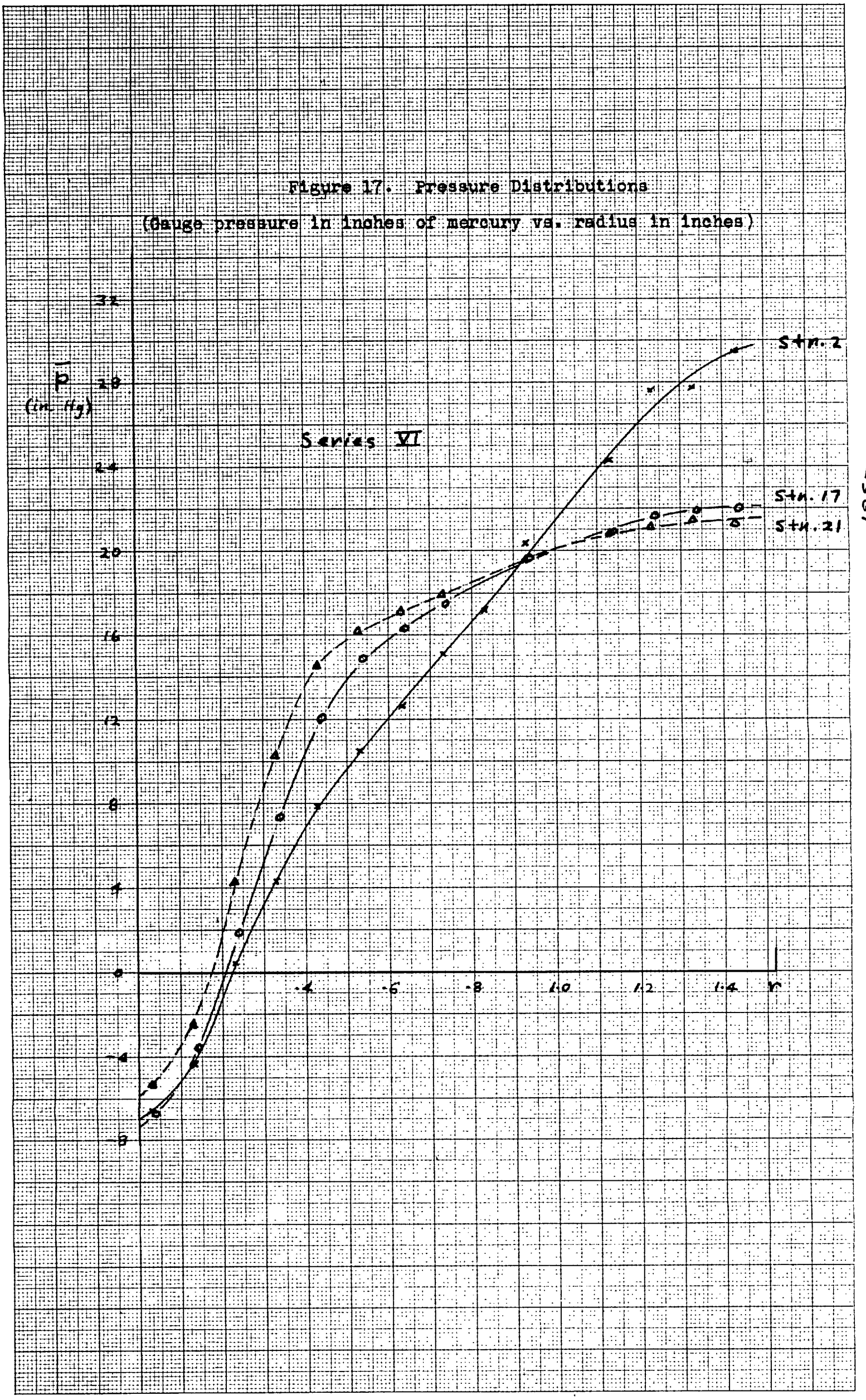


Figure 17. Pressure Distributions

(Gauge pressure in inches of mercury vs. radius in inches)



Series VII

Figure 18. Velocity Distributions

(Tangential and Axial Mach number vs. radius in inches)

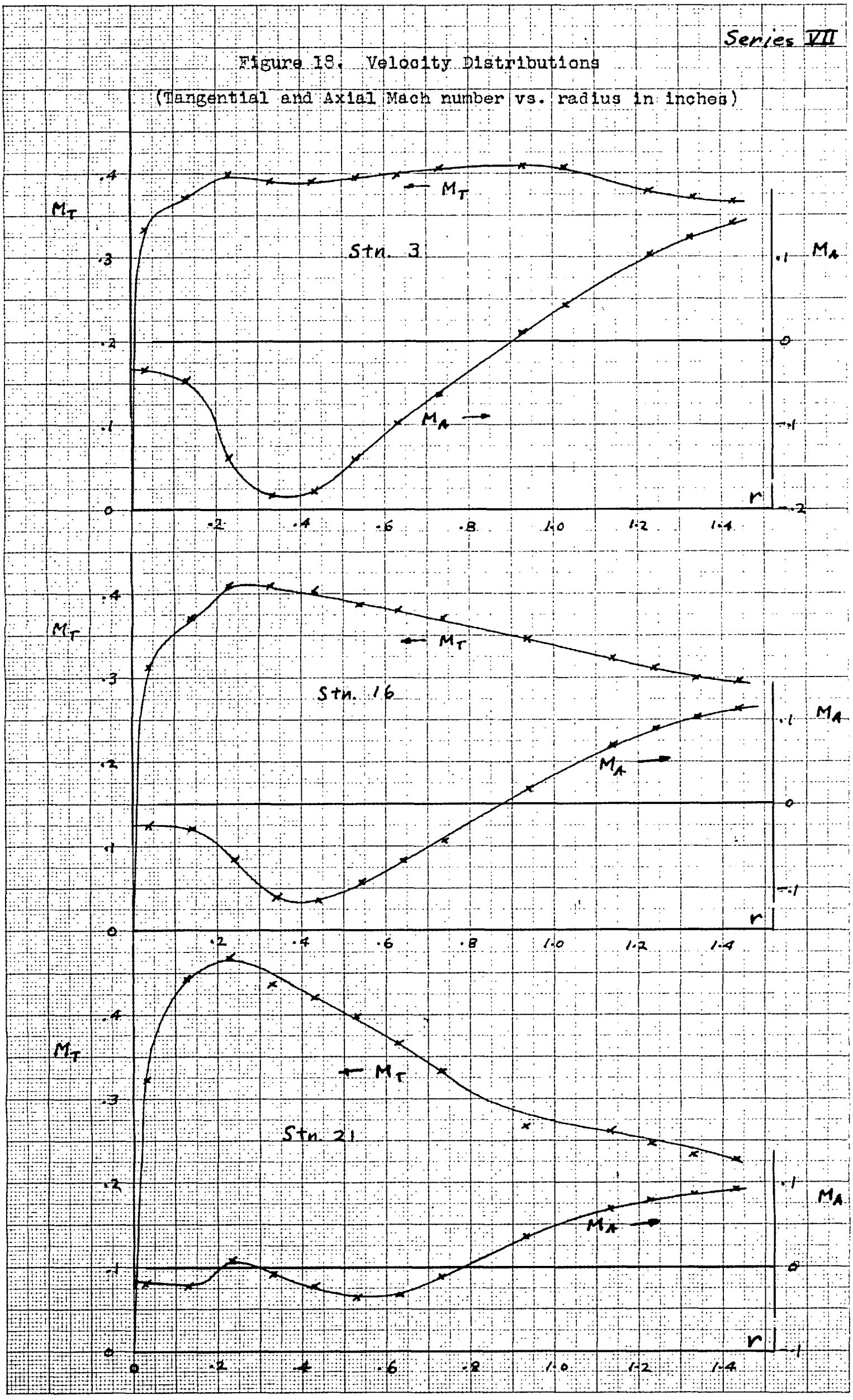
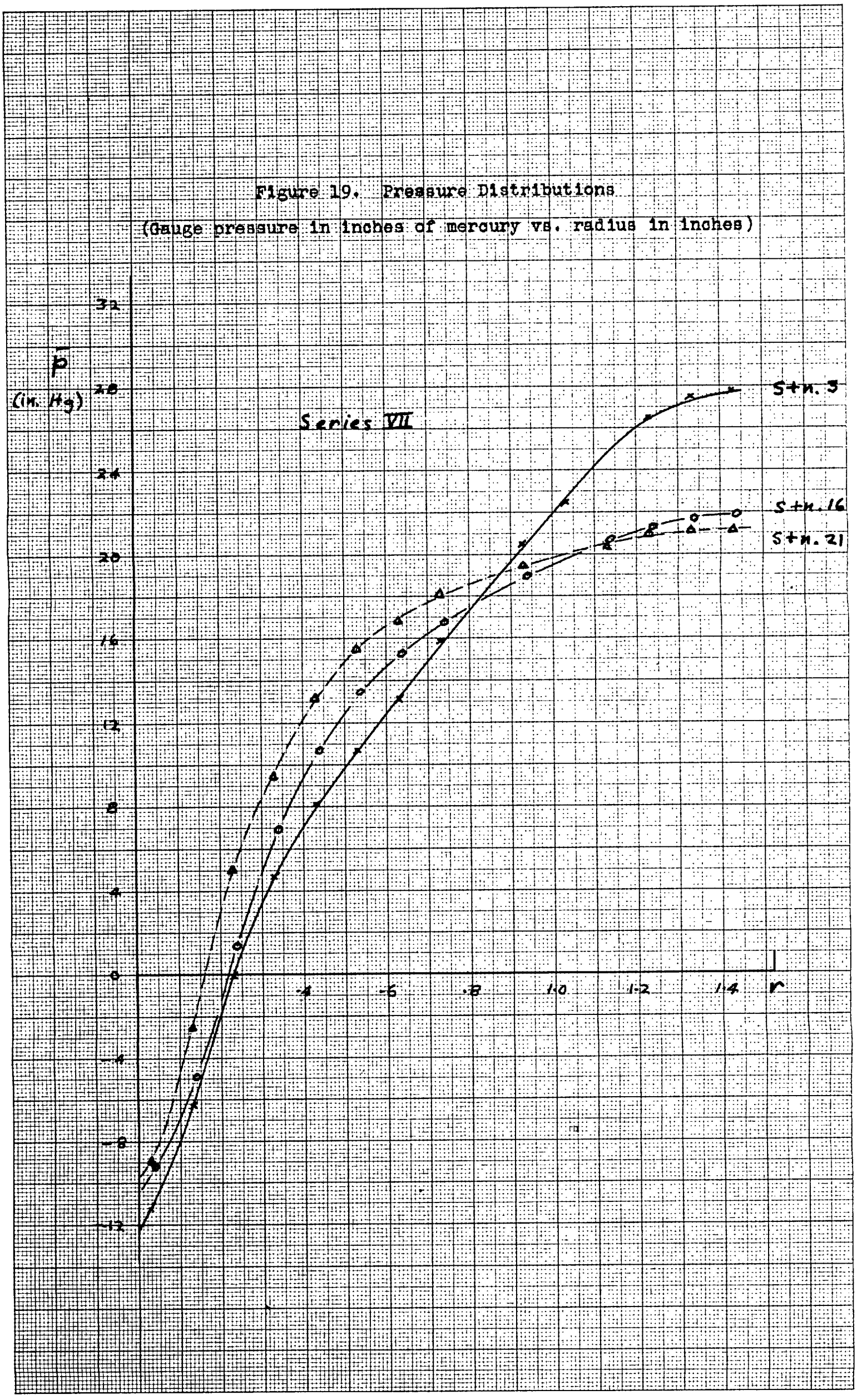


Figure 19. Pressure Distributions

(Gauge pressure in inches of mercury vs. radius in inches)

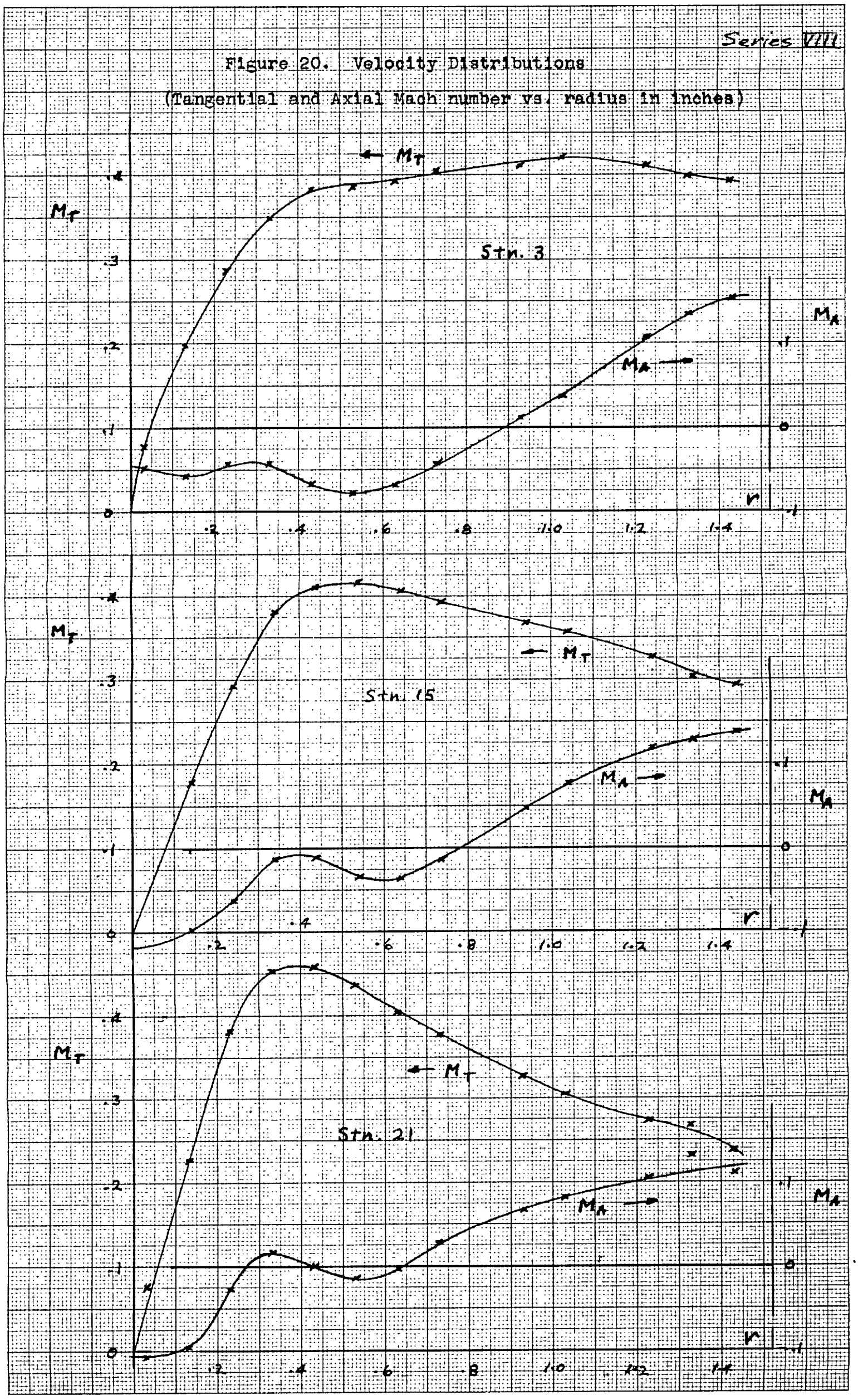



13851

Series VIII

Figure 20. Velocity Distributions

(Tangential and Axial Mach number vs. radius in inches)




13841

Figure 21. Pressure Distributions

(Gauge pressure in inches of mercury vs. radius in inches)

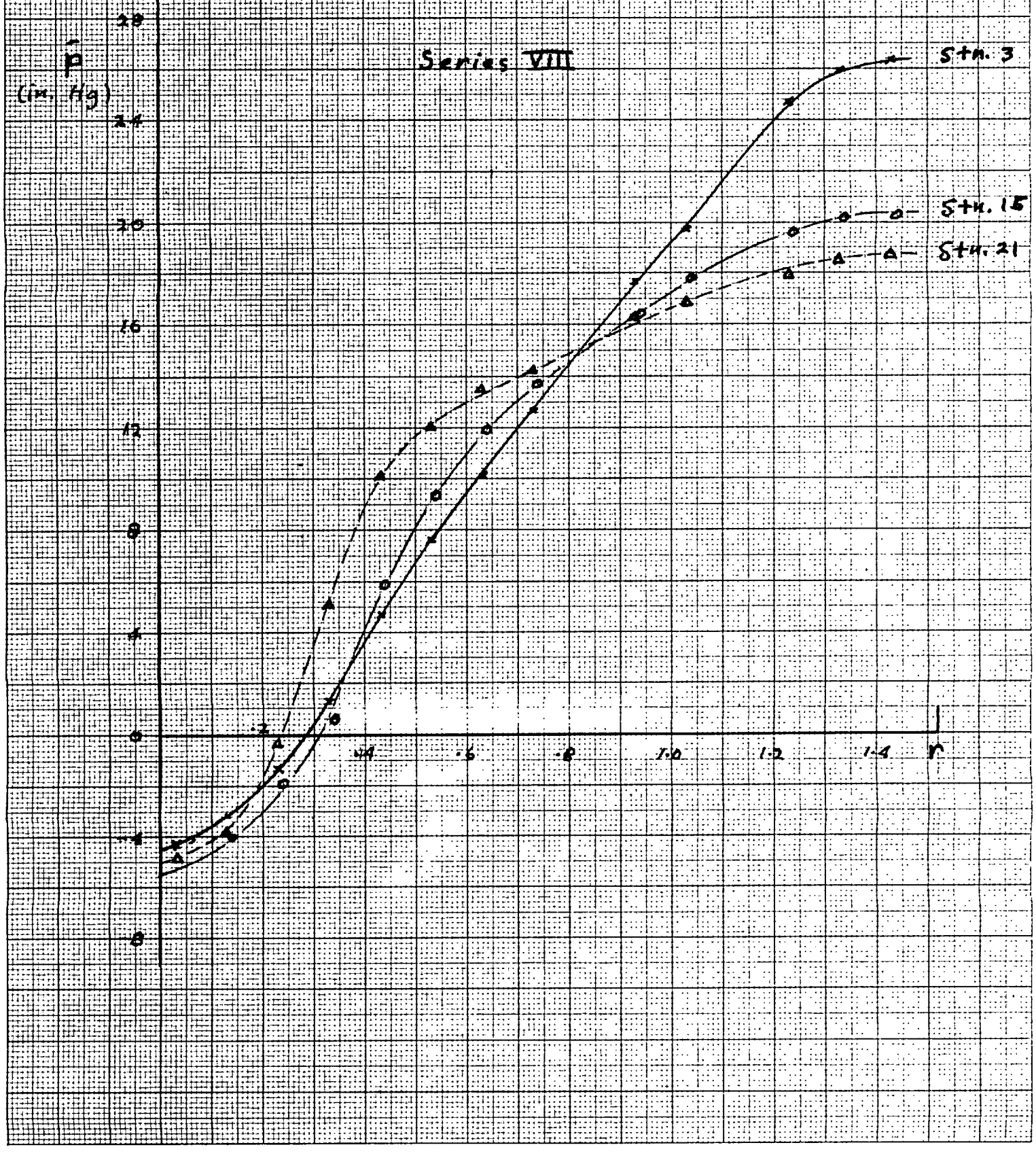


Figure 22. Recovery Temperature Distributions

(Temperature increment vs. distance from wall in inches)

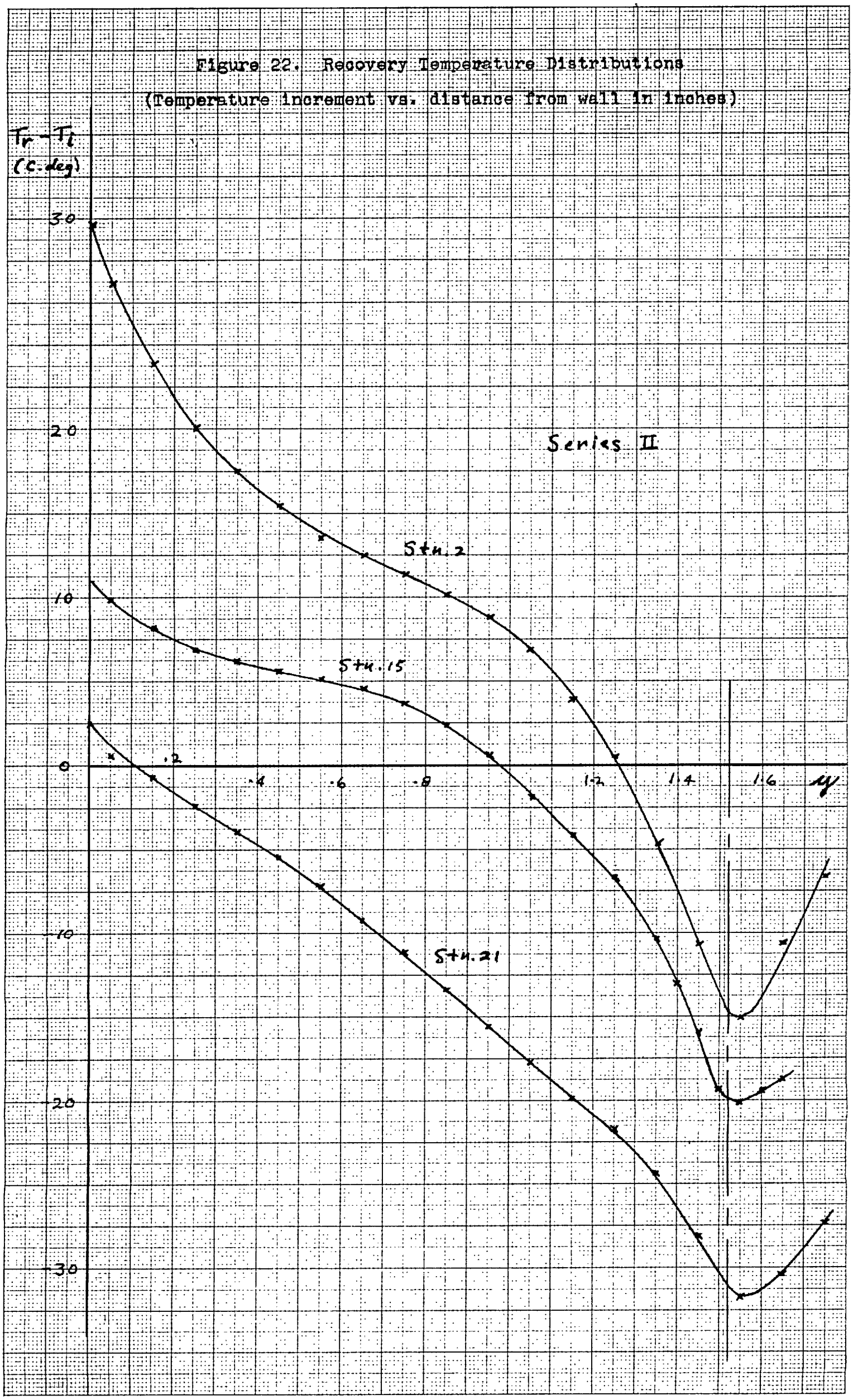


Figure 23. Recovery Temperature Distributions

(Temperature increment vs. distance from wall in inches)

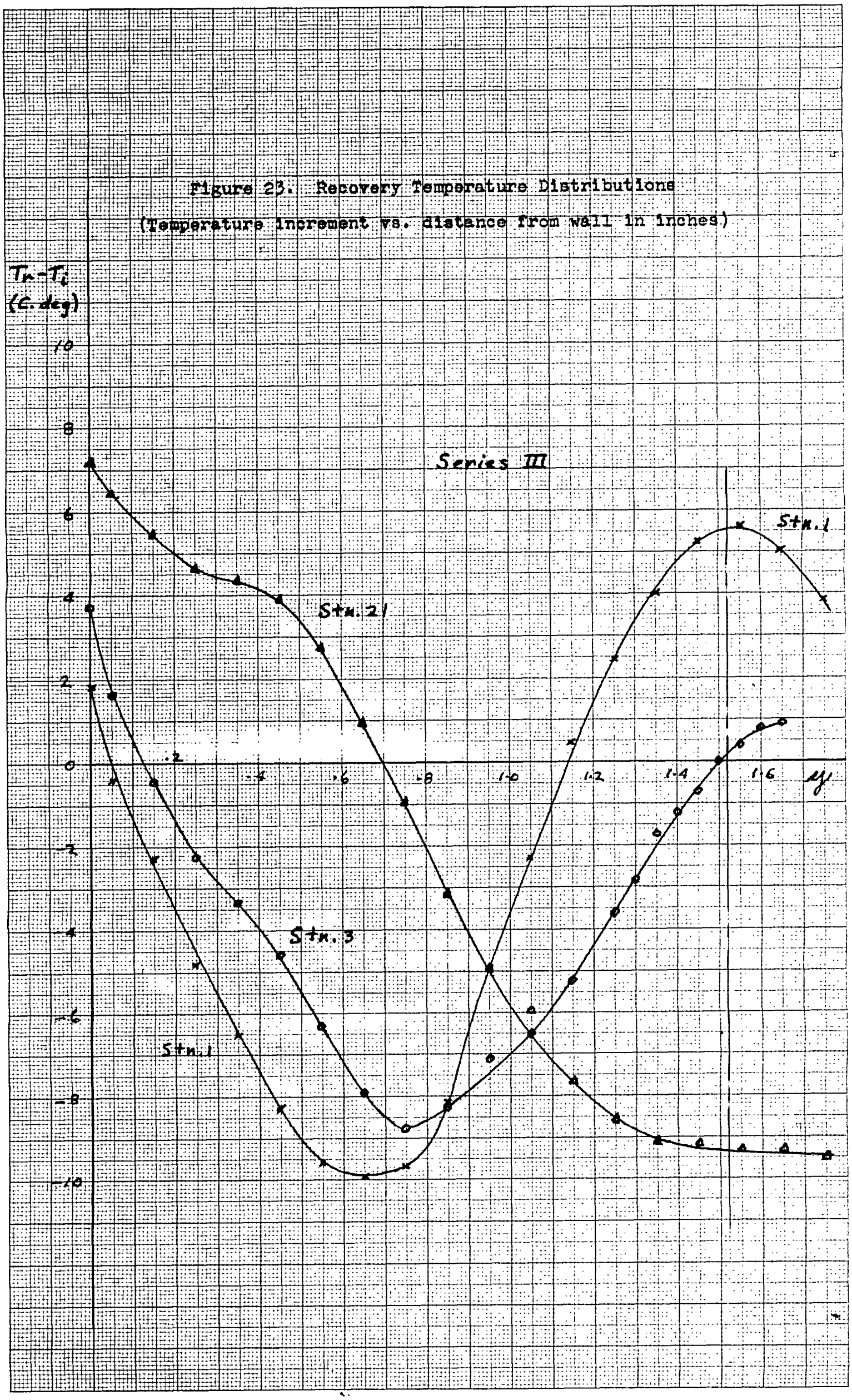


Figure 24. Recovery Temperature Distributions

(Temperature increment vs. distance from wall in inches)

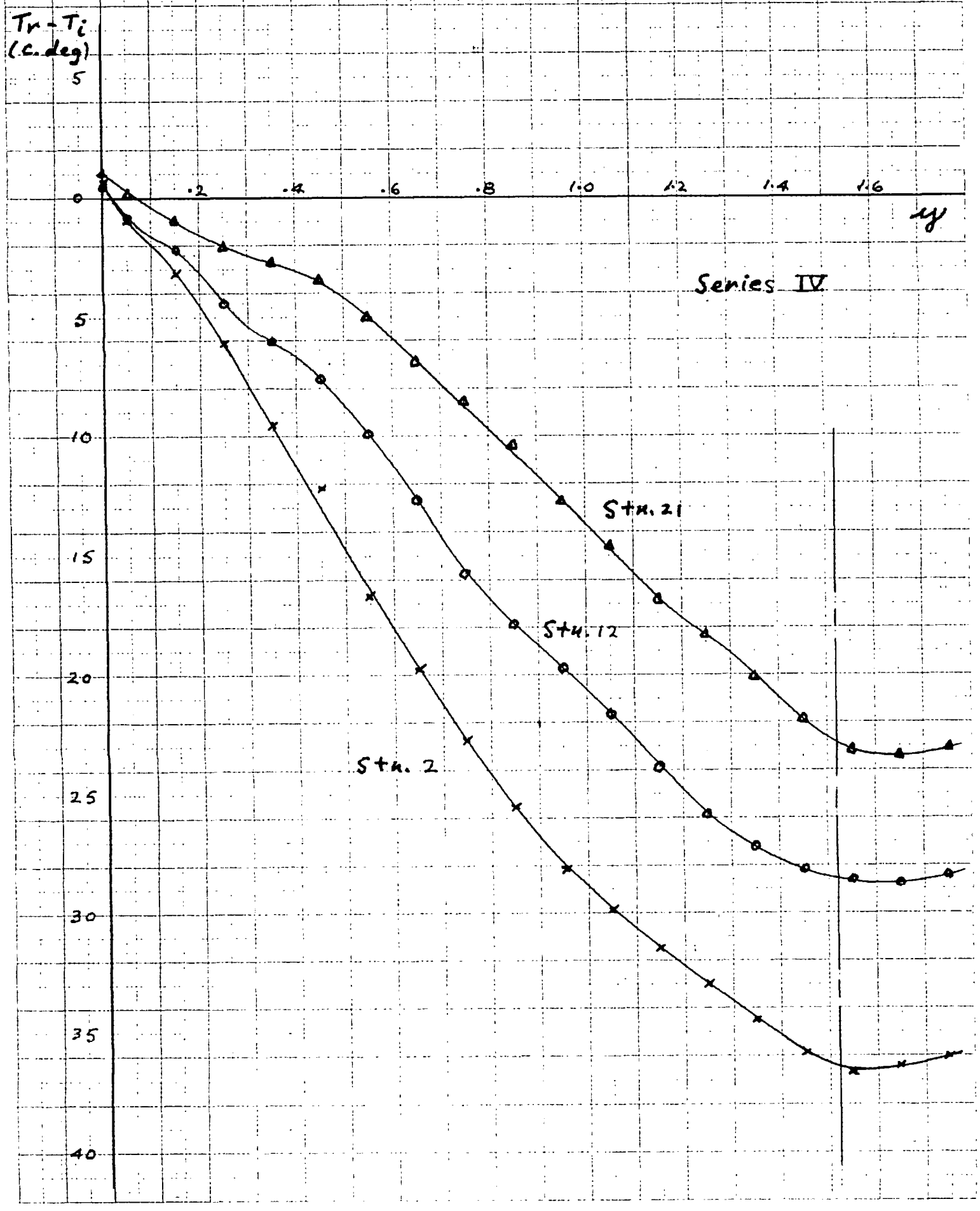


Figure 25. Recovery Temperature Distributions

(Temperature increment vs. distance from wall in inches)

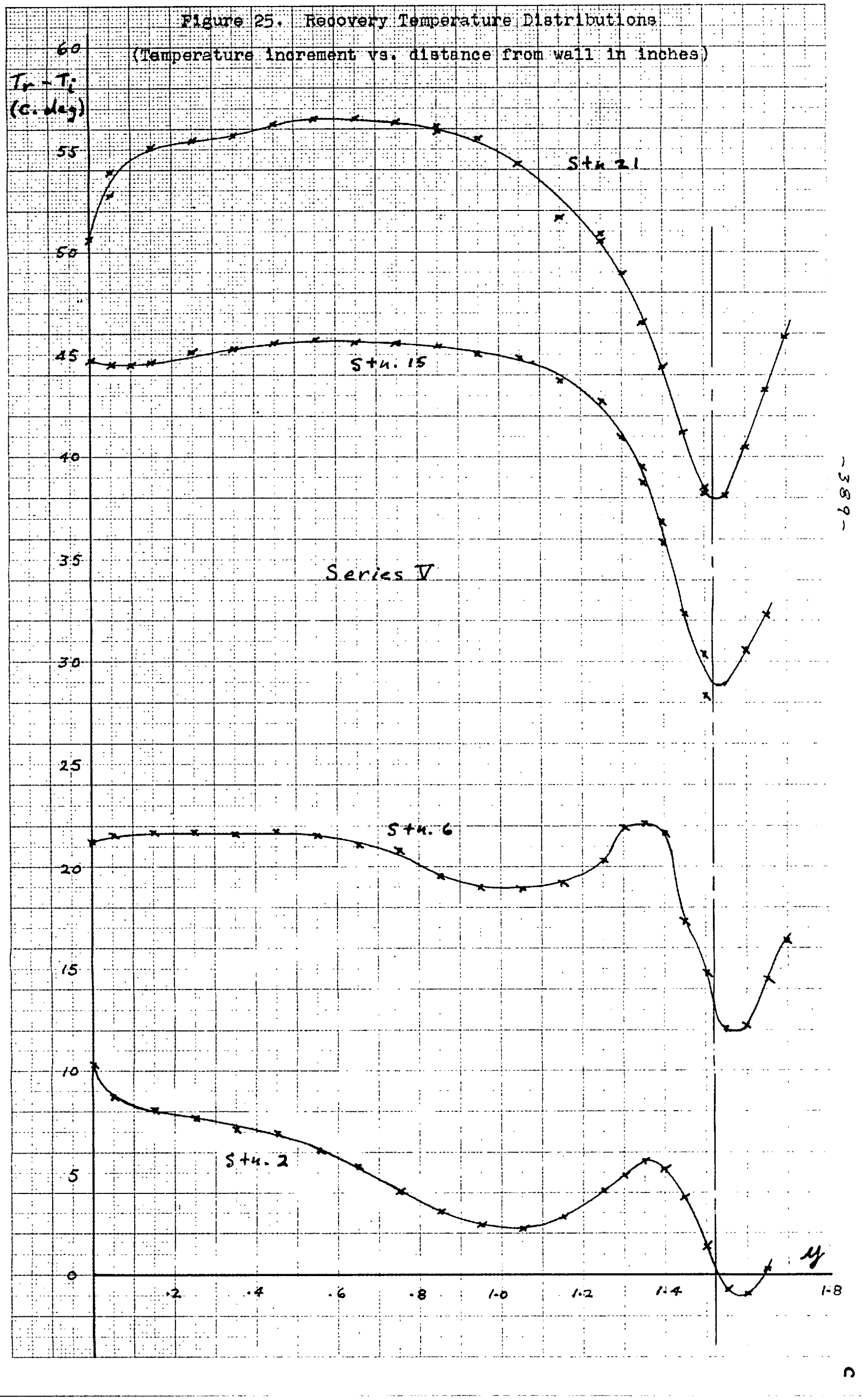
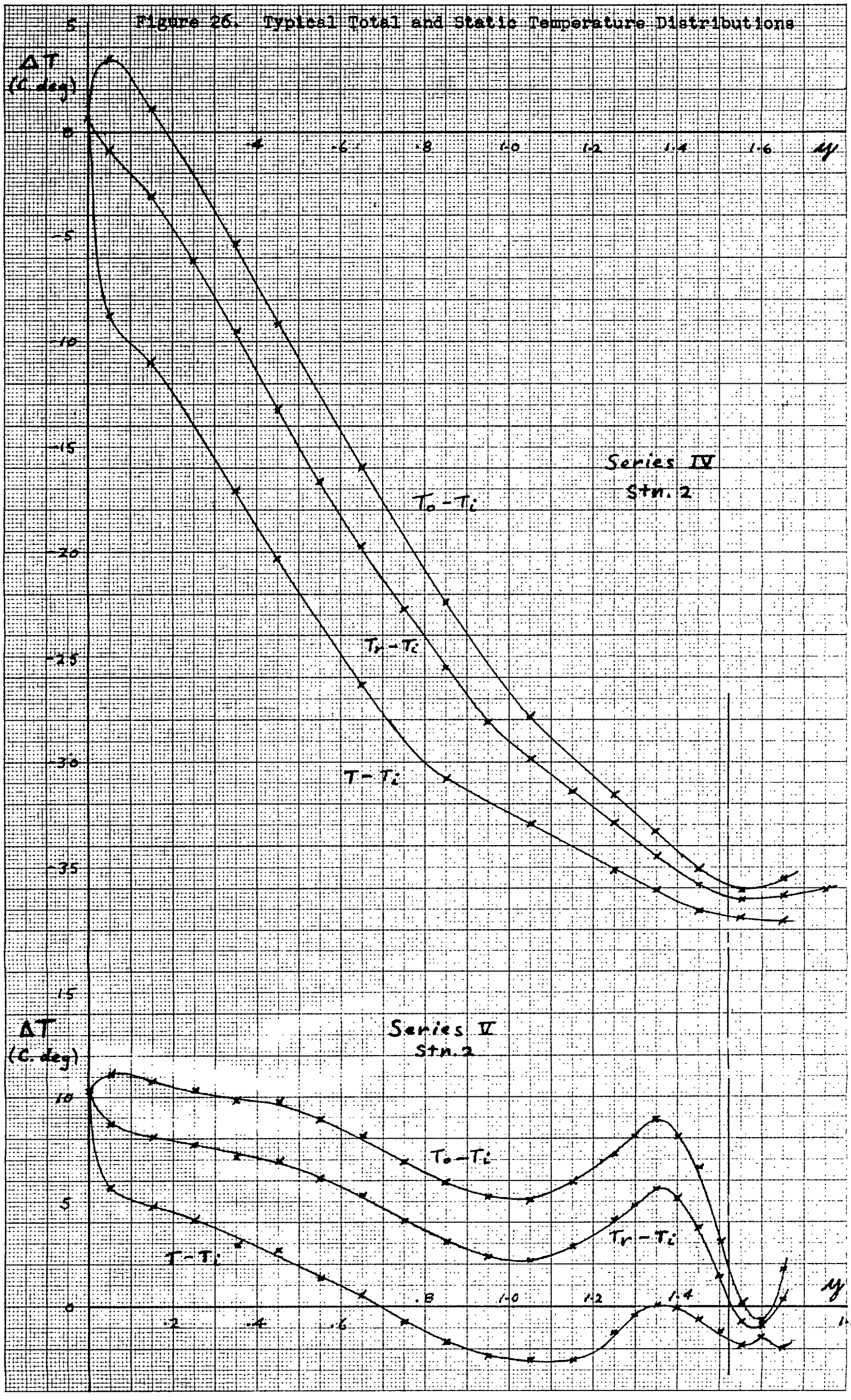


Figure 26. Typical Total and Static Temperature Distributions



C

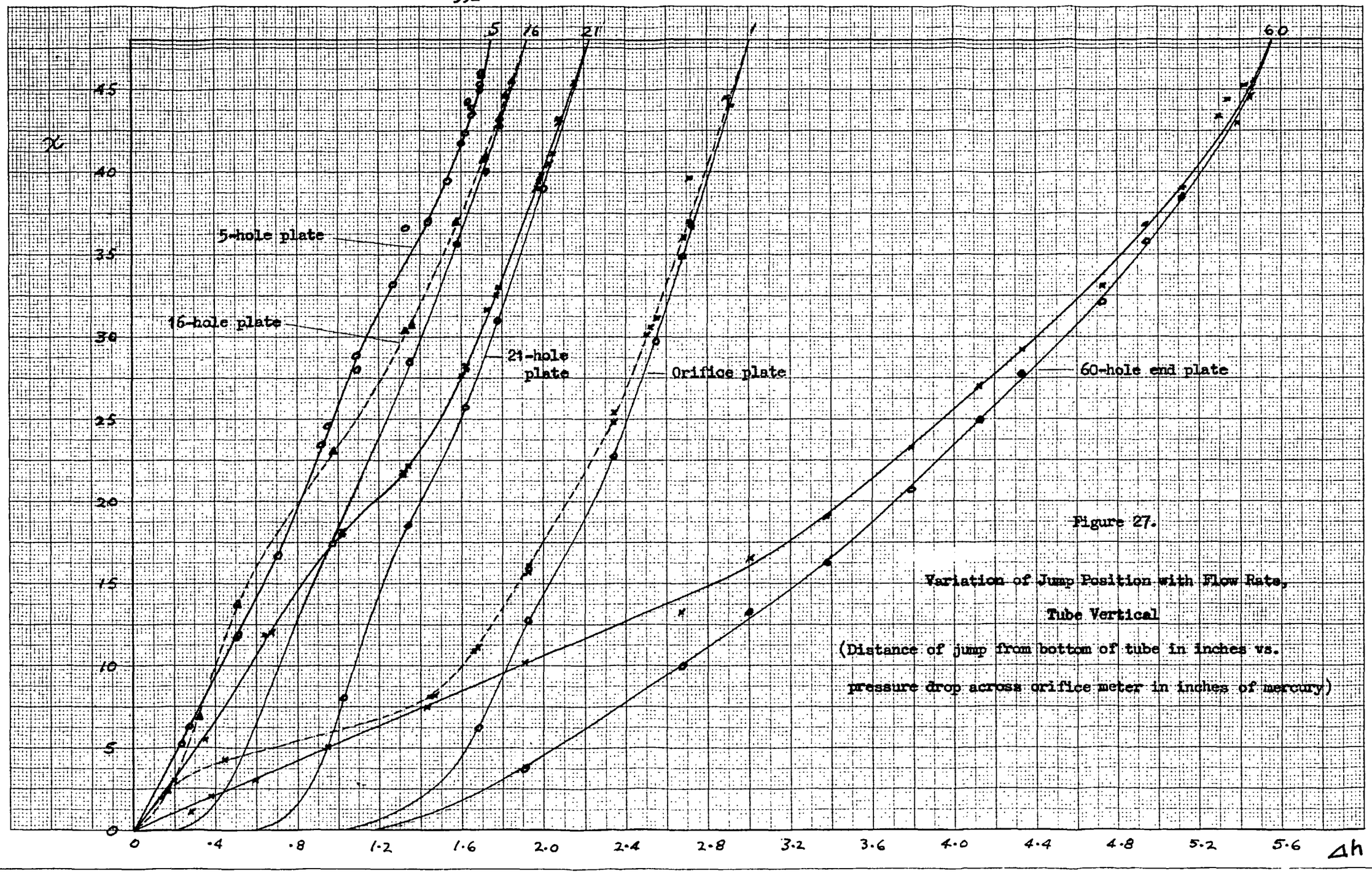



Figure 27.

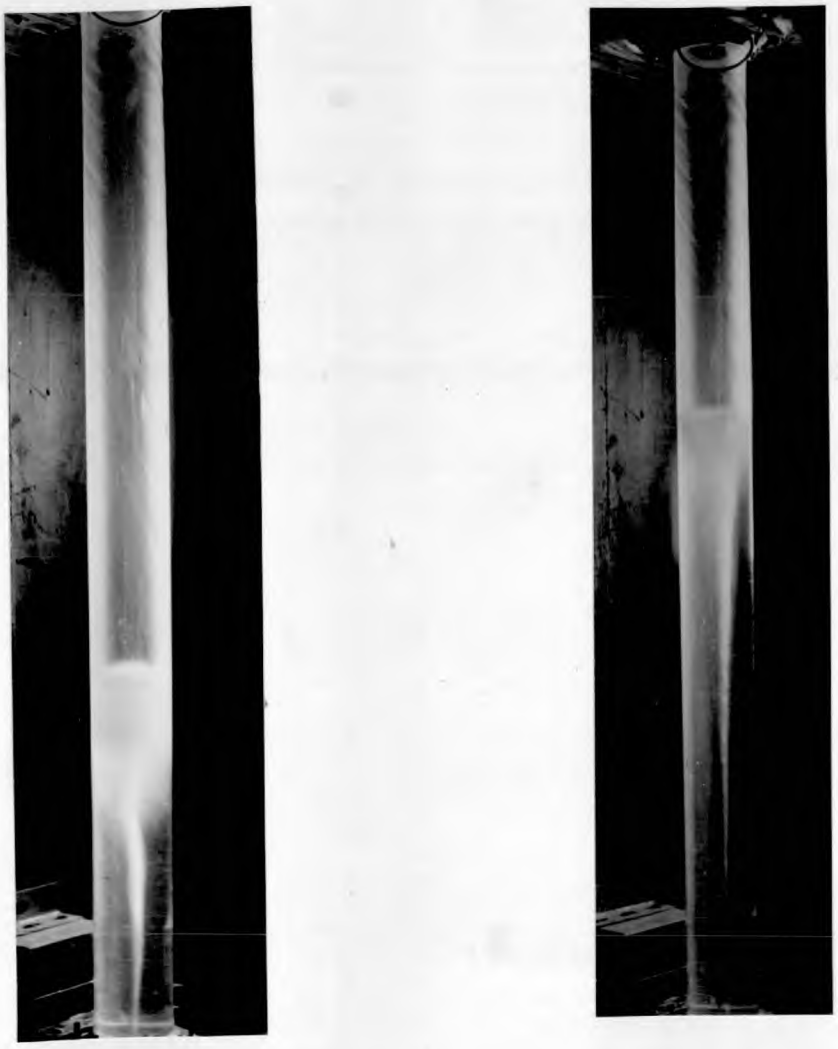
Variation of Jump Position with Flow Rate,

Tube Vertical

(Distance of jump from bottom of tube in inches vs.

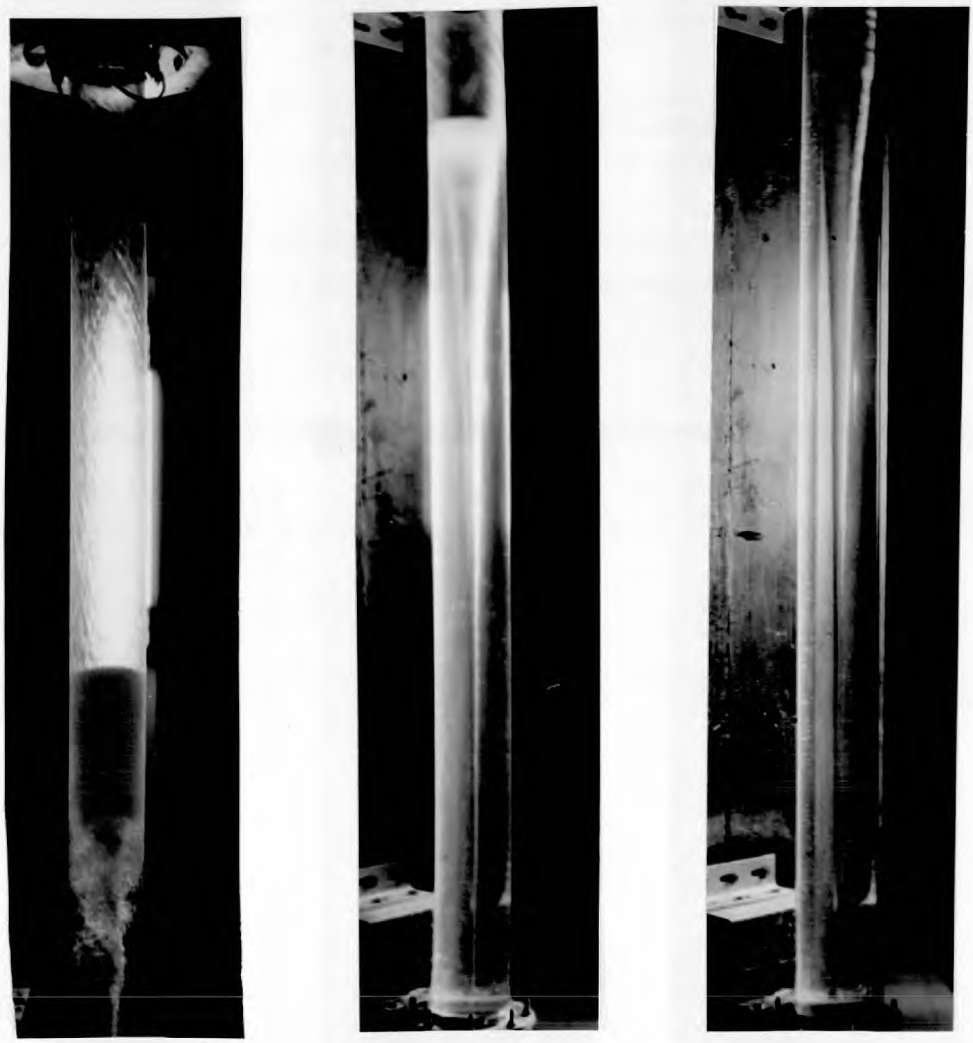
pressure drop across orifice meter in inches of mercury)

C



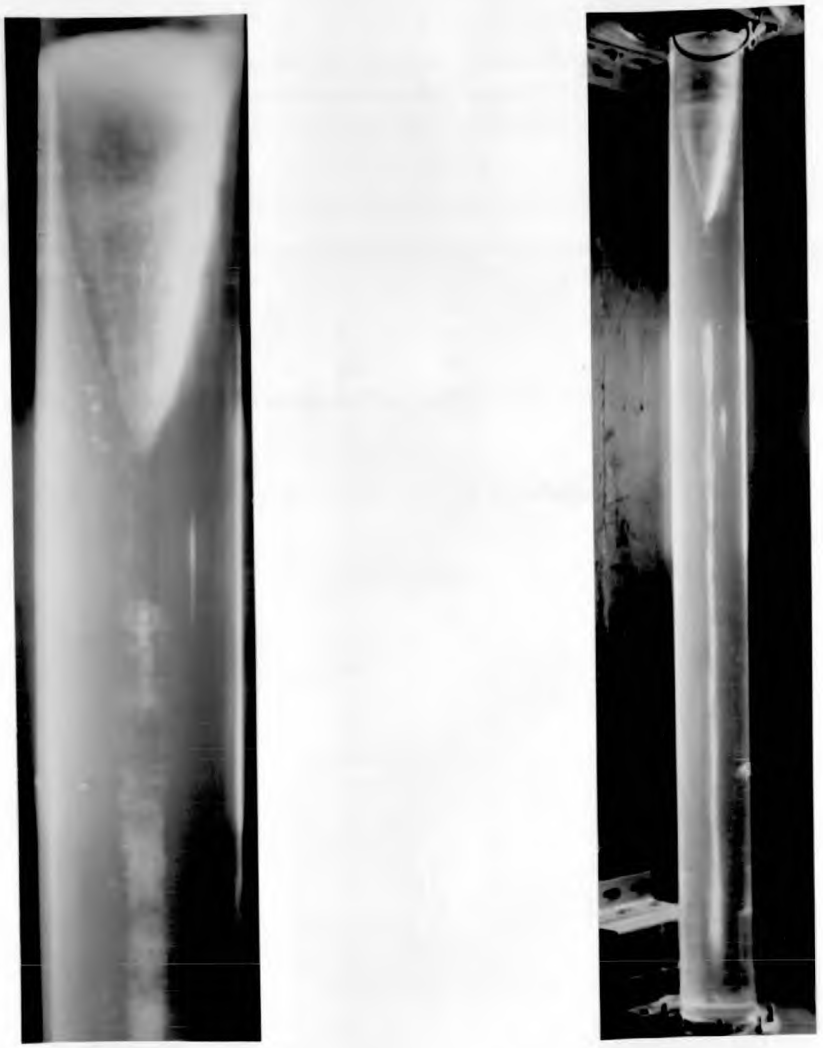
(a) (b)

Figure 28. Air Core with Tube Vertical, orifice plate at bottom



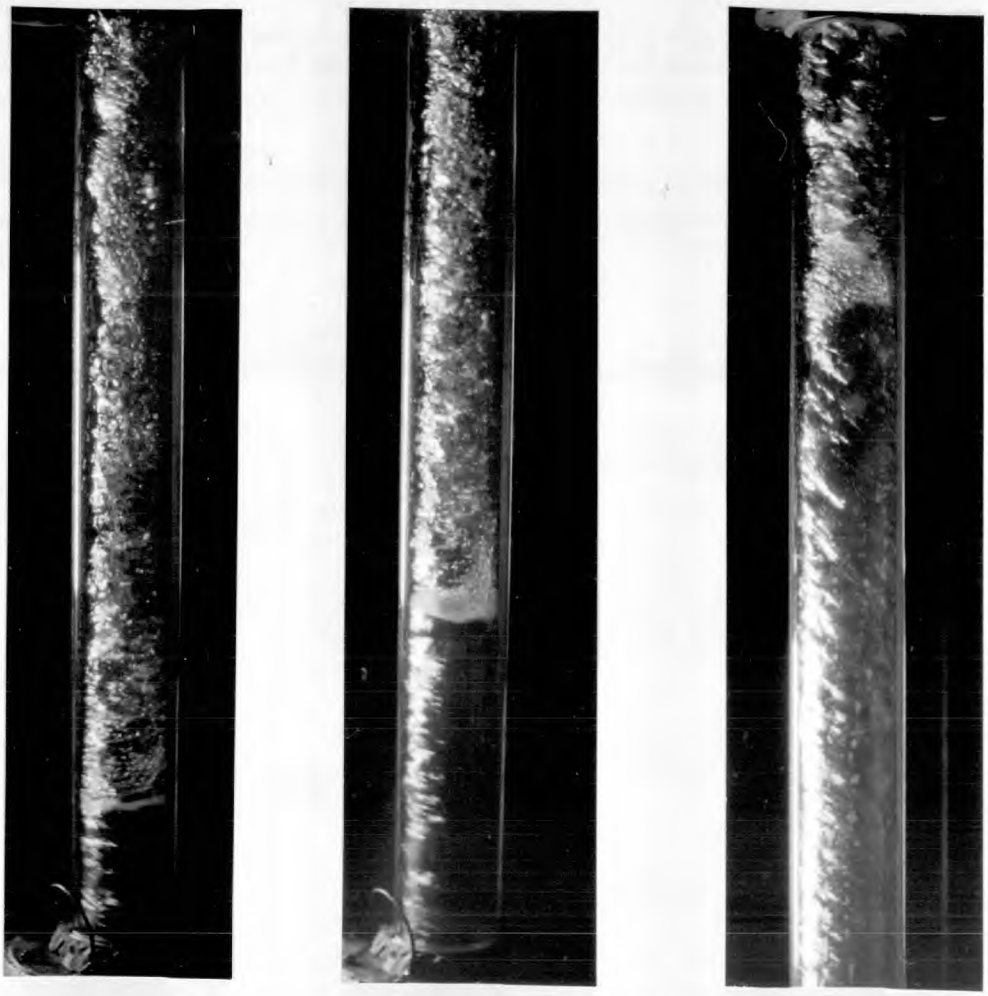
(a) (b) (c)

Figure 29. Air Core with Tube vertical, 21-hole plate at bottom



(a) (b)

Figure 30. Air Core with Tube Vertical, 16-hole plate at bottom



(a) (b) (c)

Figure 31. Jump with Tube Horizontal

C

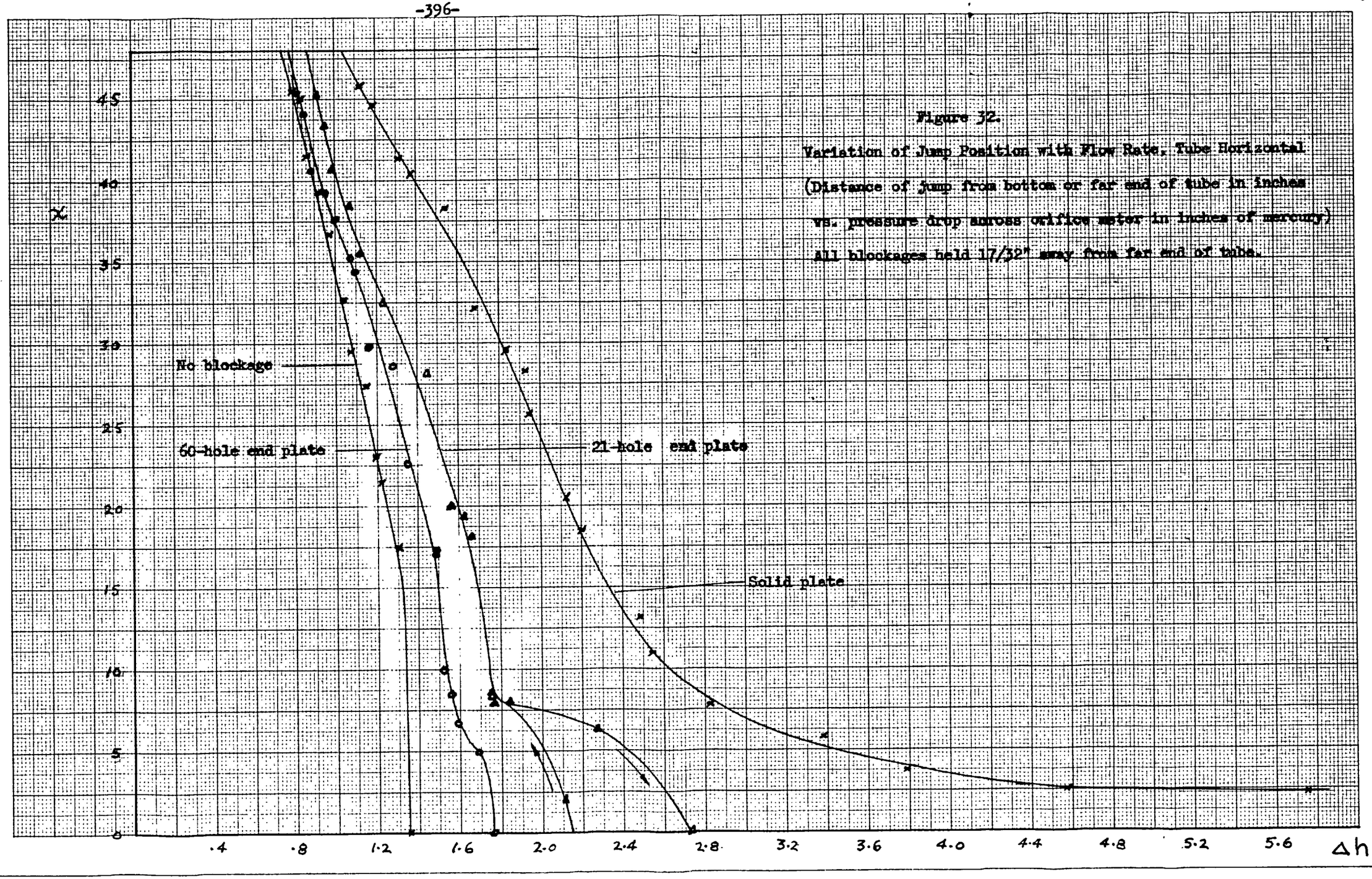



Figure 32.

Variation of Jump Position with Flow Rate, Tube Horizontal.

(Distance of jump from bottom or far end of tube in inches vs. pressure drop across orifice meter in inches of mercury)

All blockages held 17/32" away from far end of tube.

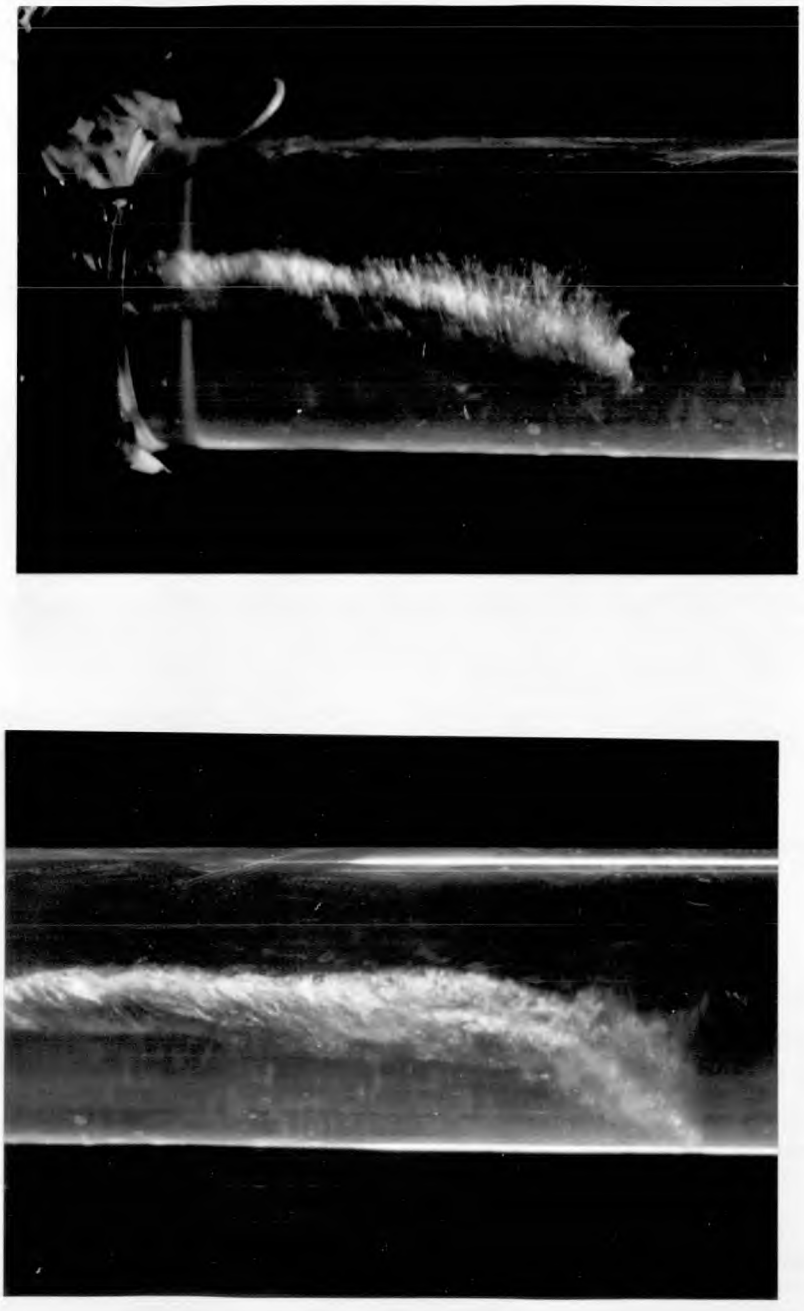
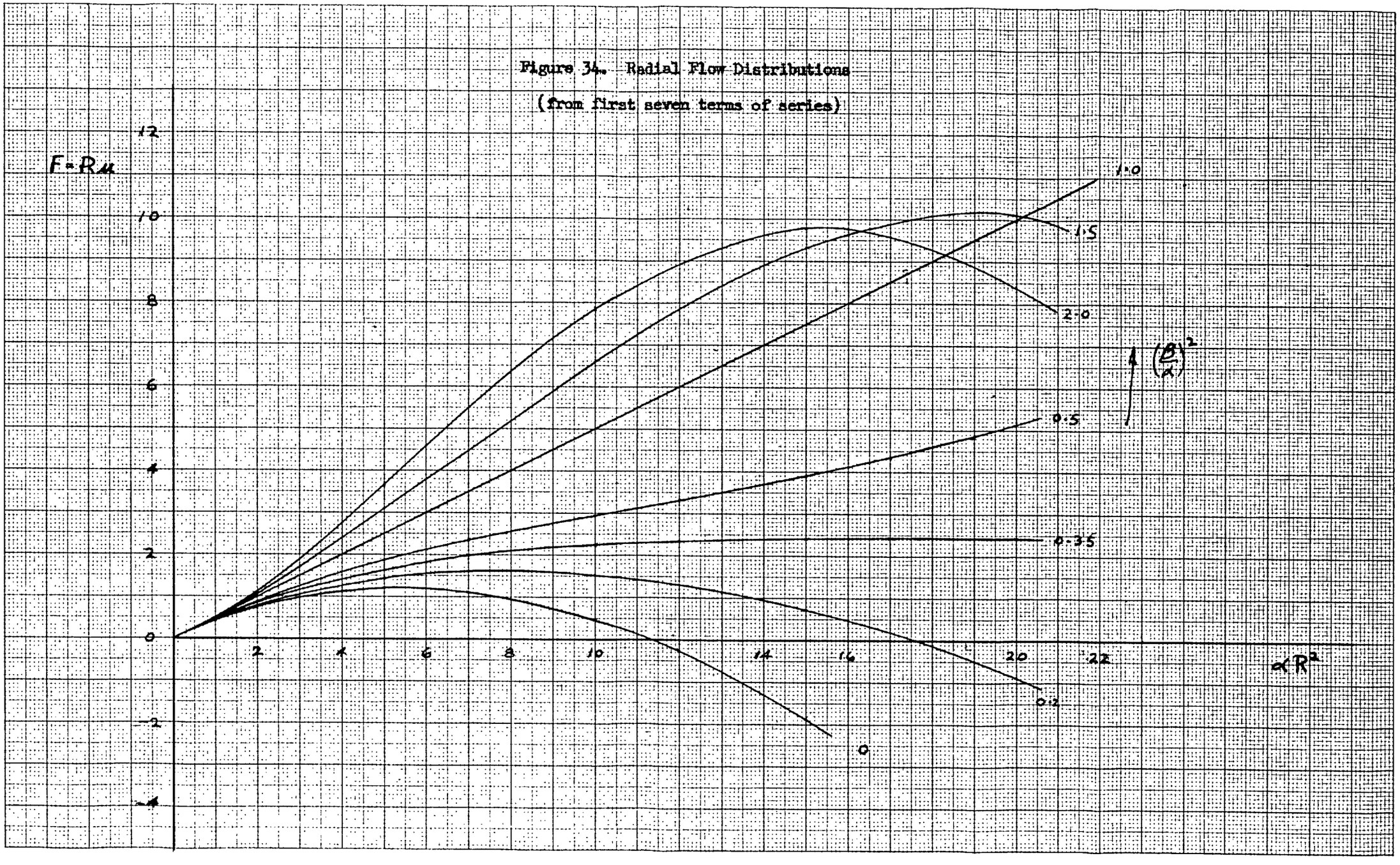


Figure 33. Whirling Core

Figure 34. Radial Flow Distributions
(from first seven terms of series)



C

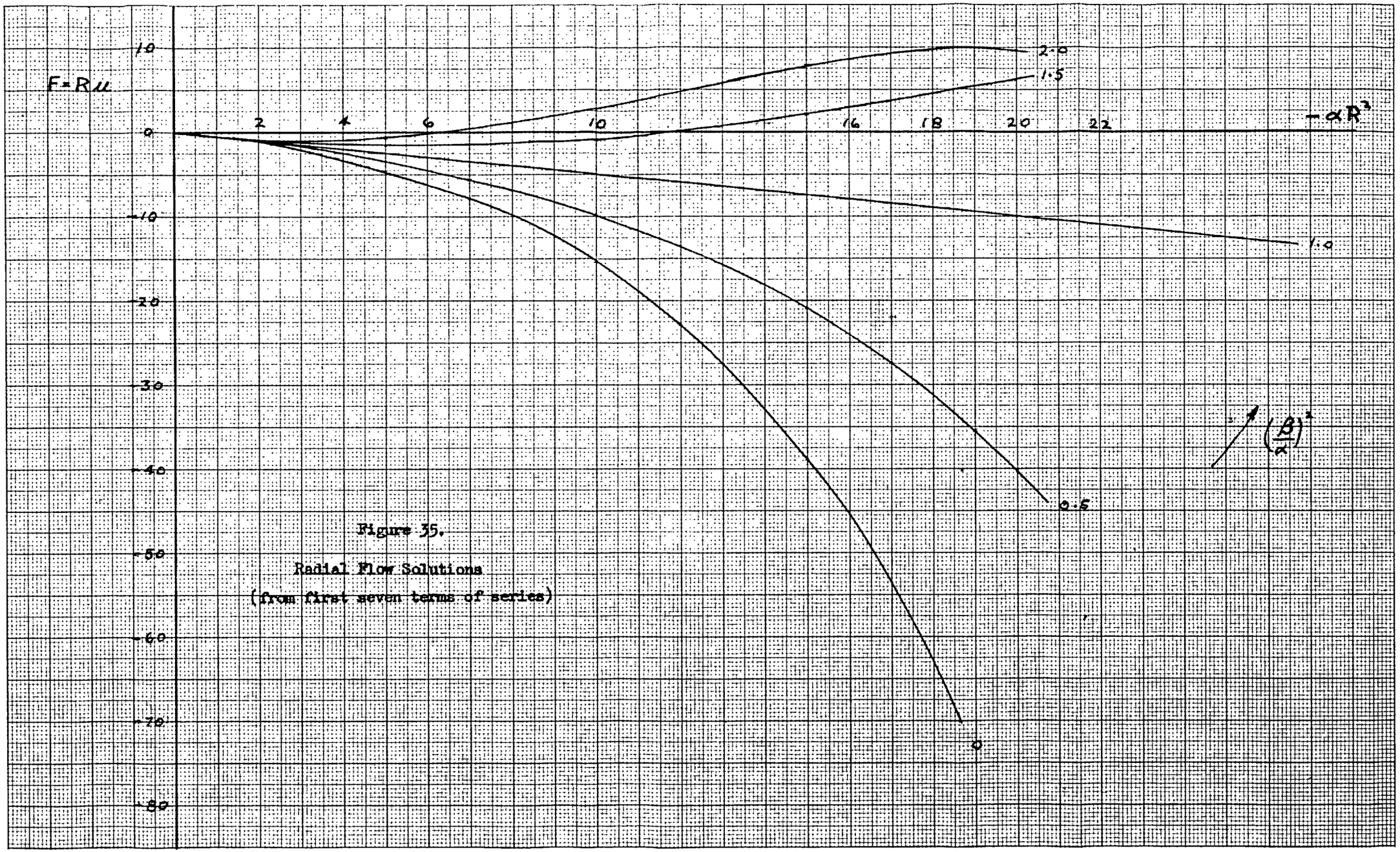
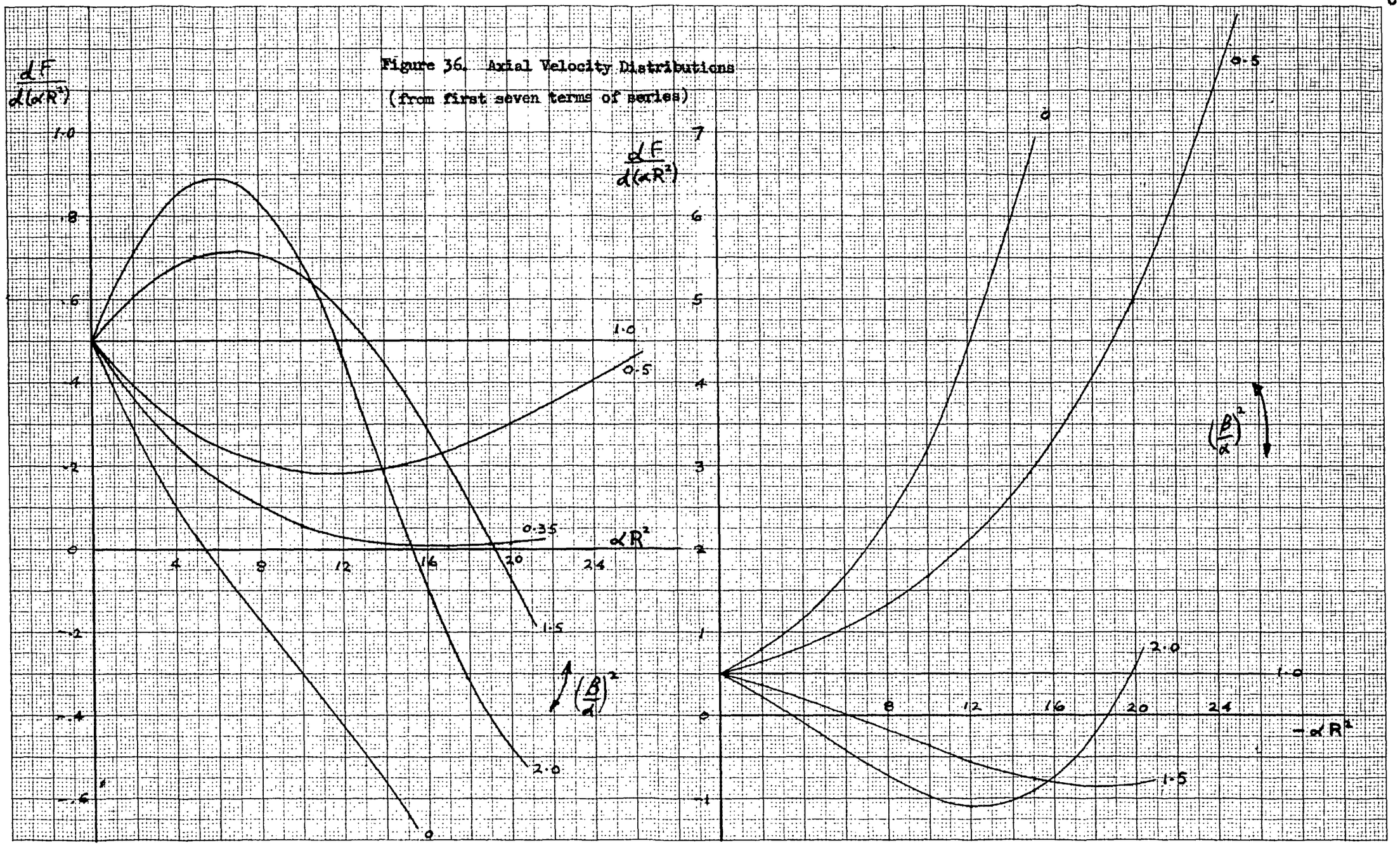



Figure 35.

Radial Flow Solutions

(from first seven terms of series)

Figure 36. Axial Velocity Distributions
(from first seven terms of series)



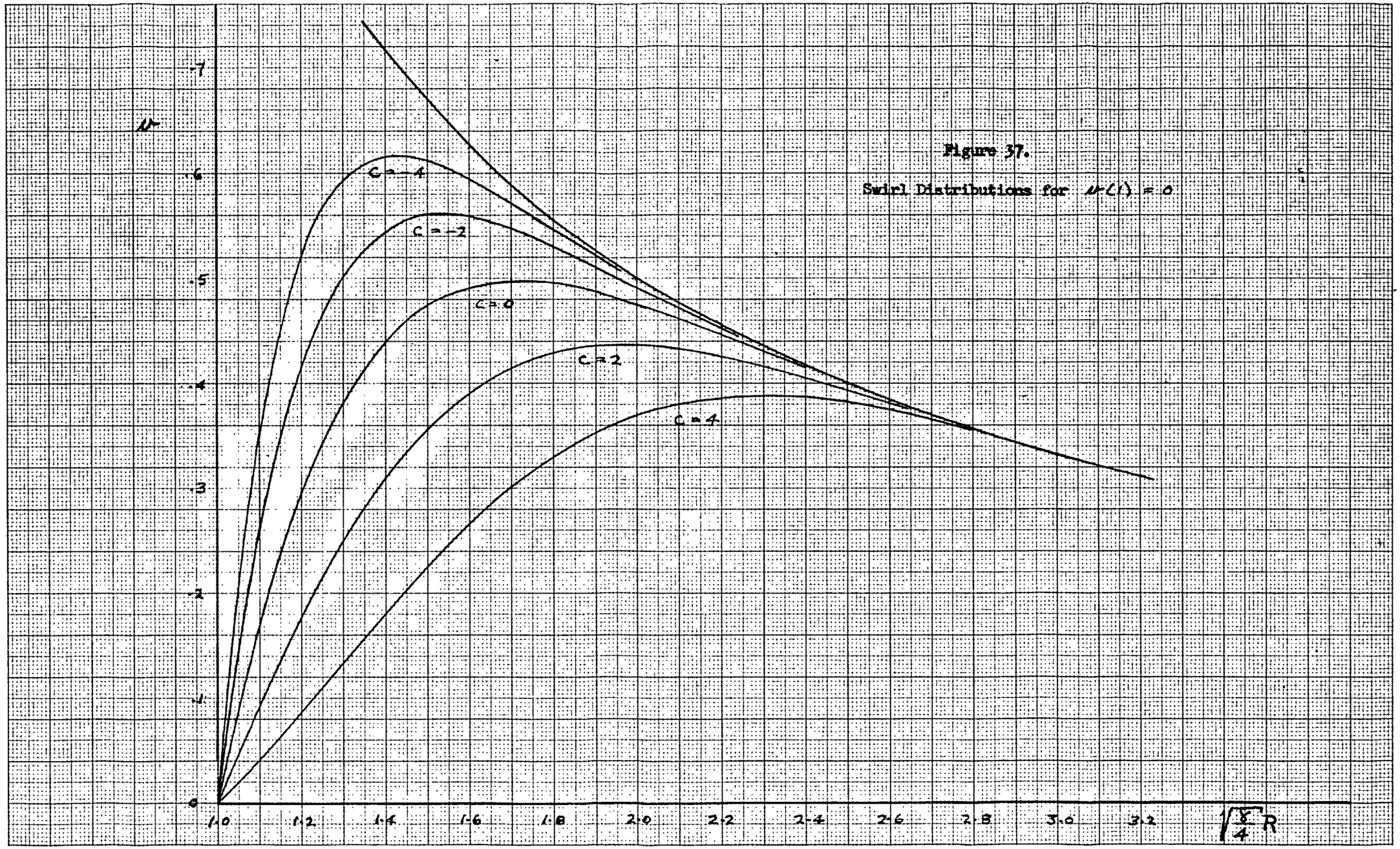



Figure 37.

Swirl Distributions for $\mu(1) = 0$

C

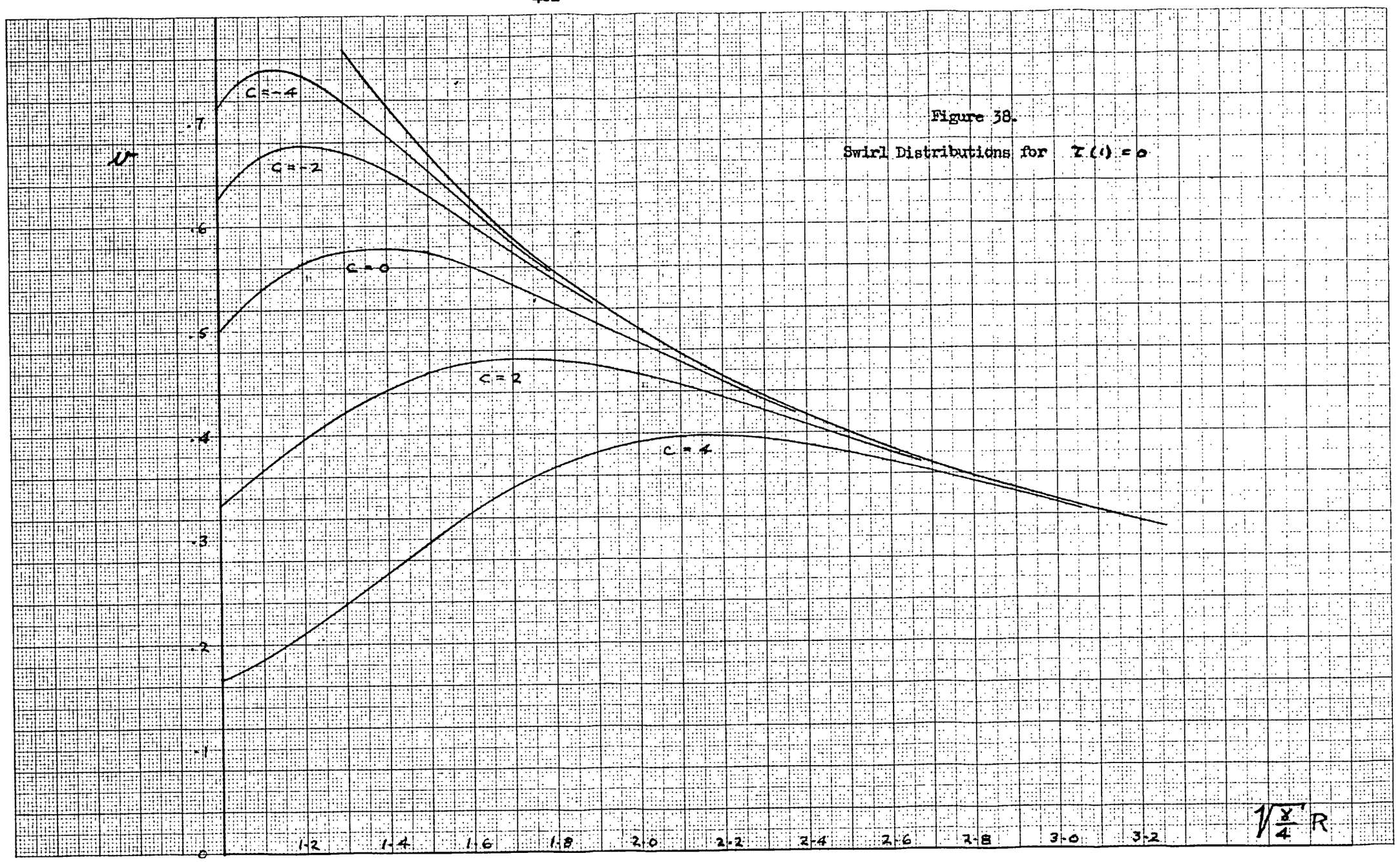



Figure 38.

Swirl Distributions for $\Gamma(1) = 0$